NOVEL METHODS OF HYDROGEN PRODUCTION: ALUMINUM-GALLIUM-INDIUM-TIN SYSTEMS AND COPPER BORON OXIDE AS PHOTOCATALYSTS

by

Yizhao Lang

A thesis submitted to the faculty of
The University of Utah
in partial fulfillment of the requirements for the degree of

Master of Science

Department of Materials Science and Engineering

The University of Utah

December 2011

The University of Utah Graduate School

STATEMENT OF THESIS APPROVAL

The thesis of **Yizhao Lang**

has been approved by the following supervisory committee members:

Ashutosh Tiwari	, Chair	**June 2, 2011**
		Date Approved
Feng Liu	, Member	**June 2, 2011**
		Date Approved
Michael Free	, Member	**June 2, 2011**
		Date Approved

and by **Anil V. Virkar** , Chair of

the Department of **Materials Science and Engineering**

and by Charles A. Wight, Dean of The Graduate School.

ABSTRACT

In recent years, hydrogen production and storage has attracted a lot of attention in both academia and industry due to its variety of applications in the energy sector. In this review, we attempt to list various methods of producing hydrogen from different sources of materials followed by the description of most recent developments in the materials perspective. We explain the role of nanotechnology in making the hydrogen production technology a viable and cost effective process. The chemical reaction cycle, mechanism and configurations of various methods of hydrogen production are elaborated in Part I of this thesis.

Among the materials for chemical methods, aluminum could be utilized as an efficient and environmental friendly energy carrier via the production of hydrogen from water. However, it requires the reaction between aluminum and water to be complete, controllable and does not require the involvement of acids and/or alkali. Such direct reaction between aluminum and neutral water, once considered impractical due to the passivation of aluminum surface in water, is enabled with the relatively recent use of catalytic gallium-based liquid alloys. In this paper we have examined the roles of different elements (Ga, In, Sn, Zn, Bi) in this type of alloy and how their compositions affect the aforementioned reaction between aluminum and water. Besides the compositions of alloys, we have also studied the activation process between the liquid alloys and aluminum powders, as well as the storage process both before and after the activation. The rate of hydrogen production from each aluminum-water reaction was measured as a function of time. The whole research is discussed in Part II of this thesis.

As photocatalysts for water splitting, $CuBO_2$, $CuAlO_2$, $CuBO_2/TiO_2$ heterojunction and $CuAlO_2/TiO_2$ heterojunction are synthesized and tested. All these materials exhibit positive water-splitting capability with a solution environment of 0.05M $Na_2S{\cdot}9H_2O$ as a hole scavenger and 0.1M NaOH as a pH modifier under simulated AM 1.5 standard sun light. The group with heterojunction $CuAlO_2/TiO_2$ shows an average hydrogen production rate of 0.509 mmol/min, 6.33% higher than the $CuAlO_2$ group. The group with $CuBO_2$ shows an average 0.979 mmol/min hydrogen production rate, the highest rate among all groups, 104.38% higher than the $CuAlO_2$ group. The details of our work on photoelectrolysis are studied in Part III of this thesis.

TABLE OF CONTENTS

LIST OF FIGURES

Figure Page

LIST OF TABLES

PART I

A GENERAL REVIEW ON HYDROGEN PRODUCTION:

METHODS AND MATERIALS

1. INTRODUCTION

The energy system of traditional fossil fuels, though still dominant and relatively economical at present, is already widely called into question by the energy experts and environmentalists, not only because of its lack of sustainability, but also due to its severe impact on the environment[1]. Several million tons of greenhouse gases such as carbon dioxide, methane, nitrous oxide, ozone and CFCs are emitted into the atmosphere each day[2]. These greenhouse gases produce several adverse impacts on the atmosphere including those that can affect people's health, such as pollution, smog and related diseases, rising sea levels, poorer air quality and other anomalous weather changes. In contrast, hydrogen, the most promising representative of novel energy carriers, showed great potential to become a widespread, clean and sustainable form of energy. With its potential reproducibility, high energy density and environmental cleanliness, hydrogen is considered an almost perfect energy source as well as energy carrier. As an energy source, hydrogen could be both renewable and distributable without regard for national boundaries[3]. A future energy system based on hydrogen and electricity is attractive not only because of its role in solving the problem of fossil fuel shortage, but also for its incomparable advantages in reducing greenhouse gases as well as all kinds of pollutions related to the burning of fossil fuels.

Even though hydrogen is the most attractive and environment friendly source of energy, most of the processes and materials used presently to produce hydrogen are not. At present, more than 96% of the hydrogen is derived from fossil fuels due to the lower cost of production. Hydrogen produced using coal and natural gas (with steam

reformation) costs ~ $1 per GGE and ~$3 per GGE, respectively (GGE= Gasoline Gallon equivalent). While the hydrogen produced using solar energy (by the means of electrolysis of water) costs ~ $9.50 per GGE. But while fossil fuels continue to be used for producing hydrogen, the whole purpose of using hydrogen for producing clean energy is undermined. As long as the hydrogen is not produced from renewable energy sources, it cannot be termed as a clean source of green energy. In order to make the hydrogen energy production affordable and clean, much more research with a clear focus on developing new materials, methods and large scale production technologies are required. Most of the technologies that are being developed to generate hydrogen energy from various renewable sources are still in the R & D stage.

Disregarding the current cost-renewability dilemma of hydrogen production described above, the whole cycle of hydrogen economy including production, storage, transportation and usage is being extensively studied by the researchers and organizations from various regions of the world. Considered as a most significant part of the hydrogen economy, hydrogen production is a critical factor determining its sustainability, effectiveness and environmental impact. While an increasingly number of new techniques like carbon nanotubes and fuel cells are used in the storage, transportation and usage of hydrogen, production of hydrogen is also studied deeply, involving divergent advanced techniques, especially nanotechnology. These new technologies may allow us to face the challenges in existing production processes as well as to apply more novel and renewable energy options into it. In this review, we will go through both the traditional methods as well as the new methods of hydrogen generation and explain how nanotechnology approaches can help in the cost-effective production of hydrogen.

1.1. References

[1] M. Momirlan and T. N. Veziroglu, Renew. Sust. Energ. Rev. **6**, 141 (2002).

[2] I. Dincer and G. Naterer, Int. J. Hydrogen Energ. **35**, 4787 (2010).

[3] G. Crabtree, Phys. Today **57**, 39 (2004).

2. METHODS OF HYDROGEN PRODUCTION AND NANOTECHNOLOGICAL ADVANCEMENTS

Hydrogen can be generated with many different methods. These methods vary so much that a lot of different ways can be used to classify them. In terms of the source of energy, hydrogen could be either produced with primary energy sources or with secondary sources. Among which, secondary energy sources used for hydrogen evolution include electricity and chemical energy, while the primary energy sources include non-renewable energy sources like fossil fuels and renewable energy sources include solar energy, wind energy and biomass. In terms of the raw materials used in the reaction, hydrogen production methods can be divided into the following classes: (1) hydrogen production by the direct reaction of chemical reagents including metals, acids and bases; (2) hydrogen production from hydrocarbons including fossil fuels and biomass; (3) hydrogen production by the direct splitting of water. In this review, we will adopt the above classification for the discussion.

2.1. Hydrogen production through direct reaction of chemicals

Hydrogen generation using available chemical reagents has been a thoroughly studied subject. The associated fundamental reactions and theories can be found in most general chemistry books. In most cases, these reactions can be roughly classified into three categories: (1) reactions involving acids (2) reactions involving bases (3) reactions between water and reactive metals.

A typical example of the first category is the reaction between sulphuric acid and zinc:

$$Zn+H_2SO_4 \rightarrow ZnSO_4+H_2\uparrow \quad (1)$$

This reaction happens in aqueous medium, though water is not consumed in the overall transformation. No external work is done to the reacting system and the reaction is exothermic. Therefore, both the materials and the energy for hydrogen generation within the process derive from the two chemicals: Zinc and sulphuric acid. The second category is similar to the first one in terms of energy transformation. However, bases, usually strong bases, can sometimes be the replacement of acids, which are the most reactive part in the reactions of the first category. Sometimes water is also involved in the reaction. In such cases, H_2O can be also considered as one of the reacting chemicals. For example, in the reaction of Silicon and Sodium hydroxide[1]:

$$2NaOH+Si+H_2O \rightarrow Na_2SiO_3 + 2H_2\uparrow \quad (2)$$

This is a spontaneous chemical reaction which produces hydrogen while supplying a large amount of heat. If both the heat and the hydrogen produced can be used efficiently, this reaction can be quite feasible and profitable.

The third category, the reaction between water and metals, is commonly categorized as a reaction between water and alkali metals, such as:

$$2Li+2H_2O \rightarrow 2LiOH+H_2\uparrow \quad (3)$$

However, other reactions, such as those between aluminum and water, could also be categorized into this type. Aluminum, as a widely used and abundant metal, can be used for water splitting and hydrogen production:

$$Al+3H_2O=Al(OH)_3+3/2H_2\uparrow \quad (4)$$

Theoretically, the reaction of 1 g of Al with water produces 1.245 L of H_2[2]. But this reaction has a limitation, due to the passivation of the Aluminum surface caused by the dense film of Aluminum oxide which prevents further reaction. However, recent studies show that, with the help of Gallium-based alloys, the reaction could be quite efficient due to the prevention of the passivation of Aluminum surface. This concept has been proved experimentally in our research laboratory.

In order to prove this concept, we have conducted experiments on three different metal alloys prepared using five different metals[3-5] (1) Ga:In:Sn = 65:25:10; (2) Ga:In:Sn:Zn = 60:25:10:5 and Ga:In:Sn:Bi = 65:22:7:4. The detailed experimental procedure for making these alloys will be reported as a separate part (Part II). From the experiments on the above three combinations of alloys, it is found that Gallium (Ga) is the element making the reaction sustain for a long time by creating a liquid alloy that effectively moistens the aluminum surface, ultimately preventing the formation of an oxide layer on the surface of the aluminum. Indium (In) makes liquid alloy with Ga when heated together with a ratio near the eutectic point. Tin (Sn) further decreases the melting temperature of the alloy. Zinc could increase the defects and cracking of the protective alumina layer, which facilitates the diffusion of the deposited In, Ga into the surface layers and improves Al reactivity. It is supposed to further decrease the melting temperature of the alloy, though it has so far proved extremely hard to mix into the

existing alloy of Ga, In, Sn at relatively low temperatures. For the first time, we have replaced Zn with Bi and the resultant alloy has been tested for the hydrogen production; bismuth has been used due to its favorable chemical and physical properties, such as its ability to lower the melting point of alloys.

The energy stored in the Al metal can be released locally into hydrogen energy through reaction with water with the help of Ga-based alloys. We have obtained 99 ml of hydrogen from the reaction of DI water with 0.2 g of Al powder which is activated by Ga-based liquid alloy for 45 hours. This amount is 39.8% of the theoretical yield of hydrogen from any reaction between water and Al. Combined with the aforementioned high rate between the amount of reacting Al and the produced hydrogen, Al can be expected to be a high-energy-capacity carrier of hydrogen in the upcoming hydrogen economy. However, since the production of Al metal is still very energy-consuming and requires other energy sources (i.e., fossil fuels), at this time, hydrogen production through reaction between Al and water is limited to be a method of energy transferring instead of energy acquiring uses, similar to other reactions previously discussed.

2.2. Hydrogen production from hydrocarbons

A number of hydrogen rich hydrocarbons, often used for combustion, could also be used in hydrogen production with their high chemical energy density within themselves. These hydrocarbons include both the nonrenewable fossil fuels and renewable biomass. Fossil fuels, especially gaseous state ones, could be readily transformed into hydrogen with the help of heat and catalysts. The efficiencies of this type of transformation are already high and still improving as new technologies become available. Biomass is usually not in the gaseous state, so the gasification is a very

important process for the hydrogen production from biomass. The efficiency of gasification is also dependent on temperatures and catalysts and for the latter, advanced technologies and materials are being progressively applied.

2.2.1. Hydrogen from fossil fuels

Fossil fuel is currently the dominating source of hydrogen production. More specifically, almost 95% of hydrogen used nowadays is produced from natural gas via steam methane reforming[6]. There are other ways of utilizing fossil fuels as a hydrogen source, such as partial oxidation, plasma reforming, autothermal reforming and coal gasification, but steam reforming is always considered playing the key role in a future hydrogen economy[7], because of its entire thermodynamical feasibility, sophisticated engineering development and high efficiency. The steam reforming of fossil fuels usually takes place in a processing device called a reformer which reacts steam at high temperature with the fossil fuel. Other than the most frequently used methane in natural gas, other hydrogen-rich fuels such as propane, gasoline, diesel fuel and ethanol could also be used to generate hydrogen by the steam reforming method.

The general hydrocarbon steam reforming reaction is[8] :

$$C_mH_n+mH_2O=mCO+(m+n/2)H_2 \quad \Delta H=\text{hydrocarbon dependent, endothermic} \qquad (5)$$

For methanol as an example, it will be[9]:

$$CH_3OH+H_2O=CO_2+3H_2,\ \Delta H=49\ \text{kJ mol}^{-1} \qquad (6)$$

And for natural gas (assuming pure methane)[10]:

$$CH_4+H_2O=CO+3H_2,\ \Delta H=206\ \text{kJ mol}^{-1} \qquad (7)$$

$CH_4+2H_2O=CO_2+4H_2,\ \Delta H=165\ kJ\ mol^{-1}$ (8)

Fuel processing requires modest temperatures depending on the specific hydrocarbon as the feedstock. For example, methanol, DME (dimethylether) and other oxygenated hydrocarbons that can be readily activated at a temperature above 180 °C and for most conventional hydrocarbons, the temperature should be above 500 °C[11-13]. Two types of catalysts are used in the process: nonprecious metal (typically nickel) and precious metals from Group VIII elements (typically platinum- or rhodium-based). Between them, the less expensive nickel catalysts are used almost universally in industry because the major limiting factors with conventional steam reformer reactors are not on kinetics and the activity of the catalyst, but on the severe mass and heat transfer limitation [14, 15].The schematic features of a steam reformer are shown in Fig. 2.1[10], in which steam

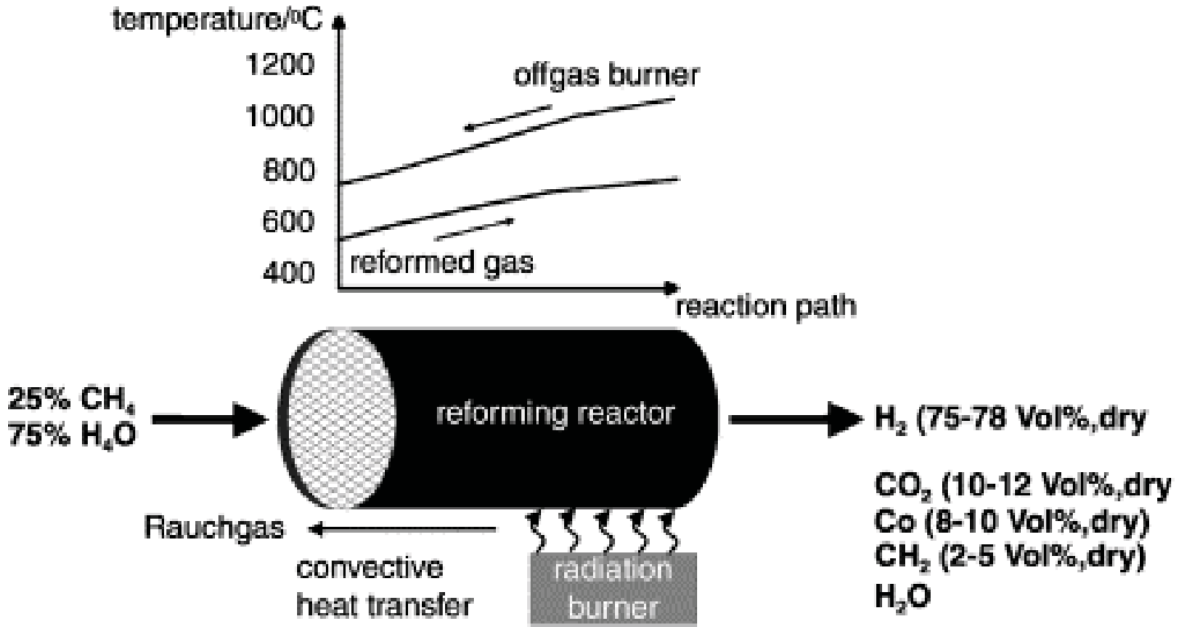

Fig. 2.1: Features of a steam reformer for methane. Reprinted with permission from Reference 10, A. Heinzel, B. Vogel and P. Hübner, Journal of Power Sources **105** 202 (2002).© 2003, Elsevier.

reforming of methane yields the best hydrogen content of all the reforming processes with 75–78 vol.%.

2.2.2. Nanotechniques applied in hydrogen production from fossil fuels

Although the previously discussed conventional steam reformer reactors do not highly depend on the reactivity of catalysts, the catalytic materials, especially nanomaterials, are considered as having increasing importance. Researchers in the University of Pennsylvania[16] synthesized a $Pd@CeO_2$ core-shell-nanostructured dispersible material which is very useful as a catalyst precursor in the methanol steam reforming reactions. The nanostructure is prepared following three steps: Firstly, the MUA-Pd nanoparticles (where MUA indicates 11-Mercaptoundecanoic acid) are prepared through a solution precipitation method borrowed from another Pd-related synthesis process[17]. The second step is the preparation of cerium (IV) tetrakis (decyloxide) [$Ce(C_{10}H_{21}O)_4$, $Ce(OR)_4$] following a solution evaporation procedure similar to their previous experiments[18, 19]. Then the final step is to prepare the $Pd@CeO_2$ core-shell nanostructure by adding the THF solution of MUA-Pd nanoparticles to the THF solution of cerium (IV) tetrakis (decyloxide), followed by the addition of a THF solution of dodecanoic acid. This synthesized $Pd@CeO_2$ nanostructure could not be used as a steam reforming catalyst alone; an Al_2O_3 substrate is necessary as a support for the catalytic function. The $Pd@CeO_2/Al_2O_3$ catalysts were prepared using the $Pd@CeO_2$ nanostructures as the starting material. The appropriate mass of degassed Al_2O_3 was then added to the $Pd@CeO_2$ solution to achieve the nominal loading for Pd and CeO_2, 1 and 9 wt %, respectively.

After the mixture was stirred overnight, THF was removed by evacuation, after which the powder was dried at 120 °C, crushed to particle sizes below 150 μm and finally calcined at 500 °C for 5 h, using a heating rate of 3 °C min^{-1} to reach the calcination temperature. The researchers tested the catalyst in methanol steam reforming reactions and, as shown in Fig. 2.2[16], obtained very promising activity on all yields including that of H_2.

Many other catalysts for hydrogen production from steam reforming of fossil fuels also utilized nano-techniques. For example, nanopowder of zirconia is used as catalysts for the steam reforming of bio-ethanol[20]. A ZrO2-modified Ni–nano-CaO sorption complex plays an important role in reactive sorption-enhanced reforming of hydrogen production[21]. Those already commercialized catalysts, like indium oxide, are also improving with the development of nanotechnology. With the significant progress that has been achieved in the preparation of nanostructured materials by utilizing the so-called nanocasting route[22]. Silica matrix acting as nanoscopic mold is developed and used as templates in the preparation of nanostructured indium oxide catalysts. Nano-structured In_2O_3 materials were obtained through the solution etching of silica framework by a 1.0 M NaOH aqueous solution[23]. The catalyst activity of the nanostructure was proved to be elevated in comparison with the commercial In_2O_3 catalyst, as shown in Fig. 2.3[23], where both mesoprous and worm-like In_2O_3 are nanostructure prepared on a silica substrate.

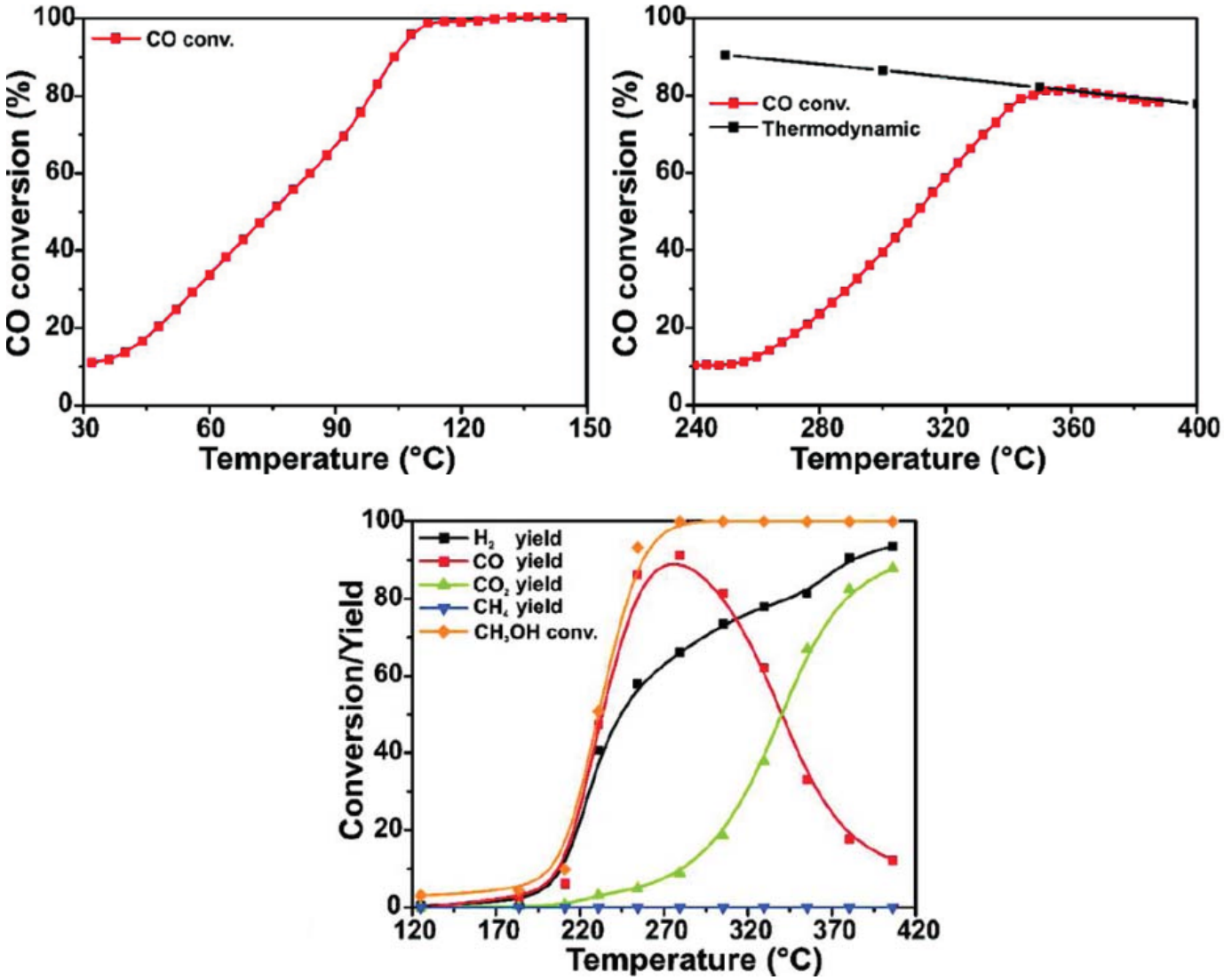

Fig. 2.2: Catalytic activity of Pd(1%)@CeO_2(9%)/Al_2O_3, prepared from Pd@CeO_2 nanostructures for methanol steam reforming reactions. Reprinted with permission from Reference 16, M. Cargnello, N. L. Wieder, T. Montini, R. J. Gorte and P. Fornasiero, Journal of the American Chemical Society **132** 1402 (2009). © 2009, American Chemical Society

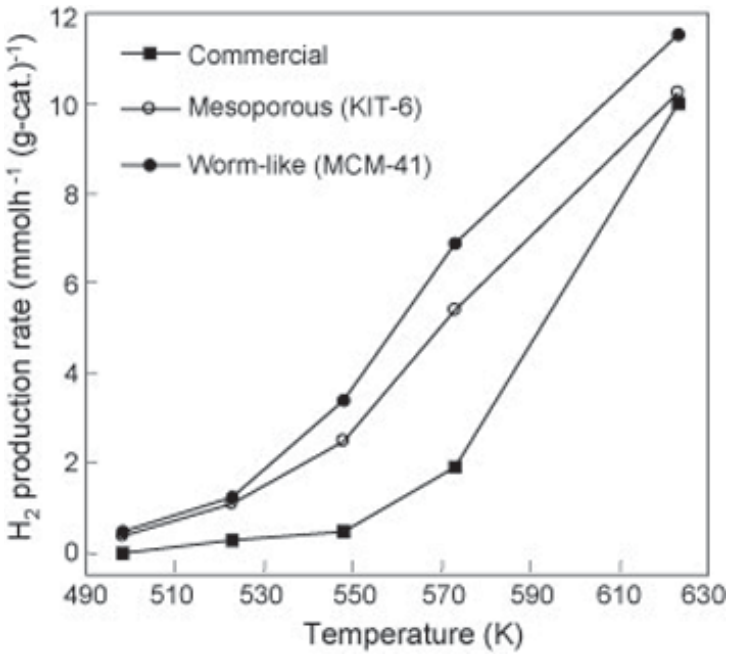

Fig. 2.3: Hydrogen production rate in the steam reforming conversion of ethyl alcohol over In_2O_3 catalysts[23]. Reprinted with permission from Reference 23, T. Umegaki, K. Kuratani, Y. Yamada, A. Ueda, N. Kuriyama, T. Kobayashi and Q. Xu, Journal of Power Sources **179** 566 (2008). © 2008, Elsevier

2.2.3. Hydrogen from biomass

Biomass, a generic term for biological materials derived from living, or recently living organisms such as forest residues, animal matter and remains of commercial crop is a renewable energy source. Chemically, biomass is carbon-based and is composed of a mixture of organic molecules containing other atoms including hydrogen. Traditionally, biomass has been utilized through direct combustion and this process is still widely used in many parts of the world. Energy from biomass fuels is used in the electric utility, lumber and wood products and pulp and paper industries. Currently, much research has been focused on sustainable and environmental friendly energy from biomass to replace conventional fossil fuels[9].

Because of the progressive depletion of conventional fossil fuels, in recent years, the utilization of biomass energy as a renewable energy source has gained particular interest[24]. The growing interest is driven by the facts including the following[25]: (1) it contributes to poverty reduction in developing countries, (2) it meets energy needs at all times, without expensive conversion devices, (3) it can deliver energy in all forms that people need (liquid and gaseous fuels, heat and electricity), (4) it is CO_2-neutral and can even act as carbon sinks and (5) it helps to restore unproductive and degraded lands, increasing biodiversity, soil fertility and water retention. Importance of biomass will increase as national energy policy and strategy focuses more heavily on renewable sources and conservation. Among other utilization of biomass, hydrogen production is considered as a very important one. Comparing to other pathways of hydrogen production, that from biomass is competitive in several ways[26]: (1) independence from

oil imports, (2) net product remains within the country, (3) stable pricing level, (4) the CO_2 balance can be improved by around 30%.

The current methods of hydrogen production from biomass can be divided into two main categories as shown in Fig. 2.4: thermochemical and biological routes. Thermochemical conversion processes such as pyrolysis, gasification, steam gasification, steam reforming of bio-oils and supercritical water gasification directly use biorenewable feedstocks to produce hydrogen[27]. Biological production of hydrogen can be classified into biophotolysis of water using green algae and blue-green algae (cyanobacteria), photo-fermentation, dark-fermentation and hybrid reactor system[30].

Gasification of biomass generally follows the reaction:

$$\text{Biomass} + O_2 \text{ (or } H_2O) \rightarrow CO, CO_2, H_2O, H_2, CH_4 + \text{other CHs} + \text{tar} + \text{char} + \text{ash} \quad (9)$$

This reaction is within a thermal treatment, which results in a high production of gaseous products and small quantities of char and ash. Combustion is involved in the gasification process to provide heat for the endothermic pyrolysis reactions[28]. The resulting gas after the high temperature process is a mixture of carbon monoxide, hydrogen and methane, with carbon dioxide and nitrogen, known as producer gas altogether[29]. After further processing including the tar distilling, possible products obtained from the whole gasification process are exhibited in Fig. 2.5. The commonly used route of biomass gasification is, firstly, to thermochemically decompose the cellulose, hemicelluloses and lignin compounds with production of char and volatiles and then to react until equilibrium while further gasifying the produced char[9].

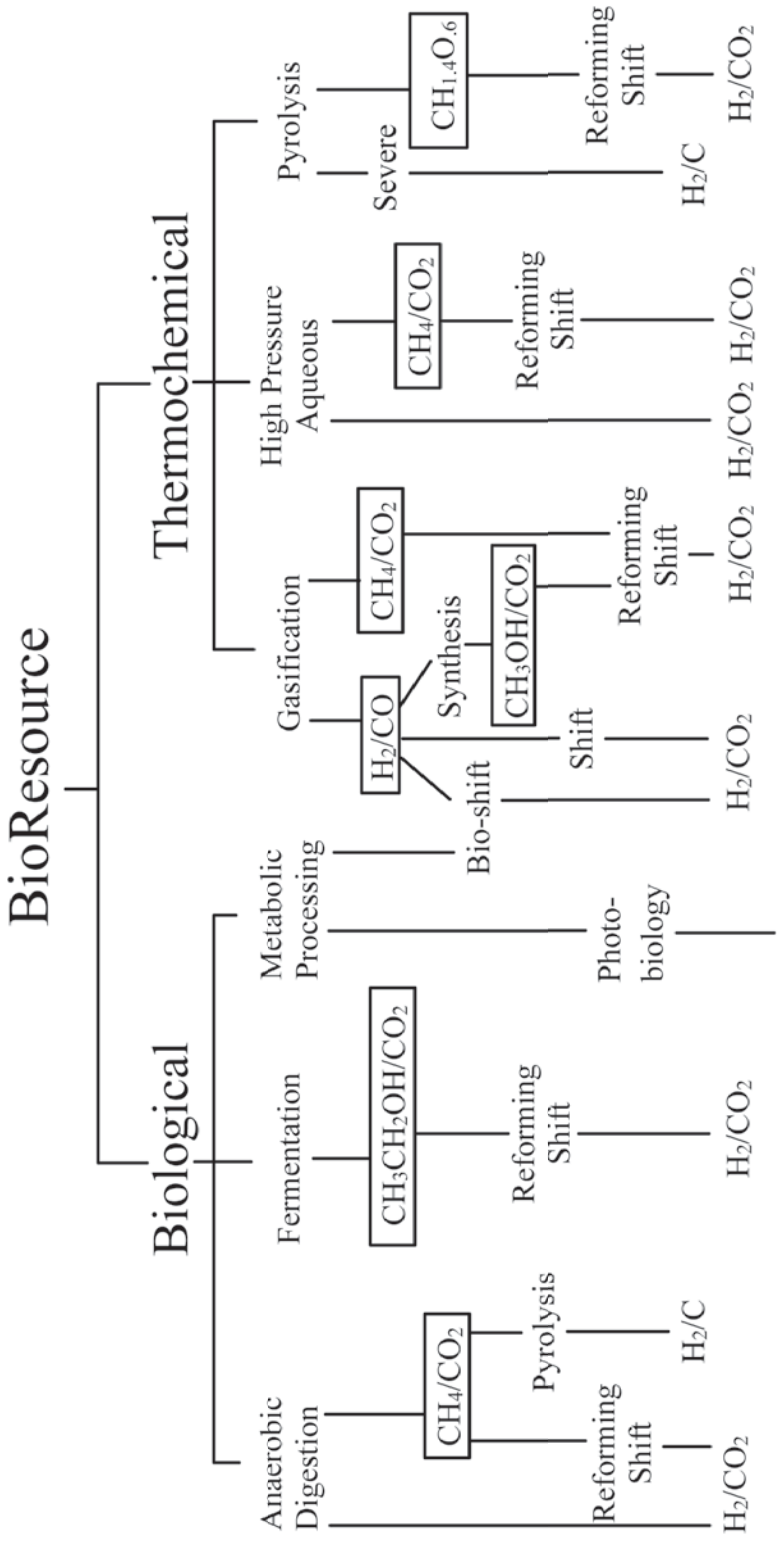

Fig. 2.4: Possible pathways from biomass to hydrogen.

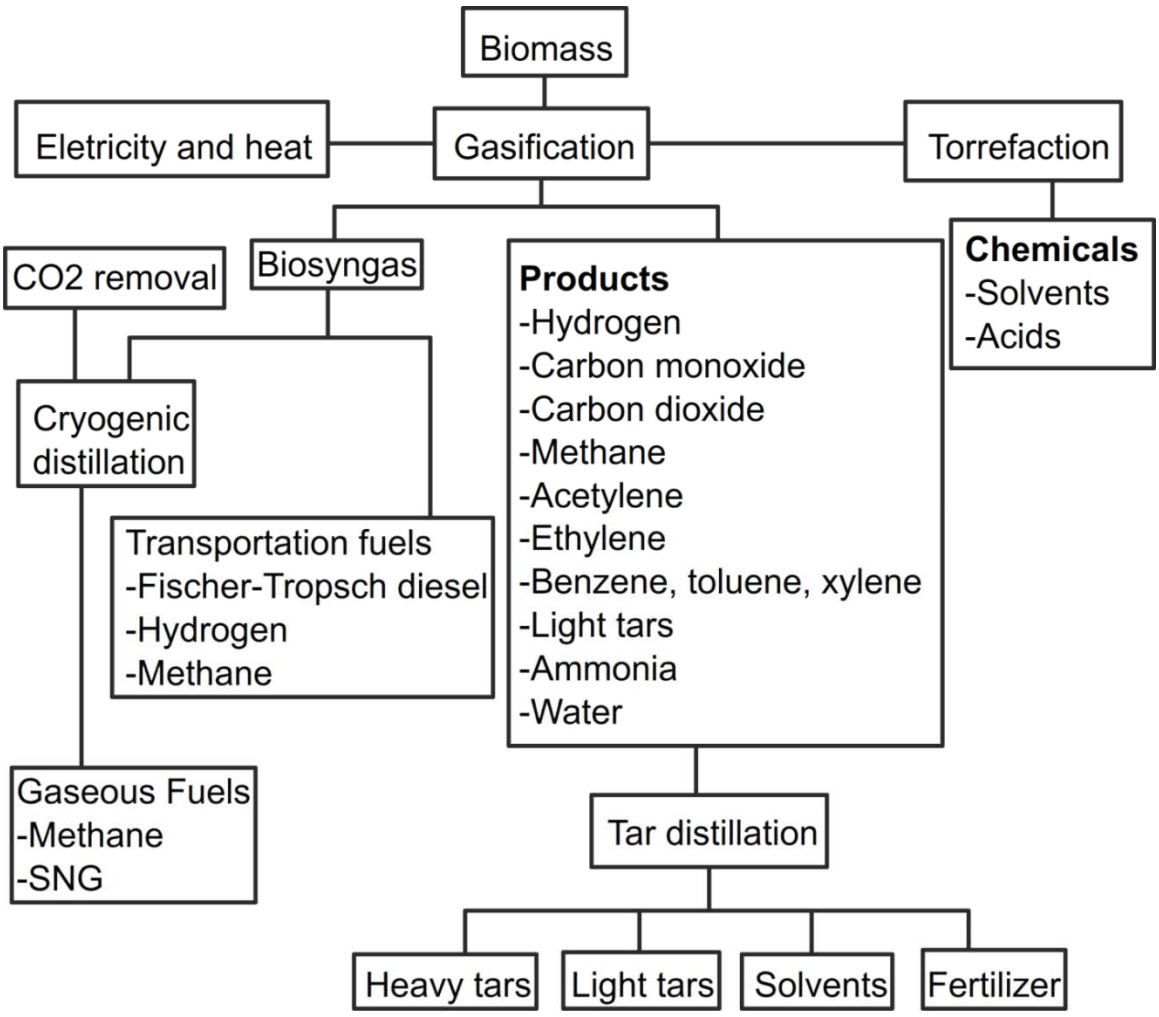

Fig. 2.5: Resulting products from gasification process.

Having been identified as a possible system for producing renewable hydrogen, biomass gasification is beneficial to exploit biomass resources, to develop a highly efficient clean way for large-scale hydrogen production and has less dependence oninsecure fossil energy sources[30]. Compared to hydrogen production from fossil fuels, the whole process would be much more renewable if the hydrogen source is biomass. However, since the hydrogen generated is still from hydrocarbons, carbon will be released, usually in the form of carbon dioxide. Although more slowly than the pace by the current direct hydrocarbon combustion, hydrogen production from hydrocarbons will still intensify global warming.

2.2.4. Applications of nanotechnology applied in hydrogen production from biomass

Nanomaterials, usually in the form of catalysts, are broadly used in the production of hydrogen from biomass. Nano-Ni-La-Fe/γ-Al_2O_3, a supported trimetallic catalyst for tar removal in biomass steam gasification, is developed to enhance the quality of the produced gas[31]. To obtain the desired nanostructure of the catalyst, a precursor of the trimetallic nano-Ni-La-Fe catalytst is incorporated into the porous γ-Al_2O_3 support substrate with deposition precipitation method. The precursor is prepared from a homogeneous aqueous solution originally prepared from $Ni(NO_3)_2{\cdot}6H_2O$, $La(NO_3)_3{\cdot}6H_2O$, $Fe(NO_3)_3{\cdot}9H_2O$ and $CO(NH_2)_2$. Among these, $CO(NH_2)_2$ functions as a homogeneous precipitation agent to enable a gradual and homogeneous basification of the solution with the increasing temperature to avoid local high pH, which resulted in the subsequent and homogeneous precipitation of nickel precursor in solution. The homogeneous solution is then transferred onto the γ-Al_2O_3 supports, sealed and finished

deposition-precipitation through oil bath heating. After the precipitation of the precursor is formed on γ-Al_2O_3 supports, cooling, filtering and washing processes were performed. Then the final structure of nano-Ni-La-Fe/γ-Al_2O_3 is completed with a calcination process in a muffle furnace at 550°C for 1 h in air atmosphere. The whole surface of the supported trimetallic catalyst and nanoparticles on it were respectively characterized by SEM and TEM analysis and presented in Fig. 2.6[31].

The activity and the performance of the nanostructured trimetallic catalyst in the application of biomass gasification are evaluated by comparing the cases. The tar yield after adding catalyst was reduced significantly, with the tar removal efficiency reaching 99% for catalytic gasification at 800°C, while the gas yield markedly increased with adding catalyst. The percentages of C_2 and CH_4 in the product gas after catalysis were obviously reduced, while that of the valuable H_2 increased markedly to over 10 vol% due to catalysis.

Another similarly structured catalyst, nano-NiO/γ-Al_2O_3, is also proven to be useful for the hydrogen production from biomass gasification. The experiments carried out by Wuhan Polytechnic University, PR China[32], demonstrated that their newly developed nano-NiO/γ-Al_2O_3 catalyst in rice husk biomass air–steam gasification gave a promising 99% tar removal rate at 800 °C while the overall gas yield increased remarkably. Also, due to the presence of catalysts, the percentage of H_2 in the product gas was obviously enhanced over 10 vol%. All this evidence supports that using the prepared nano-NiO/γ-Al_2O_3 catalyst in biomass gasification can significantly improve the quality of the produced gas and meanwhile eliminate efficiently the tar generation. The same group also tested the same nano-NiO/γ-Al_2O_3 on the biomass of palm oil waste instead of rice husk and led to the same conclusion that nano-NiO/γ-Al_2O_3 catalyst, with extremely small particle size, contributed greatly in both the gas quality and the yield[33].

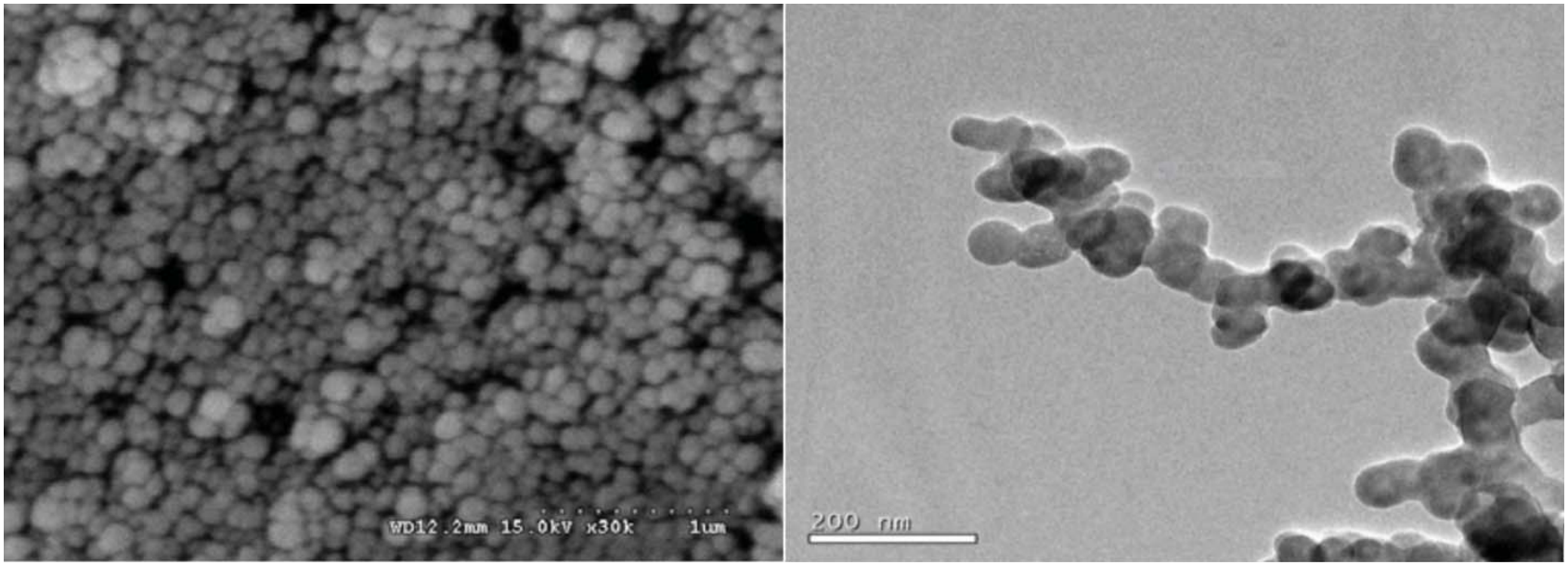

Fig. 2.6: SEM image of the supported trimetallic catalyst surface (left) and TEM micrograph of nanoparticles on the trimetallic catalyst surface (right)[31]. Reprinted with permission from Reference 31, J. Li, BioResources **4** 1520 (2009). © 2008, BioResources.

2.3. Hydrogen production by direct water splitting

Theoretically, the most promising route for hydrogen production is through water splitting. Since the resultant of hydrogen consumption is always H_2O, the complete reaction from the production of hydrogen to the consumption of it would be a perfect cycle if H_2O is also the initial hydrogen source. Such a simplified cycle would be both beneficial to the environment and economical for the intermediate processes.

To split water and release hydrogen, different energy sources were studied. For example, electrolysis of water is an easy way to produce hydrogen. However, the transformation of energy from electricity to hydrogen is not efficient and electricity itself is not an ultimate energy source in nature. Thermolysis of water is the thermal decomposition of water at very high temperature. It uses heat as the energy source. For water alone, the temperature required (2000°C~3000°C) is too high for any practical use, but catalysts can accelerate the dissociation of the water molecules at lower temperatures. Photoelectrochemical water splitting is considered a very promising method among them all, because it revealed the possibility of generating hydrogen through solar energy, the stable and almost incessant energy source. Some recent studies focused on the combination of different types of water splitting methods. It is extrapolated that a 10% efficiency of thermal photocatalytic generation of H_2 could be achieved at approximately 400°C in high pressure vessel with the help of catalysts[34] . These three major methods of water splitting will be discussed in detail in the following sections.

2.3.1. Thermolysis and thermochemical decomposition of water

Thermal decomposition, also called thermolysis, is defined as a chemical reaction in which a compound breaks up into at least two other substances when heated. The

reaction is usually endothermic as heat is required to break chemical bonds in the compound undergoing decomposition. The decomposition temperature of a substance is the temperature at which the substance decomposes into smaller substances or into its constituent atoms.

In this review, thermolysis mainly refers to the thermal decomposition of water. Even without the assistance of any specific technology, when heated to a high enough temperature, water will break up into hydrogen and oxygen. By separating the equilibrium mixture of these two generated gases, the desired pure hydrogen can be obtained.

The net reaction

$$H_2O \rightarrow H_2 + 1/2O_2 \quad (10)$$

produces only hydrogen and oxygen.

However, thermodynamically, the Gibbs function (ΔG, or free energy) of the aforementioned water decomposition does not become zero until the temperature is increased to about 4700 K[35] (detailed temperature varies with condition parameters); sometimes it is considered about 4300K as shown in Fig. 2.7[36]. Although the theoretically thermodynamic balance is not a prerequisite condition of hydrogen evolution, a temperature of at least 2100°C must be maintained in the reactor to make the process economically feasible[37]. And to maintain such a high in-reactor temperature, the inner structural component of the reactor should at least resist a temperature of 2300°C. It makes the selection of reactor materials and the separations of the two gases extremely difficult. Even at about 2200°C, most nonoxide refractory materials are already

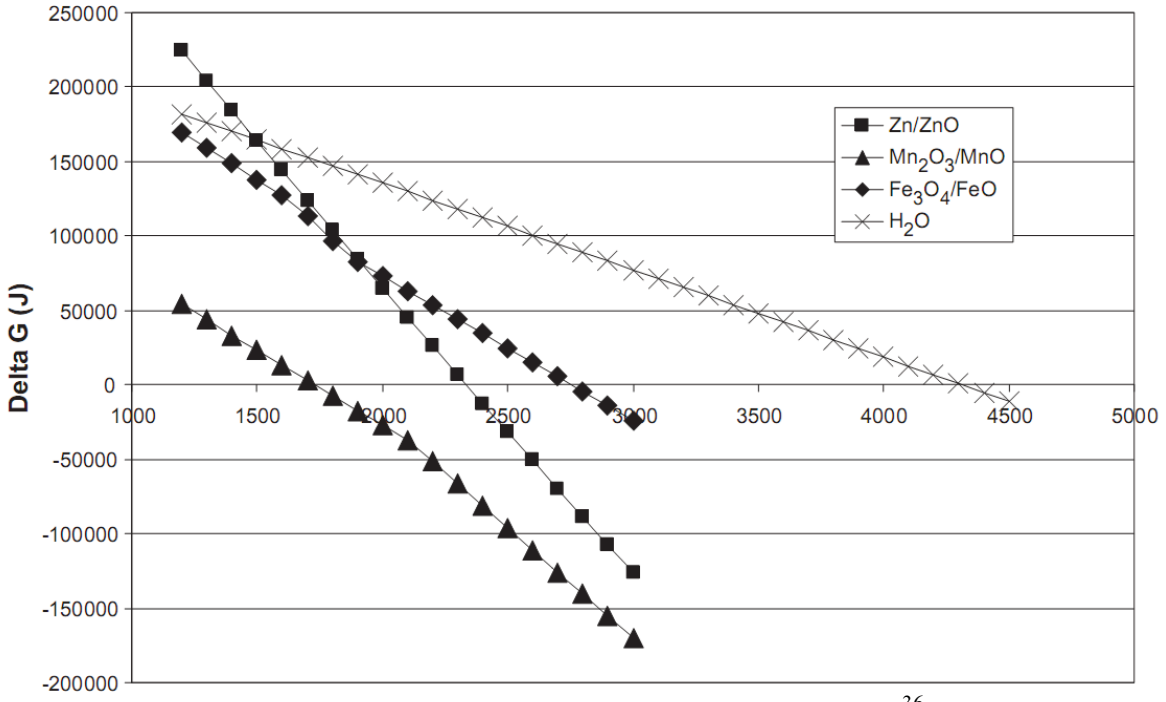

Fig. 2.7: Gibbs energy change of reaction for decomposition reactions[36]. Reprinted with permission from Reference 36, C. Perkins and A. W. Weimer, Int. J. Hydrogen Energy **29** 1587 (2004). © 2004, Elsevier.

unstable and H_2 is expected to have a reactive effect on oxides at these extremely high temperature[38]. Besides, the consumption of energy in the process increases dramatically with the required temperature because of the huge radiation losses at such temperatures.

All these problems make the feasibility of direct water thermolysis challenging. As a result, in practical experiments, the thermal decomposition of water for hydrogen production usually involves more than one step of chemical reactions instead of direct thermolysis. Such a process is termed a "thermochemical water splitting cycle" and the function of chemical reactants within the cycle can be considered as that of catalysts.

In these cycles, the decomposition temperature requirement is represented by that of the endothermic "high-temperature step", which is followed by one or more exothermic "low-temperature" reaction steps. The temperature requirement in the "high-temperature step" (700°C-2000°C)[39] is considerably lower than in direct thermal water splitting. Sometimes it can be decreased to a degree that is low enough for the usage of solar energy, providing a promising route of converting solar power into hydrogen energy. At the same time, the previously mentioned difficulties on energy losses and reactor materials under high temperature are largely reduced, giving a higher efficiency and a wider range of material selection. Also, the gas separation of hydrogen and oxygen can be done at a relatively lower temperature, thus being easier and less dangerous.

The concerns within the evaluation and selection of these cycles include energy losses between each process step in transferring, the overall chemical process complexity and, if using solar energy, the heat of reaction for the solar step. It is ideal to have cycles with opportunities for energy recovery, simple and few-step process designs and low operating temperature. Meanwhile, it is also crucially important that all the chemical reagents other than water in the cycles are supposed to be completely regenerated and recycled within each cycle, otherwise the major advantage of thermolysis, i.e. water being the only net reactant, would be nullified and the sustainability and renewability would be undermined.

More than 400 cycles were considered possible for thermochemical hydrogen evaluation by the U.S. Department of Energy. Among this large pool, researchers evaluated and chose nine technically and practically feasible candidates[39]. They are broadly cataloged into "high temperature" and "low temperature" cycles in Table 2.1[36].

Table 2.1: Thermochemical water splitting cycles. Reprinted with permission from Reference 39, C. Perkins and A. W. Weimer, AIChE Journal **55**, 286 (2009). © 2009, American Institute of Chemical Engineers.

Cycle	Reaction Steps
High Temperature Cycles	
Zn/ZnO	$ZnO \xrightarrow{1600\text{-}1800^\circ C} Zn + 1/2O_2$ $Zn + H_2O \xrightarrow{400^\circ C} ZnO + H_2$
FeO/Fe_3O_4	$Fe_3O_4 \xrightarrow{2000\text{-}2300^\circ C} 3FeO + 1/2O_2$ $3FeO + H_2O \xrightarrow{400^\circ C} Fe_3O_4 + H_2$
Cadmium carbonate	$CdO \xrightarrow{1450\text{-}1500^\circ C} Cd + 1/2O_2$ $Cd + H_2O + CO_2 \xrightarrow{350^\circ C} CdCO_3 + H_2$ $CdCO_3 \xrightarrow{500^\circ C} CO_2 + CdO$
Hybrid cadmium	$CdO \xrightarrow{1450\text{-}1500^\circ C} Cd + 1/2O_2$ $Cd + 2H_2O \xrightarrow{25^\circ C,\text{electrochemical}} Cd(OH)_2 + H_2$ $Cd(OH)_2 \xrightarrow{375^\circ C} CdO + H_2O$
Sodium manganese	$Mn_2O_3 \xrightarrow{1400\text{-}1600^\circ C} 2MnO + 1/2O_2$ $2MnO + 2NaOH \xrightarrow{627^\circ C} 2NaMnO_2 + H_2$ $2NaMnO_2 + H_2O \xrightarrow{25^\circ C} Mn_2O_3 + 2NaOH$
M-Ferrite (*M* = Co, Ni, Zn)	$Fe_{3-x}M_xO_4 \xrightarrow{1200\text{-}1400^\circ C} Fe_{3-x}M_xO_{4-\delta} + \delta/2O_2$ $Fe_{3-x}M_xO_{4-\delta} + \delta H_2O \xrightarrow{1000\text{-}1200^\circ C} Fe_{3-x}M_xO_4 + \delta H_2$
Low Temperature Cycles	
Sulfur-Iodine	$H_2SO_4 \xrightarrow{850^\circ C} SO_2 + H_2O + 1/2O_2$ $I_2 + SO_2 + 2H_2O \xrightarrow{100^\circ C} 2HI + H_2SO_4$ $2HI \xrightarrow{300^\circ C} I_2 + H_2$
Hybrid sulfur	$H_2SO_4 \xrightarrow{850^\circ C} SO_2 + H_2O + 1/2O_2$ $SO_2 + 2H_2O \xrightarrow{77^\circ C,\text{electrochemical}} H_2SO_4 + H_2$
Hybrid copper chloride	$Cu_2OCl_2 \xrightarrow{550^\circ C} 2CuCl + 1/2O_2$ $2Cu + 2HCl \xrightarrow{425^\circ C} H_2 + 2CuCl$ $4CuCl \xrightarrow{25^\circ C,\text{electrochemical}} 2Cu + 2CuCl_2$ $2CuCl_2 + H_2O \xrightarrow{325^\circ C} Cu_2OCl_2 + 2HCl$

In this table, all the high temperature cycles utilize the oxidation of a metal or metal oxide with water as the hydrogen release step and the reduction of the corresponding metal oxide as the major energy converting step, which could be done with solar energy or nuclear energy. Two intensely studied cycles as the representatives of them are those of Zn/ZnO and FeO/Fe_3O_4 [40, 41]. Their advantages include: (1) They have only two steps, making the energy losses between steps minimized and the whole procedure relatively simple; (2) Hydrogen and oxygen are obtained in separate steps, leaving little hazard of explosion from their mixture; (3) Clear-cut circulation of steps requiring and not requiring solar energy makes both day-time with sunlight and night-time without sunlight well used.

Those low temperature cycles are slightly more complicated chemically. Their endothermic steps are quite similar with the energy converting steps of high temperature cycles, though usually more complex catalytic or electrolytic chemicals are used rather than those of high temperature cycles. However, at the cost of the greatly reduced operation temperature, these cycles involve more steps therefore more potential energy losses and much more processing complexity. Besides, more gas phase intermediate products other than hydrogen and oxygen within the cycles make the procedure more dangerous, resulting in the preference of indirect solar absorption heating other than directly concentrated sun light.

2.3.2. Nanotechnology applied in thermolysis and thermochemical decomposition of water

For both thermochemical decomposition of water and direct thermolysis, separation of different gases has been an important research focus. Especially in direct thermolysis and

high temperature cycles, the separation of hydrogen and oxygen at that high temperature (T>2500K) is the most severe problem. If the separation is not done properly, the two gases may recombine into water again, or form a very explosive mixture when the temperature is lowered.

To overcome this problem, porous ceramic membranes are developed. Material selection for the porous membranes is quite limited because of the high temperature and, sometimes, high pressure. Zirconia is frequently used due to both its high melting temperature to withstand the harsh condition in the reactor and its excellent hydrogen permeability. However, even though the melting temperature (2715°C) of zirconia is much higher than the basic working temperature, the sintering temperature (1800°C) is remarkably lower. Continuous operation in this environment results in an equivalent effect as continuous sintering, i.e. closure of pores and loss of permeability.

To overcome this problem, much research has been done and technologies have been used. Researchers in the Weizmann Institute of Science, Israel[43], used sol-gel method for preparing homogeneous powders of relatively large spherical zirconia particles, which lowered by 200 °C of the equivalent sintering temperature of the membrane made from it. More specifically, a sample made from sol-gel processed zirconia powders with diameter $d \geqslant 50$ μm emerged from the heat treatment at 1900°C/1.5 h+1980°C/1.5 h with almost unchanged open porosity (OP ~35%) while other samples made from smaller particles were completely destroyed at this temperature (Fig. 2.8[43]) Their attempts are partially successful in bridging the gap between the normal sintering temperature of stabilized zirconia and the reactor operating temperature.

In comparison to direct thermolysis, nanotechnology played an even more

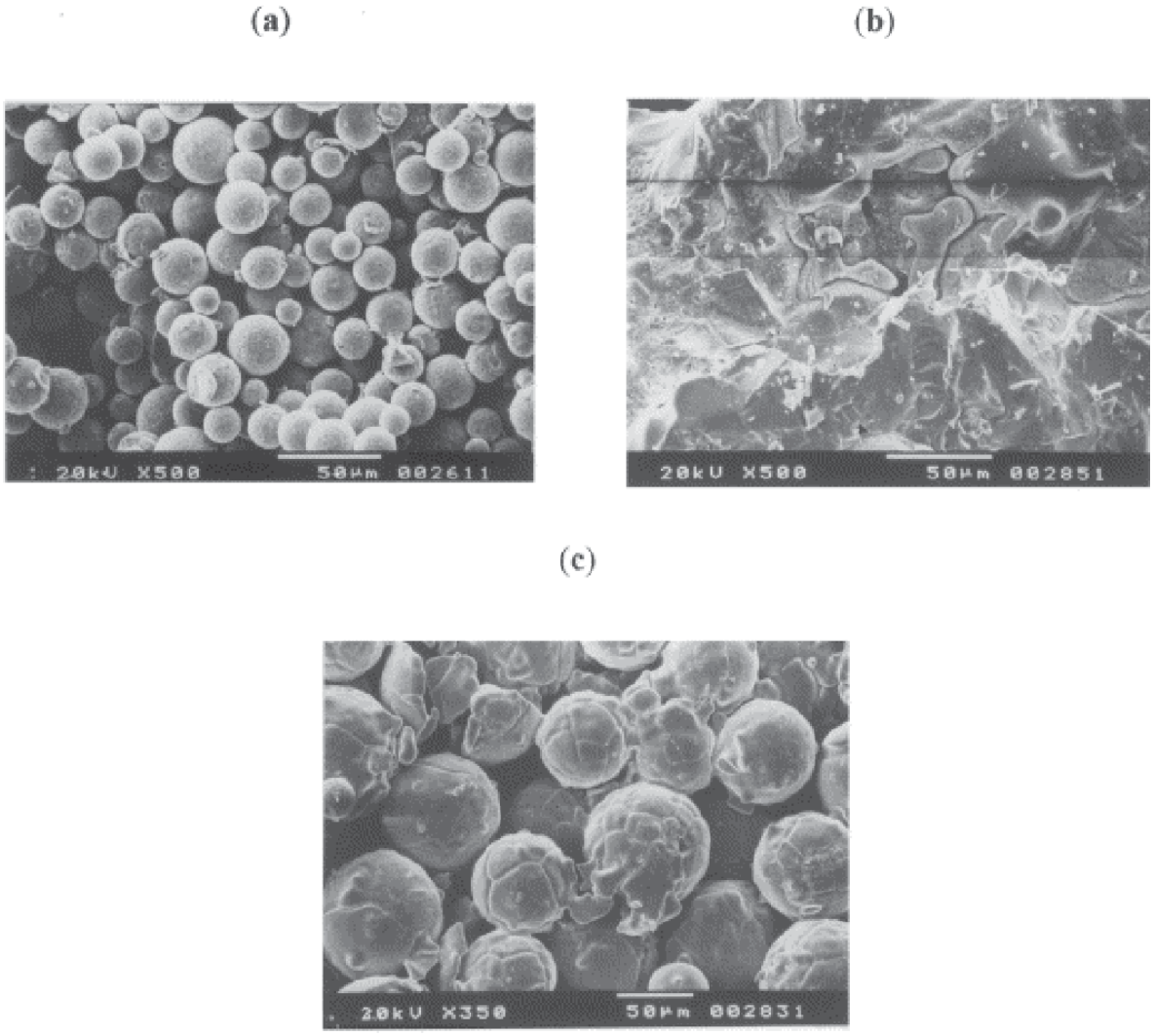

Fig. 2.8: Membrane from Sol–Gel powder. (a) $d \leqslant 25$ µm particles, 1750°C/5 h heating. (b) $d \leqslant 25$ µm, 1750°C/5 h+1900°C/1.5 h+1980°C/1.5 h heating. (c) $d \geqslant 50$ µm, 1750°C/5 h+1900°C/1.5 h+1980°C/1.5 h heating.[43] Reprinted with permission from Reference 43, A. Kogan, Int. J. Hydrogen Energy **25** 1043 (2000). © 2000, Elsevier.

significant role in thermochemical water decomposition cycles. The nature of nanostructure can be expected to be very useful for the catalytic materials in both high and low temperature cycles. Researchers in the Swiss Federal Institute of Technology, Zurich[44] explored the use of Zn-nanoparticles in the production of solar hydrogen via the Zn/ZnO water-splitting thermochemical cycle. Their novel reactor concept for hydrogen production by hydrolysis of Zn features three temperature controlled zones that can

overpap: a Zn nanoparticle-H_2O(g) mixing zone, a Zn-nanoparticle formation by steam-quenching zone and a Zn(g)–H_2O reaction zone, as shown in Fig. 2.9[44].

To achieve this concept, they designed a prototype laboratory-scale reactor consisting of a 100 cm length, 5.25 cm i.d. Inconel tube placed inside a concentric cylindrical furnace. A ceramic crucible containing molten zinc is located in the center of the heated region. Inert carrier gas is discharged into this Zn-evaporation zone above the melt through a 2.2 mm i.d. tube that is supported by a stainless steel flange. The flange closes the feed side of the reactor and has a port with a pressure transducer. A stainless

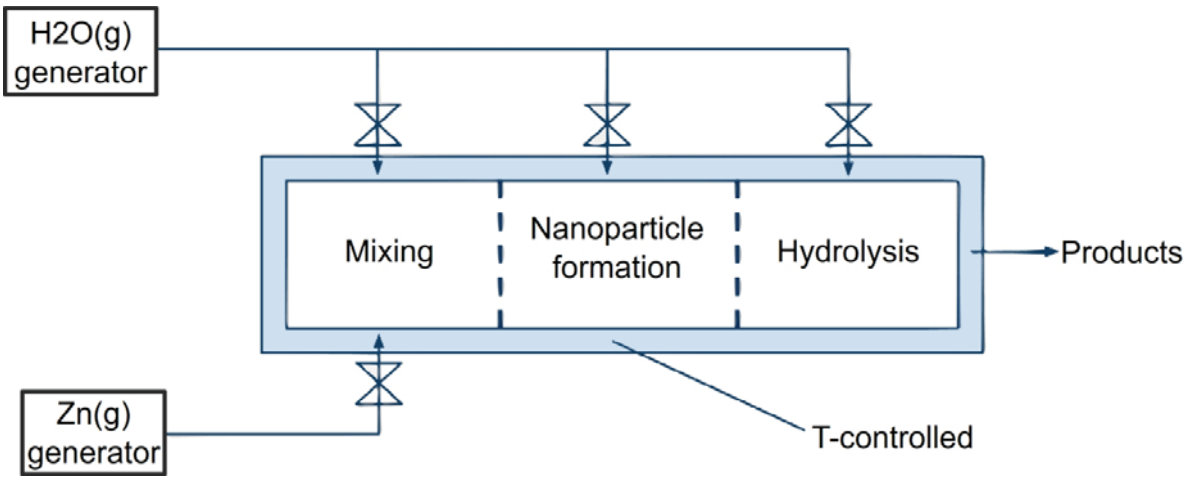

Fig. 2.9: Schematic of the aerosol reactor concept featuring three temperature-controlled zones for mixing, nanoparticle formation and hydrolysis reaction[44]. Reprinted with permission from Reference 44, K. Wegner, H. C. Ly, R. J. Weiss, S. E. Pratsinis and A. Steinfeld, Int. J. Hydrogen Energy **31** 55 (2006). © 2006, Elsevier.

steel lance consisting of a 1.65 cm i.d. centre tube and a 4.8 cm o.d. annulus is positioned right after the ceramic crucible and serves as the 3-zone reactor for mixing, nanoparticle formation and hydrolysis reaction. In this design, the nanoparticle formation and reaction zones overlap. Steam, pure or diluted with an inert gas, is introduced in counter-flow to the Zn-laden carrier gas through an array of 12 equally-sized nozzles of 2.5 mm inner diameter, uniformly arranged over the annulus at the front side of the lance. A stainless steel gas-return cap guides the steam perpendicularly to the Zn-laden carrier gas stream coming from the evaporation zone, thus forming a T-ring-mixer. The $Zn(g)–H_2O(g)$ mixture flows with the aid of a vacuum pump through the center tube of the lance where quenching, nanoparticle/nanodroplet formation and hydrolysis reaction takes place[44]. The schematics are shown in Fig. 2.10.

The advantages of using nanoparticles in the cycle include: (1) high specific surface area augmenting the reaction kinetics, heat transfer and mass transfer; (2) high completeness of oxidation due to large surface-to-volume ratio; (3) easy forming of fine entrainment which smoothes the flow of processing.

Inspired by the use of Zn-nanoparticles, other nanoparticles also are studied to be utilized in the cycles of thermochemical decomposition. Researchers in the Processes, Materials and Solar Energy laboratory, France[2] developed a similar process based on the SnO_2/SnO water-splitting cycle. After the thermal reduction occurs under atmospheric pressure at about 1600 °C, SnO nanoparticles are hydrolysed efficiently in the temperature range 500–600 °C and achieved a H_2 yield over 90%.

Solar reduction step: $SnO_{2\,(s)} \rightarrow SnO(g)+1/2O_2$ (endothermic, 1600°C) (11)

Hydrolysis step: $SnO(s)+H_2O(g) \rightarrow SnO_{2\,(s)}+H_2$ (exothermic, 550°C) (12)

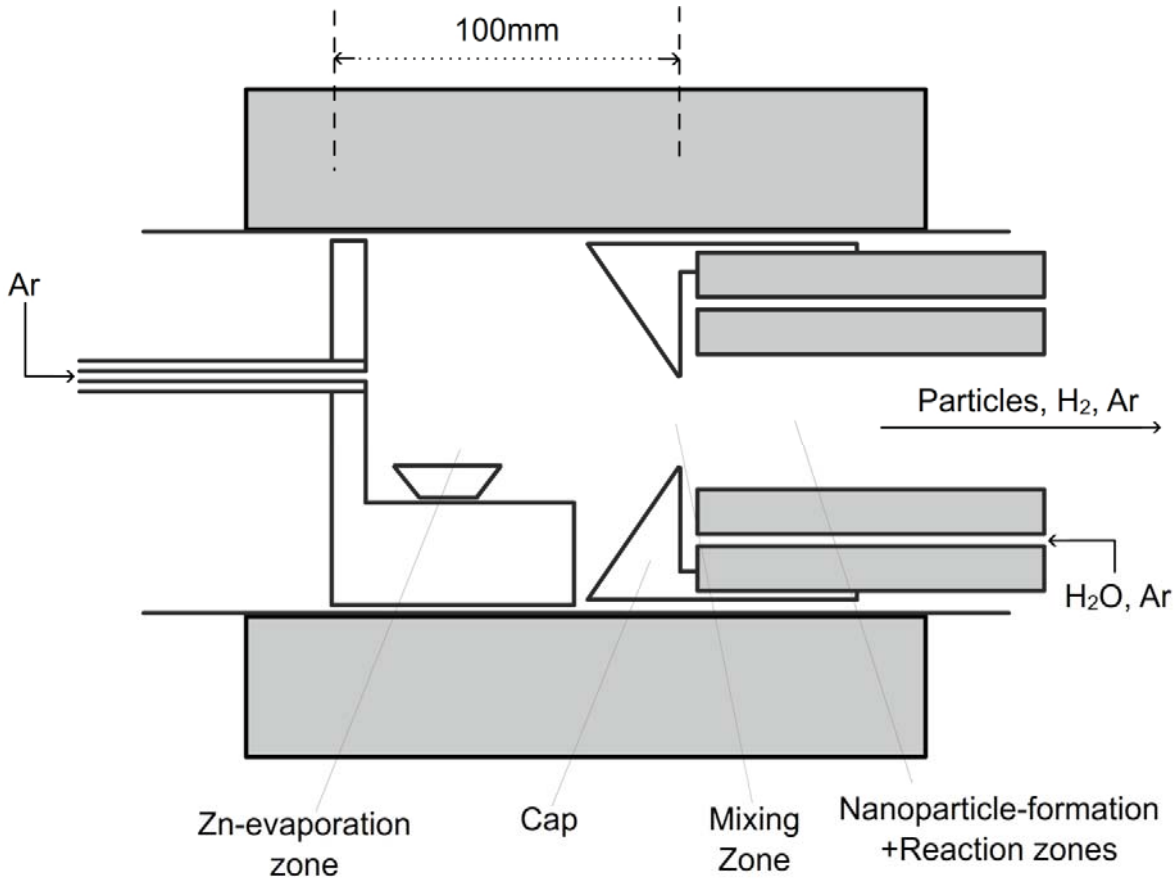

Fig. 2.10: Scheme of the prototype laboratory-scale reactor for the formation of Zn-nanoparticles and their in situ hydrolysis[44]. Reprinted with permission from Reference 44, K. Wegner, H. C. Ly, R. J. Weiss, S. E. Pratsinis and A. Steinfeld, Int. J. Hydrogen Energy **31** 55 (2006). © 2006, Elsevier.

Their experimental set-up can be seen in Fig. 2.11[45]:

2.3.3. Direct electrolysis of water

Electrolysis of water to produce hydrogen is a comparatively simple and efficient way among most methods. It already has a history of more than 200 years[46]. Around 4% of hydrogen gas produced worldwide is still created by electrolysis. Besides its efficiency and fitness for onsite application, the byproduct of the electrolysis, heavy water, is a very useful substance used in nuclear application. However, although there are so many obvious advantages of generating hydrogen by the electrolysis of water, its vulnerability cannot be overlooked: the energy used in electrolysis, i.e. electrical energy, is a secondary energy itself. By merely converting electrical energy into hydrogen energy, the overall usable energy is at the best in a balance. Unless combined with other renewable energy techniques, hydrogen evolved by electrolysis could not play a very important role in solving energy crisis. Fortunately, such attempts of combination are already done by some researchers, with renewable energies like wind energy, making the electrolysis of water again a promising candidate for hydrogen production.

The net reaction of the electrolysis of water can be simply written as[47]:

$$2H_2O(\text{liquid/vapor}) + \text{electrical energy} \rightarrow 2H_{2\,(}g) + O_{2\,(}g) \qquad (13)$$

Its half reaction can be balanced in two ways:

With acid:

$$\text{Cathode (reduction): } 2\,H^+(aq) + 2e^- \rightarrow H_{2\,(}g) \qquad (14)$$

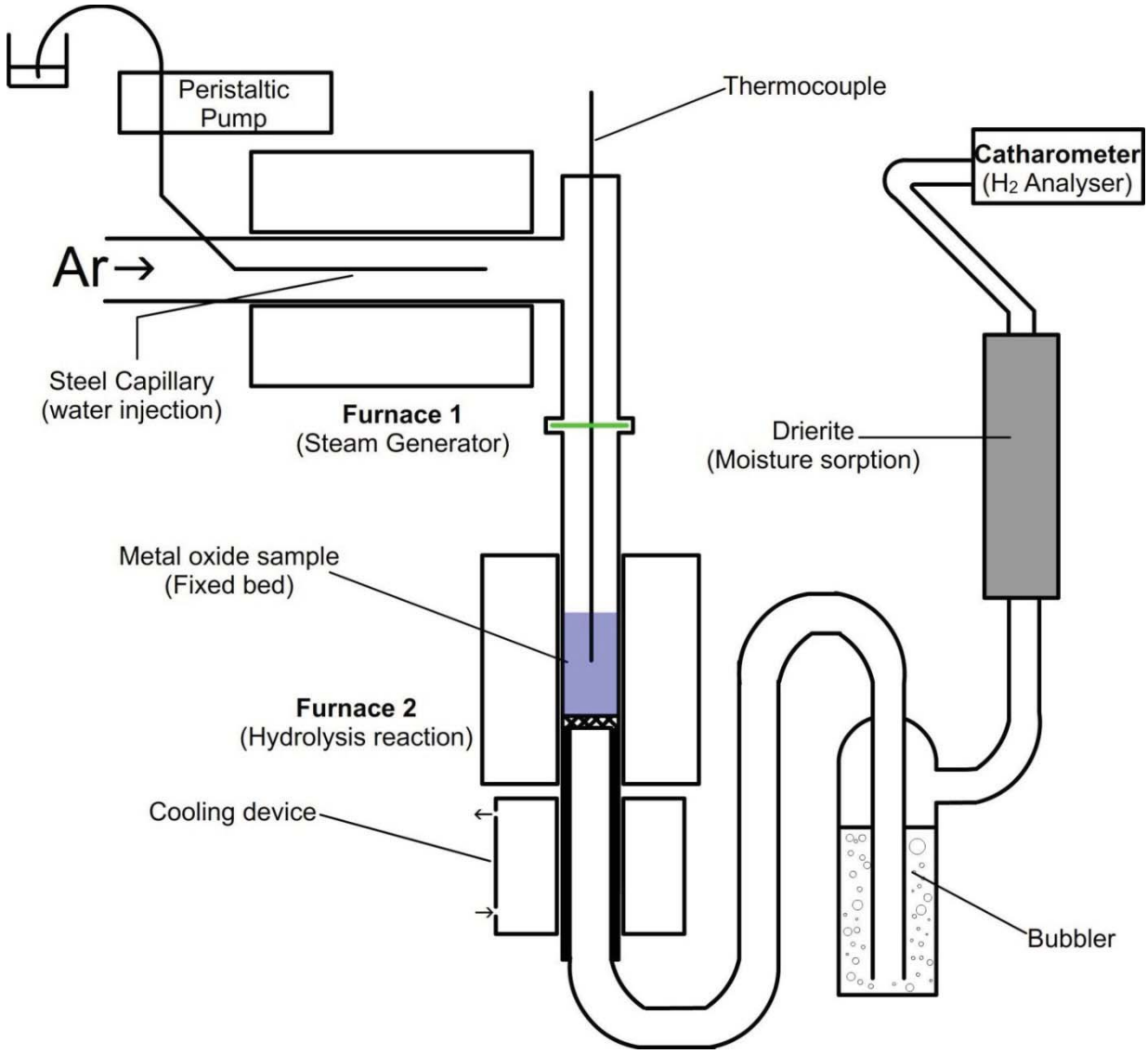

Fig. 2.11: Experimental set-up for the production of hydrogen from hydrolysis of SnO nanoparticles[45]. Reprinted with permission from Reference 45, S. Abanades, P. Charvin, F. Lemont and G. Flamant, Int. J. Hydrogen Energy **33** 6021 (2008). © 2008, Elsevier.

Anode (oxidation): $2\ H_2O(l) \rightarrow O_{2\ (}g) + 4\ H^+(aq) + 4e^-$ (15)

With base:

Cathode (reduction): $2\ H_2O(l) + 2e^- \rightarrow H_{2\ (}g) + 2\ OH^-(aq)$ (16)

Anode (oxidation): $4\ OH^-(aq) \rightarrow O_{2\ (}g) + 2\ H_2O(l) + 4\ e^-$ (17)

The standard potential of electrolyzing pure water into hydrogen can be calculated thermodynamically. At 1 bar and 25 °C, the Gibbs free energy ΔG of the water splitting reaction is 237.178kJ/mol[48]. From chemical kinetics, the thermodynamic reversible potential[49]

$E = V_{rev} = \Delta G/nF = 1.23V$ (18)

where n is the moles of electrons and F is the Faraday constant.

At this voltage, the reaction is endothermic because of the change of entropy ΔS. Taking the thermal factor into account, when no heat is absorbed or generated, the electrical energy is equal to the enthalpy $\Delta H = \Delta G + T\Delta S = 285.83KJ/mol$ at standard condition. Therefore, the thermoneutral voltage can be calculated as

$V_{tn} = \Delta H/nF = 1.48\ V$ (19)

Although it is possible to electrolyze pure water directly, the process will be very slow due to the low overall conductivity caused by low autoionization of pure water. One way to overcome this difficulty is to largely increase the potential applied, but it will be very energy inefficient. It is more widely used to add a water-soluble electrolyte into the water to be electrolyzed to increase its conductivity.

There are some basic rules which need to be followed in choosing an electrolyte when the desired product is hydrogen. Because a cation from the electrolyte is in competition with the hydroxide ions to obtain an electron, a cation with a greater standard electrode potential than a hydrogen ion will be reduced in its stead and no hydrogen gas will be produced. Similarly, if the electrolyte anion is with less standard electrode potential than hydroxide, oxygen gas will not be generated and the water-splitting process will not be complete.

Cations with lower electrode potential than H^+ and can therefore be used include Li^+, Rb^+, K^+,Cs^+, Ba^{2+}, Sr^{2+}, Ca^{2+}, Na^+ and Mg^{2+}. Acid could also be used because the added cation is H^+ itself. Anion is often chosen as sulfate (SO_2, SO_3, SO_4) or simply as hydroxide to form strong bases like sodium hydroxide and potassium hydroxide. Nowadays, more new types of electrolyte such as solid polymer electrolyte functioning with Nafion[50] are introduced into application.

The electricity used in the electrolysis for hydrogen production could be generated from energy resources including nuclear, wind, solar and bioenergy. Among these resources, solar, especially solar photovoltaic energy[51], possesses many special attributes and is the only renewable resource which could actually meet the predicted demand of the middle of this century[52] (with nuclear energy being the only nonrenewable resource).

2.3.4. Nanotechnology applied in direct electrolysis of water

As a long-history hydrogen production method, electrolysis itself was continuously developing and adapting new techniques such as Hofmann voltammeter, high pressure electrolysis, high temperature electrolysis and so on. More recently, with the booming of advanced nanotechnology, nanotechniques are also widely applied in electrolysis of water.

Researchers in the Gwangju Institute of Science and Technology, Republic of Korea, fabricated Ni nanopottery structure using a well-controlled electrodeposition process into a nanoporous alumina template[53]. They applied the nanostructure as a cathode catalyst for hydrogen evolution reaction in alkaline water electrolysis and found it both stable and effective.

As shown in Fig. 2.12[53], in step (a) gold nanobowl is formed into alumina template by DC sputtering of gold to provide good electrical contacts, followed by electrodepostion of Ni nanopottery and then in (b), further galvanic electrodepostion is done to form the top holes of the Ni nanopottery. With the increasing electrodeposition time, either smaller diameter holes as in (d) or nanorod with no hole at all as in (c) could be obtained. Both side elevation and top view of the formed Ni nanopottery structure are done with SEM as shown in Fig. 2.13[53]and Fig. 2.14[53].

This Ni nanopottery structure introduces both higher quantity of and larger surface reactive sites for hydrogen adsorption into the electrolysis hydrogen evolution reaction. As a result, the catalytic activity is greatly boosted compared to traditional cathode catalyst and even some other nanostructures like Ni nanorod and nanofilm.

Besides the aforementioned Ni nanopottery, carbon nanotube is also novelly

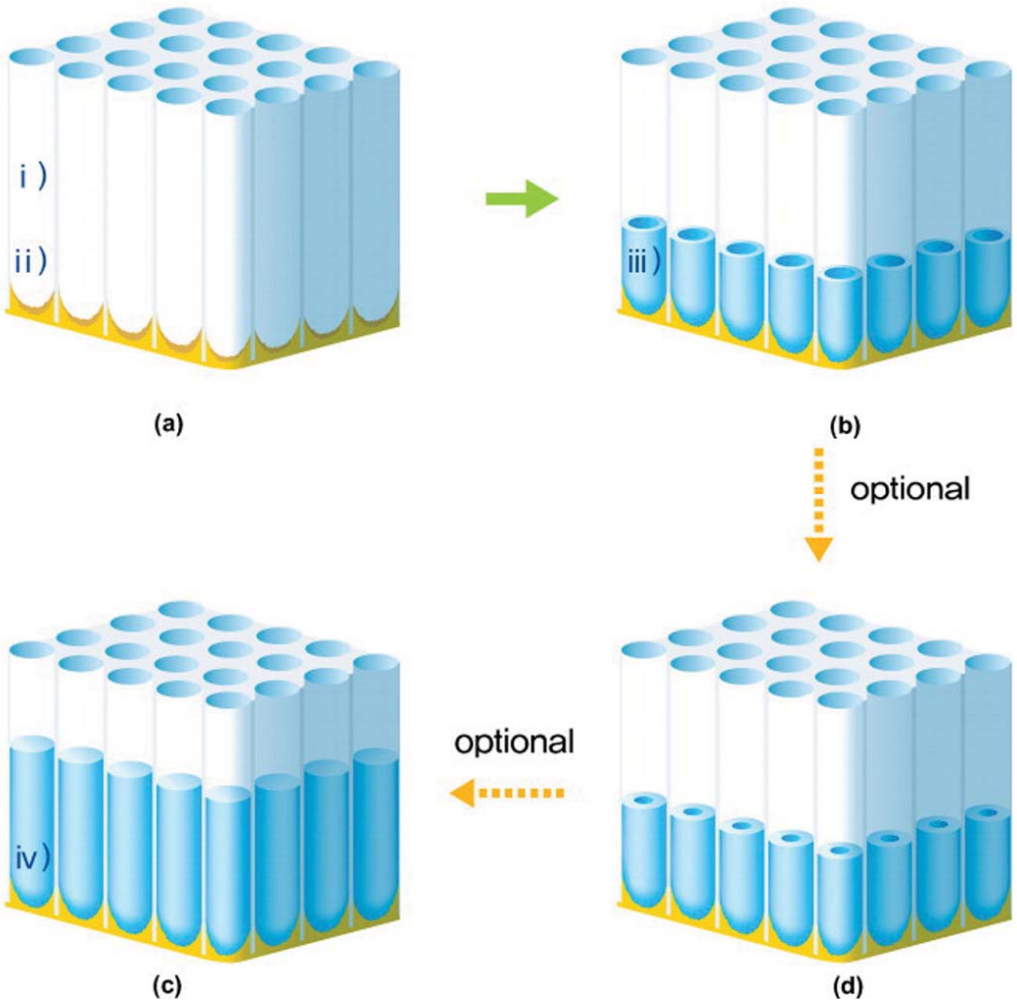

Fig. 2.12: Conceptional diagram of Ni nanopottery formation[53]. Reprinted with permission from Reference 53, Y. Yi, J. K. Lee, H. J. Lee, S. Uhm, S. C. Nam and J. Lee, Electrochemistry Communications **11** 2121 (2009). © 2009, Elsevier.

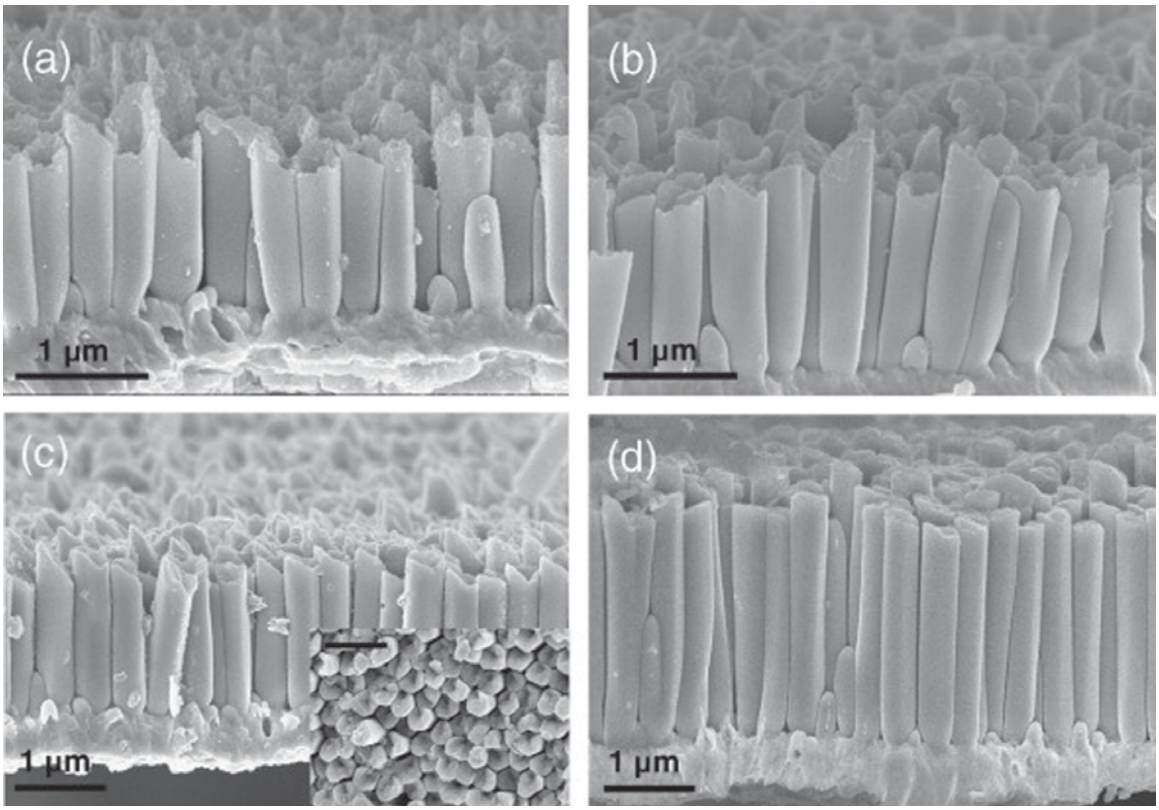

Fig. 2.13: SEM images of Ni nanostructure obtained at different electrodeposition times. Applied current is −10 mA/cm^2. (a) Electrodeposited for 150, (b) 300, (c) 350 and (d) 600 s[53]. Reprinted with permission from Reference 53, Y. Yi, J. K. Lee, H. J. Lee, S. Uhm, S. C. Nam and J. Lee, Electrochemistry Communications **11** 2121 (2009). © 2009, Elsevier.

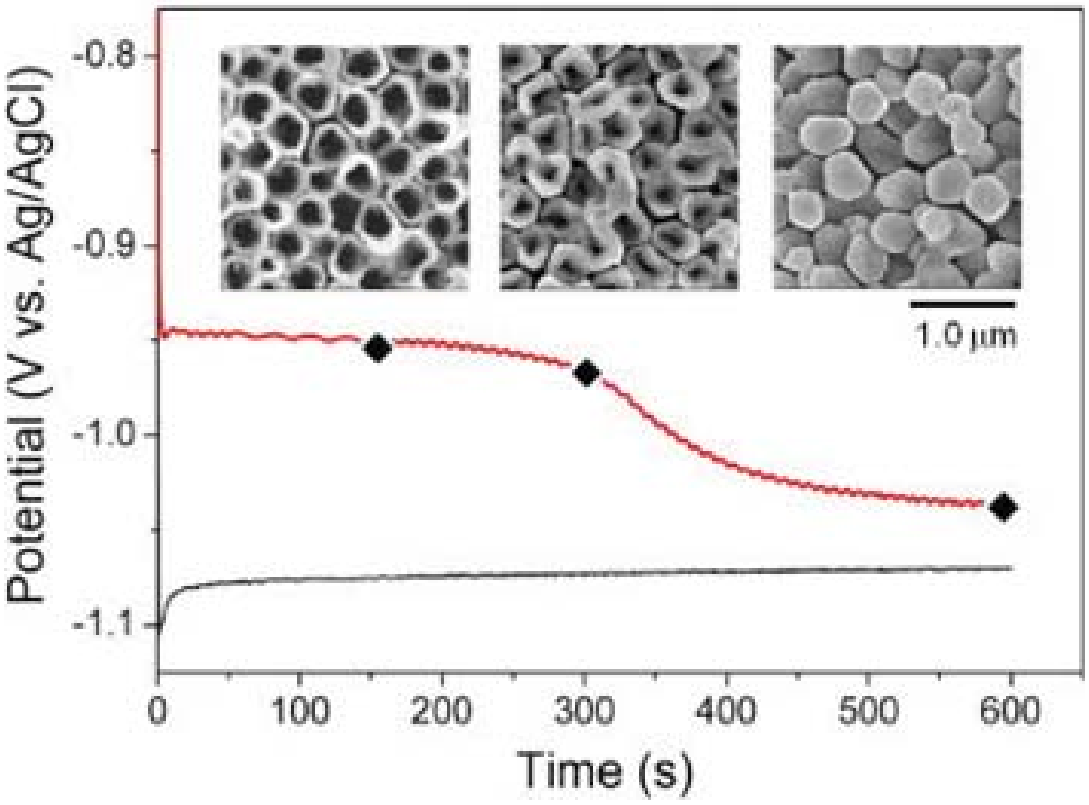

Fig. 2.14: A plot of potential variation at a current of −10 mA/cm^2 and inset shows the corresponding top-view of SEM images[53]. Reprinted with permission from Reference 53 Y. Yi, J. K. Lee, H. J. Lee, S. Uhm, S. C. Nam and J. Lee, Electrochemistry Communications **11** 2121 (2009). © 2009, Elsevier.

applied as a cathode related material in electrolysis of water[54]. The electrically conducting surface of the nanotube arrays is very useful as (a) cathode for hydrogen generation and absorption (b) electrolyzing water. Moreover, hydrophobic carbon nanotube-based electrochemical cell is considered as an alternative solution to hydrogen sorting due to the unique combination of hydrophobicity and conductivity of carbon nanotube forests.

As the final product shown in Fig. 2.15[54], researchers in the California Institute of Technology have grown the aligned nanotubes via chemical vapor deposition with a two-stage thermal CVD system. The main process was done at 825°C, using SiO_2 as the substrate for growth. A mixture of ferrocene as Fe-catalyst and toluene as carbon source was injected beforehand. While heating, as a gas solution carrier, a flow of 800 sccm of argon gas was maintained. The diameter of the grown nanotubes ranged from 15 to 50 nm and their length approximately 800 μm. (a) and (b) in the figure show that the foamlike microstructure of the aligned nanotubes is across the entire multiwalled carbon nanotube network (c) and (d) indicate that, at the surface of the nanotube forest, entanglement that provides surface connectivity and electrical pathways for high electrical conductivity is formed.

The real application can be seen if Fig. 1.16[54], in which the tungsten electrodes were used as both anode and cathode. In Fig. 2.16 (b) the tungsten needle inserted into the water droplet was working as anode while the other one immersed in the carbon nanotube forest was functioning as cathode. Bubbles observed surrounding the tungsten anode are oxygen bubbles, indicating the occurrence of electrolysis. The static contact angle between the nanotube forest surface and the water droplet was measure to be around 144°,

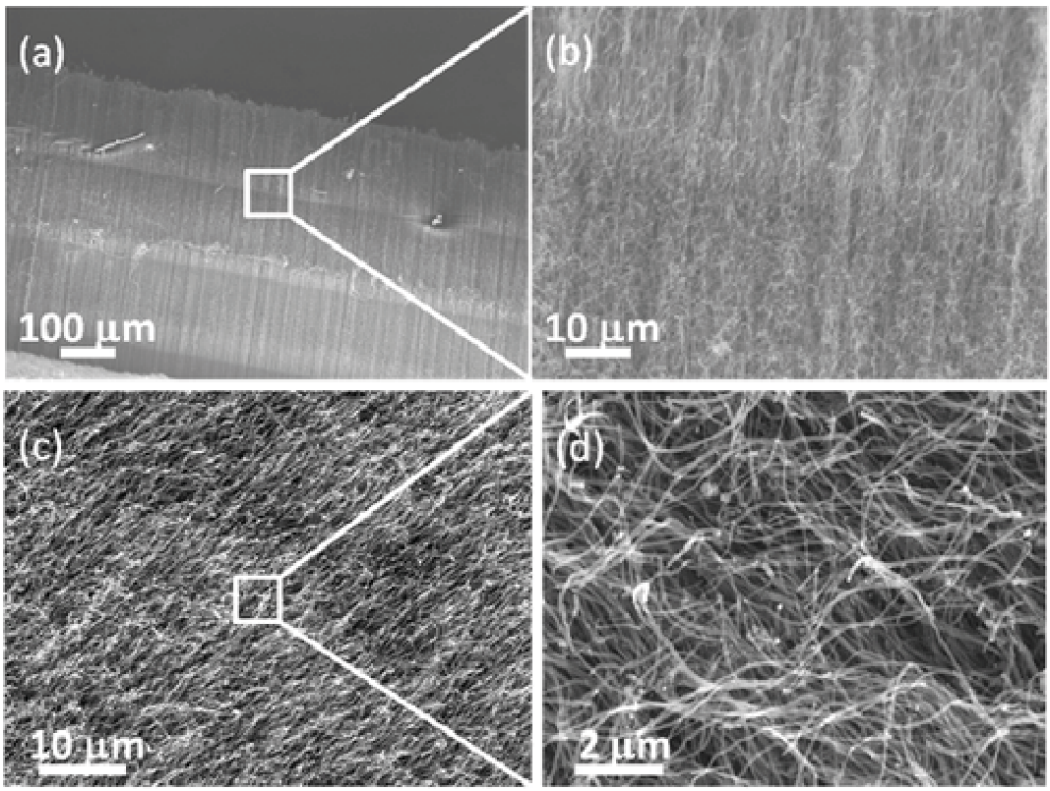

Fig. 2.15: SEM graphs of typical multiwalled carbon nanotubes[54]. Reprinted with permission from [54], A. Misra, J. Giri and C. Daraio, ACS Nano **3** 3903 (2009).© 2009, American Chemical Society

exhibiting a highly hydrophobic behavior related with the extremely high surface roughness.

Hydrogen generation using this device was proved by the results from GC measurements, while a control experiment using hydrophobic paraffin film with two tungsten electrodes both in the water drop generated no traceable amount of hydrogen. This comparison suggested the fast chemical reactivity of the vertically aligned CNT forests attributed to their large surface area and catalytic activity and their high potential efficiency in systems for water decomposition.

Nanosized Ni particle, as one of the alternative H_2 electrode materials for SOECs,

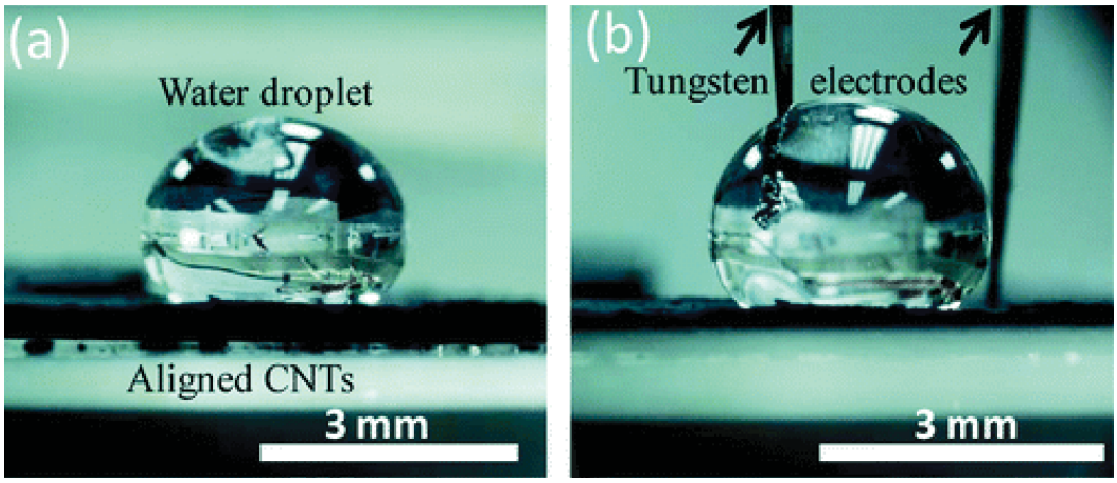

Fig. 2.16: Digital micrographs of the deionized water droplet sitting on the hydrophobic surface of the CNT forest[54]. Reprinted with permission from Reference 54, A. Misra, J. Giri and C. Daraio, ACS Nano **3** 3903 (2009).© 2009, American Chemical Society

is also successfully applied in high temperature electrolysis of water and steam. Highly dispersed nanosized Ni particles, prepared by researchers in the University of Yamanashi, Japan, are proved feasible to reduce the contact resistance between the samaria-doped ceria cathode and solid electrolyte[55]. At 900°C, with optimal load of nanosized Ni particles, the polarization resistance of the samaria-doped ceria electrode is measured to be 0.18 Ω cm^2 at 900°C, which shows a promising potential. Besides, samaria-doped ceria electrode with highly dispersed nanosized Ni particles exhibits a decent stability in humidified H_2 at 800 °C and 0.6 A cm^{-2} over 1100h[56].

2.3.5. Photoelectrolysis and photocatalytic decomposition of water

As mentioned in previous paragraphs, electrolysis of water always transforms electrical energy into hydrogen-carried chemical energy. As a result, whether the hydrogen production is renewable depends on where the electrical energy is from.

Obviously, using electricity from fossil fuels will hardly make the energy cycle sustainable. Only processes based on renewable energy sources could be considered. One widely accepted route is to firstly collect solar energy and convert it into electrical energy and then to electrolyze water with the energy collected[51]. However, this route includes two steps, therefore inevitably resulted in two times of energy loss within conversion.

Photoelectrolysis can be considered as a variation of electrolysis directly using light. Within a photoelectrolytic process, the conversion of light into electrical current and the chemical transformation of H_2O into H_2 are integrated into a single step with a single electrode. Considered as the most efficient renewable method of hydrogen production[49], interests are widely shown world-widely by researchers aiming at making hydrogen as a clean and sustainable energy source.

The general operating principle of a photoelectrochemical cell (PEC) is illustrated in Fig. 2.17. The semiconductor electrode in the figure is usually an n-type semiconductor photoanode that functions as the working electrode, absorbing photon and produces oxygen. The counter electrode, reducing H^+ ion into H_2, can either be a metal cathode like platinum or a p-type semiconductor cathode. If the counter electrode is chosen as a p-type semiconductor cathode, the working electrode can also be a metal anode. In sum: at least one of two the electrodes should be a semiconductor, with n-type as anode and p-type as cathode and the semiconductor electrode is supposed to be photoactive.

The three separated steps of reactions in the illustration:

$$h\nu \rightarrow h^+ + e^- \quad (20)$$

$$2H^+ + 2e^- \rightarrow H_2\uparrow \quad (21)$$

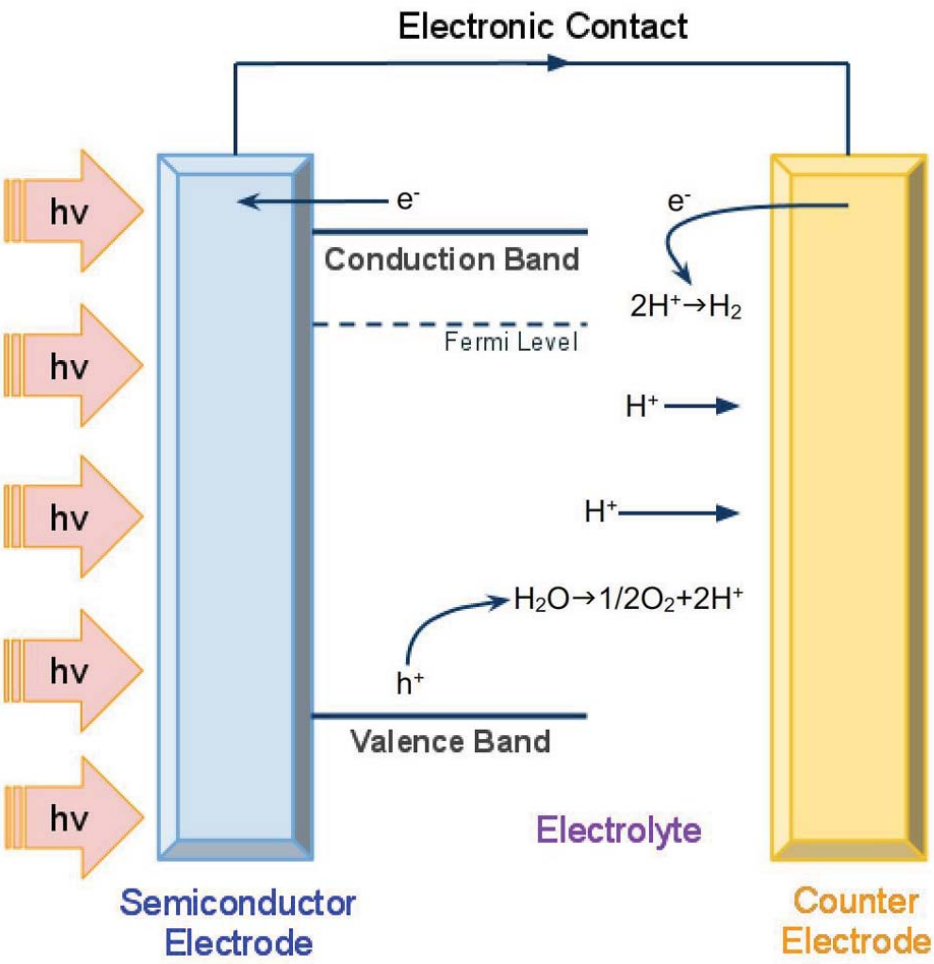

Fig. 2.17: General illustration of hydrogen production by a photoelectrochemical cell during water photoelectrolysis.

$$2h^{+}+H_2O \rightarrow 1/2O_2\uparrow+2H^{+} \quad (22)$$

can be expressed into one overall reaction:

$$2hv+H_2O \rightarrow H_2\uparrow+1/2O_2\uparrow \quad (23)$$

This is an endothermic process and its standard Gibbs free energy change ΔG^0 is 237.14kJ/mol. According to the relationship

$$\Delta G^0=-nF\Delta E^0 \quad (24)$$

The standard electric potential ΔE^0 is 2.46eV. Since this is a two-electron redox process, the electromotive force ΔE is equal to or greater than 1.23V for possible decomposition of water. This is actually the same value of direct electrolysis.

Photocatalytic water decomposition is slightly different from the photoelectrochemical water decompostion described above, although their mechanisms are generally the same[57-62]. The major difference is regarding the location of the sites of reaction (2) and (3). While in the photoelectrochemical process, the two reactions take place separately at the photoanode and the photocathode and evolving oxygen gas and hydrogen gas, respectively, in the photo-catalytic process, both reactions simultaneously occur on the surface of the photocatalyst, generating a mixture of both gases[58]. A schematic diagram of an ideal photocatalytic water-splitting device is shown in Fig. 2.18, with the semiconductor particle acting as photocatalyst. The photocatalyst functions as

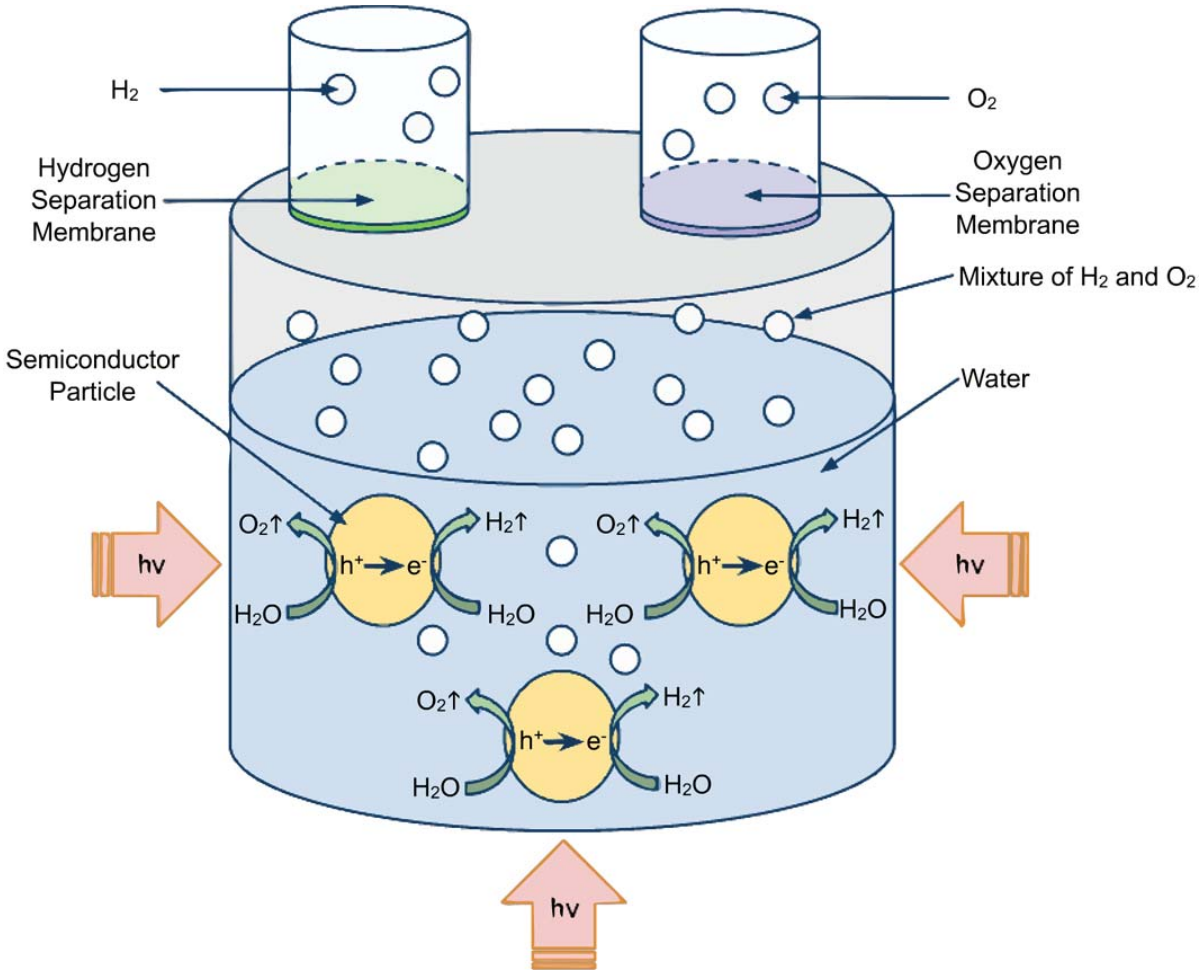

Fig. 2.18: Photocatalytic water decomposition with suspending semiconductor particles behaving as electrochemical cells.

both the working electrode and the counter electrode of the photoelectrochemical cell at the same time. Hydrogen and oxygen mixture gas are generated from water splitting with light absorbed. The mixture of gas could be then separated with respective separation membranes. The separation could be done easily at relatively low temperature.

As can be seen in Table 2.2, many different materials have been studied as photocatalysts[59-62] and most of our focus has been on metal oxide semiconductors like TiO_2 and delaffosite $CuAlO_2$. Modified TiO_2photocatalysts are studied on the

Table 2.2: Some selected data related to photocatalytic water decomposition methods and their efficiencies

Method	Condition	Efficiency	Year	Reference
Decomposition of oxalic acid over platinized TiO2	100 ml 4.9×10^{-3} M oxalic acid solution; photocatalyst: 0.05 g (0.5 wt.% Pt–TiO2) ; irradiation time: 3 h	58 μmol/h hydrogen generated	2001	59
NiO(0.2 wt.%)/$NaTaO_3$:La(1.5%) photocatalyst	Photocatalyst powder dispersed in pure water; NaOH added into a reactant solution; light source being a 400 W high-pressure mercury lamp	7.2 mmol/h of hydrogen	2003	60
Delafossite CuAlO2	0.1M S2− solution at pH, 13.72 48 ± 0.1 °C and illuminated by a 500W halogen lamp	Generation rate of 0.19 ml/(h*mg)	2005	61
CuAlO2/TiO2 heterojunction	(300 mg)/TiO_2 (75 mg); temperature 50±0.1 °C; Environment: 200 ml of aqueous S^{2-} solution(0.025 M) three tungsten lamps each one of 200W for 40 min pH about 11	5265 μmol of H_2 obtained	2007	62
CuAlO2 nanoparticle catalysts	0.2 g batch of $CuAlO_2$ powder mixed as a slurry with 170 ml of undoped, filtered, deaerated and de-ionized water	Hydrogen generation rates increased from 715 to 6244 ppm/h as the temperature rose from 460 to 510 K	2009	34

photocatalytic hydrogen production as suspended particles. Researchers in Cairo, Egypt and the Clean Energy Research Institute, USA, deeply studied TiO_2anatase in powder form and its modification by RuO_2. With 2 g/L of RuO_2/TiO_2 photocatalyst suspended in 6% methanol solution with 1.5% activated carbon, a continuous evolution of hydrogen along with time is achieved by photolysis[63].

Our research group also did related study on the synthesis and the application of these two materials as photocatalysts on hydrogen evolution. These two semiconductors have one important advantage over other photocatalytic materials in terms of high chemical stability against photochemical erosion during the water-splitting process. However, we can also observe from the data, unfavorably, that although the efficiency of hydrogen production with this method is improving and acceptable at the experimental level, it is still far less than any feasible expectation of practical application. A lot more progress is required for photocatalytic hydrogen production to be applied in practice.

In our experiments, four groups of $CuAlO_2$ catalyst powders consisting of different ratios of Cu were prepared with high temperature process. As shown in Table 2.3, different (n) indicating different molar ratios of Cu in $Cu_{(n)}AlO_2$ were chosen and corresponding amounts of CuO and $Al(NO_3)_3{\cdot}9H_2O$ were calculated. We dissolved $Al(NO_3)_3{\cdot}9H_2O$ in DI water and CuO in nitric acid separately. After they are both fully dissolved following a long time of magnetic stirring, we mix them together in one beaker and heat while continuing stirring to make the mixture homogeneous. When all liquid in the beaker is evaporated, we collect the solid in the beaker and transfer it to a clean crucible. After calcinations at 1100°C (Fig. 2.19), $Cu_{(n)}AlO_2$ powders as final products were obtained. In order to get smaller sizes of $CuAlO_2$ particles, we applied the ball

Table 2.3: Initial reactants of different groups of $Cu_{(n)}AlO_2$

Group No.	n	CuO (g)	$Al(NO_3)_3 \cdot 9H_2O$ (g)	$Cu_{(n)}AlO_2$ (g)
1	1.00	0.6492	3.0615	1.0
2	1.02	0.6553	3.0304	1.0
3	1.05	0.6644	2.9843	1.0
4	1.10	0.6789	2.9106	1.0

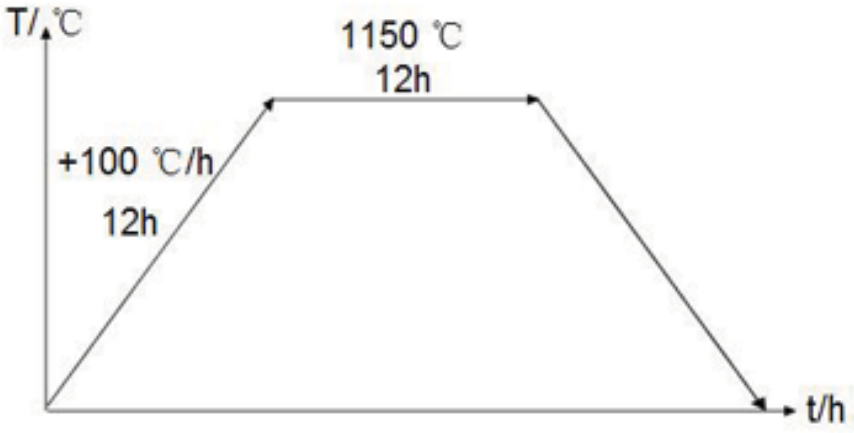

Fig. 2.19: The temperature used for calcination.

milling method on the obtained powders. The weight ratio between the zirconia milling balls and $CuAlO_2$ samples is taken as 10:1. The operating time of ball milling is 20 hours.

DI water is used to make the concentration of S^{2-} 0.25M. Then the ball-milled $CuAlO_2$ powders are added into the same solution for 3 g/L. After 5 min stirring, we flushed the solution with N_2 for 30 min and then kept it at 50°C for better reactivity than room temperature. Finally, we focused our lights on the beaker to provide the luminous energy. X-Ray Diffraction on the four groups of $Cu_{(n)}AlO_2$ particles was done using Philips X'Pert XRD, their patterns shown in Fig. 2.20. It can be seen that no phanerous CuO phase in the final products appeared on the patterns along with the increase of Cu amount. All four patterns are very close to the standard $CuAlO_2$ phase, without any unexpected peak on the patterns. The self-compensation for the extra amount of Cu in the system can be explained by the loss of Cu and permeation of Al due to the Alumina container being at high temperature.

SEM characterizations were also done on the $CuAlO_2$ samples as shown in Fig. 2.21. From the SEM images we can see that after the ball milling, the general particle size decreased; meanwhile, the surface area of the particle dramatically increased. In the hydrogen generation experiments, very small bubbles could be observed.

Because of the turbidity of the solution, the number of bubbles per minute can hardly be counted. Roughly, on one side, about 10 per min on average can be seen, while the control group of DI water alone shows half the number due to the gasification of water itself. The extra amount of bubbles are possibly of the hydrogen produced, but to make sure of its nature, a much larger production rate than this is required for further examination.

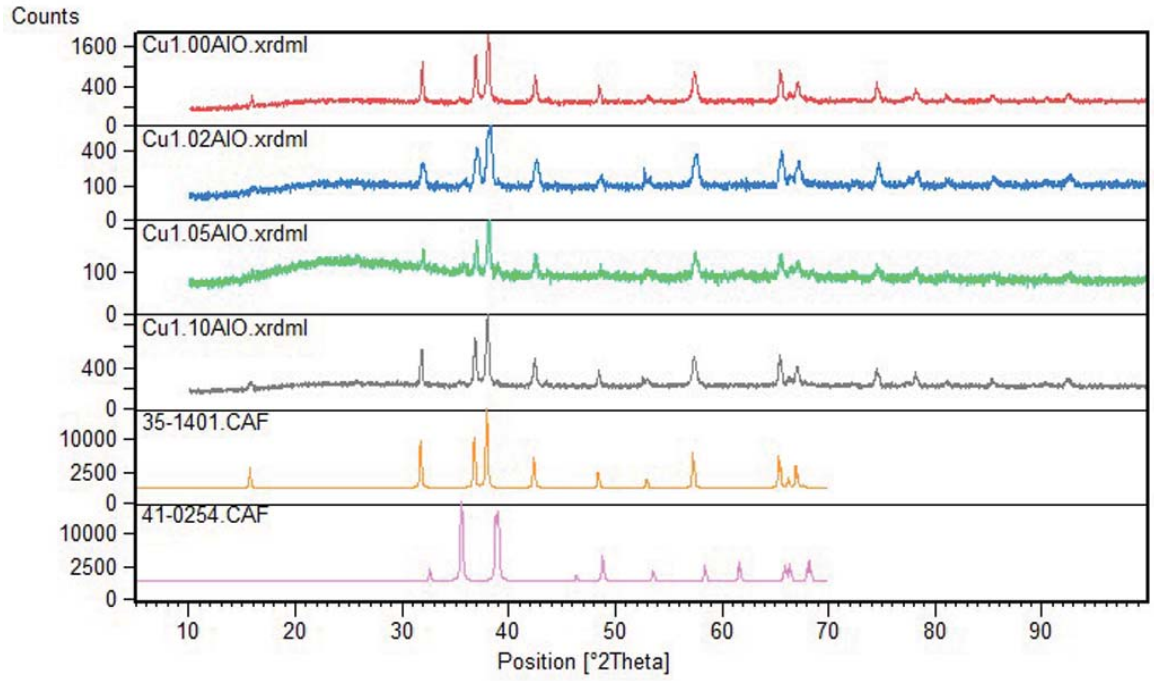

Fig. 2.20: The first four patterns are measured XRD patterns of the prepared $CuAlO_2$ powders

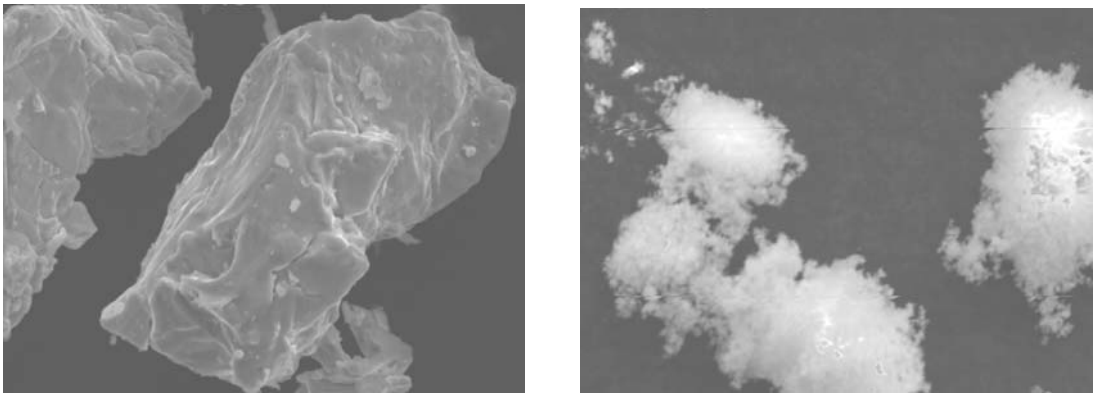

Fig. 2.21: The SEM pictures of the $CuAlO_2$ particles before (left) and after (right) ball milling

2.3.6. Nanotechnology applied in photoelectrolysis and photocatalytic decomposition of water

Both photoelectrochemical and photocatalytic water decomposition are very suitable objects for the application of advanced nanotechnology, because one of the most characteristic properties of nanomaterials is their distinct catalytic ability due to the extremely large specific surface areas. A very important nanotechnique applied in both photoelectrochemical cell and photocatalytic water splitting is the nanocrystalline semiconductor electrode[57]. As we know, one challenging obstacle between the ideal efficiency of photochemical process and its real working condition is the recombination of electrons and holes. If the recombination time is not considerably larger than that of the electron activation or injection, most electrons would recombine with holes again and the light energy absorbed would be wasted. Photoelectrodes made from nanocrystalline semiconductor materials such as colloidal TiO_2 solved this problem because their electron injection occurs several thousand times faster than charge recombination[64]. This property of nanometersized semiconductor particles is widely exploited for light-to-electrical energy conversion, including not only photoelectrolysis and photocatalytic decomposition but also direct electricity generation like dye-sensitized solar cells. To make these nanocrystalline semiconductor particles into usage, a substrate is necessary to connect them and provide a pathway for electrical conduction, as shown in Fig. 2.22[57]. Two processing routes were developed for this connection. In the first approach, a suspension of nanoparticles is directly applied on the conducting substrate and then they are sintered together to form electrical contact allowing charge transport from particles to substrate[64]. In the other approach, by a chemical or electrochemical deposition process, particles are

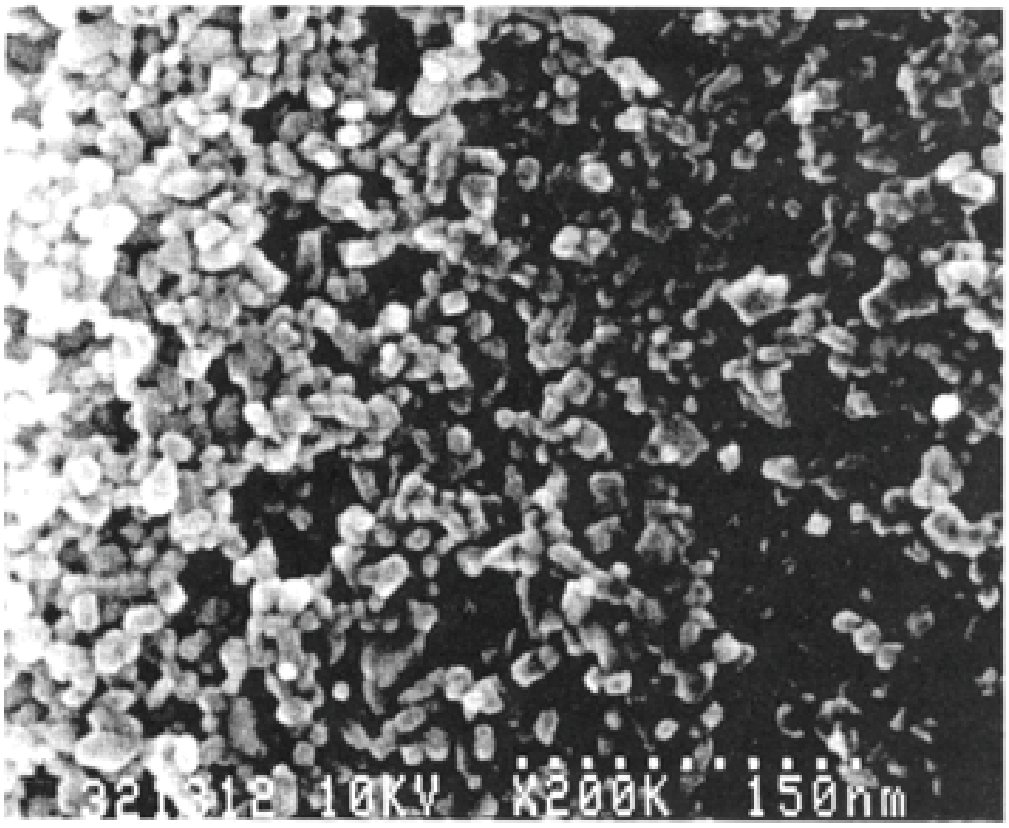

Fig. 2.22: SEM picture of nanocrystalline TiO_2 deposited on conducting glass [57]. Reprinted with permission from [57], A. Hagfeldt and M. Graetzel, Chemical Reviews **95**, 49 (1995). © 1995, American Chemical Society.

directly formed onto the substrate[65].

Nanotechnology is not only used on mainly-functional semiconductors, but also on accessory materials used with them. CdS and CdSe nanocrystallites are deposited on mesoporous TiO_2 films to improve the charge transport characteristics of the semiconductor-sensitized TiO_2 films and increase the performance of the photoelectrodes. Researchers in National Cheng Kung University, Taiwan, studied the appropriate heat treatment parameters in the annealing of the semiconductor sensitizers (CdS, CdSe and CdS/CdSe) being assembled on mesoporous TiO_2 films to enhance the

performance of the photoelectrodes in a process of photoelectrochemical hydrogen generation. They developed an optimized heat treatment route, i.e., firstly annealing a TiO_2/CdS electrode at 300^oC, then annealing at 150^oC after the assembly of CdSe nanocrystallites[66]. Electrodes prepared through this route appear to have improved performance because the serious oxidation and decomposition of the sensitizers due to over-annealing are avoided while the counter-diffusion at the CdS/CdSe interface during co-annealing is also averted.

Besides nanocrystalline, nanoporous thin film materials are also applied as photoanodes. Researchers in the University of California, Santa Barbara, experimented and synthesized highly crystalline mesoporous TiO_2. Then they filled the pores with carbon to prevent pores from collapsing in the following annealing process at 500^oC. The C-TiO_2 thin film photoanode shows a solar spectrum photoconversion efficiency of 2.5% at zero bias and 40 mW/cm^2 illumination. This efficiency is approximately 4-10 times higher than their control sample of comparable crystallinity[67]. The only observed drawback of this material is that it sacrificed the excellent charge transfer properties of TiO_2. To solve this problem, several combined methods are developed; one of them is a bilayer structure coupling the TiO_2 layer with a thin layer of C-TiO_2, another is to obtain a thin absorption layer of copper oxide covering the TiO_2, though both of them are currently with some technical difficulties in the uniform coverage of the underlying material architecture.

Other nanoporous metal oxides besides TiO_2 are also widely studied as potential materials used in photoelectrolysis and photocatalysis for their photochemical properties. Researchers in Pennsylvania State University, University Park, synthesized self-organized nanoporous iron (III) oxide (haematite) via potentiostaticanodization of iron foil. The pore diameters of the nanoporous structure range from 50 to 250 nm with a pore

depth around 500 nm. The diameters can be controlled by varying the applied potential and electrolytic composition. Annealing is done in a nitrogen atmosphere at 400 ^{o}C for the crystallization and structural retention of the synthesized structure. The crystallized Fe_2O_3 nanoporous film, having a 2.2 eV band gap, exhibited a net photocurrent density of 0.51 mA cm^{-2} in 0.5 M H_2O_2 +1 M NaOH at 0.6 V versus Ag/AgCl under simulated AM 1.5 sunlight[68]. The FESEM images of the structure are shown in Fig. 2.23[68].

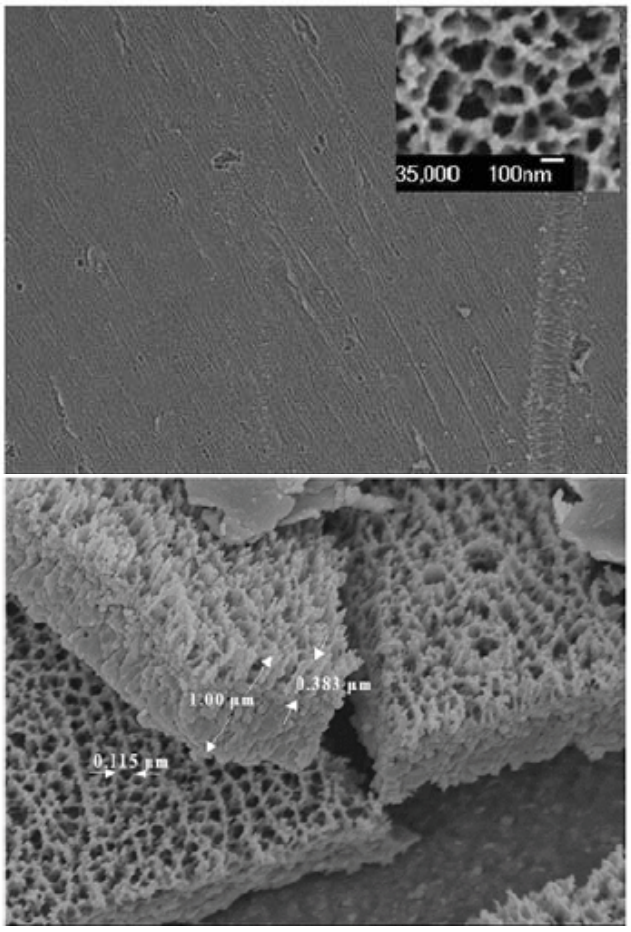

Fig. 2.23: FESEM images of a sample annealed at 400 $^{\circ}$C for 30 min: the upper image shows the uniformity of pore formation across the sample (the inset shows the pore diameter after annealing); the lower cross-sectional image shows the pore depth as 383 nm, the pore diameter as about 100 nm and the barrier oxide thickness as approximately 600 nm[68].Reprinted with permission from Reference 68, H. E. Prakasam, O. K. Varghese, M. Paulose, G. K. Mor, C. A. Grimes, Nanotechnology **17**, 4285 (2006). © 2006, IOP.

Nanotubes, especially TiO_2 nanotubes, are proved to be valuable for their applications in photoelectrolysis and photocatalysis as well[69,70]. As an ordered nanostructure, nanotube has the advantage of higher electron transport through the system over the aforementioned porous nanoparticulate films. Researchers in Pennsylvania State University, University Park[71], used anodization technique to fabricate titania with a unique nanoarchitecture consisting of vertically oriented, immobilized, highly ordered high-aspect ratio nanotubes as shown in Fig. 2.24[71]. Nanotube arrays annealed at 600°C show a hydrogen generation efficiency of water photoelectrolysis at Watt-normalized rate of 1.75 mL/W h under AM 1.5 illumination. They are proved to be stable against photocorrosion because no detectable variation in the hydrogen generation rate with time is observed over their testing periods of several months.

More improvements following the development of TiO2 nanotube arrays are accomplished by later researchers. One relatively novel study is the carbon-doped TiO2 nanotube array. As we know, a narrow band gap of the semiconductor photoanode is very helpful for the utilization of visible-light energy in the maximization of water splitting efficiency. And one of the best ways to narrow the band gap is to dope the TiO2 with C, S, or N. The most common method for preparing a carbon-doped TiO2 film is by direct oxidation of the Ti metal in the flame of a burner[72]. However, this method cannot well control the morphologies of the carbon-doped TiO2 by the flame oxidation method.

Researchers at the University of Texas at Austin introduce the carbon dopant into the TiO_2 nanotube arrays, with a process of annealing at high temperature (500-800°C) under controlled CO gas flow[73]. A conversion efficiency of 0.55% was obtained from

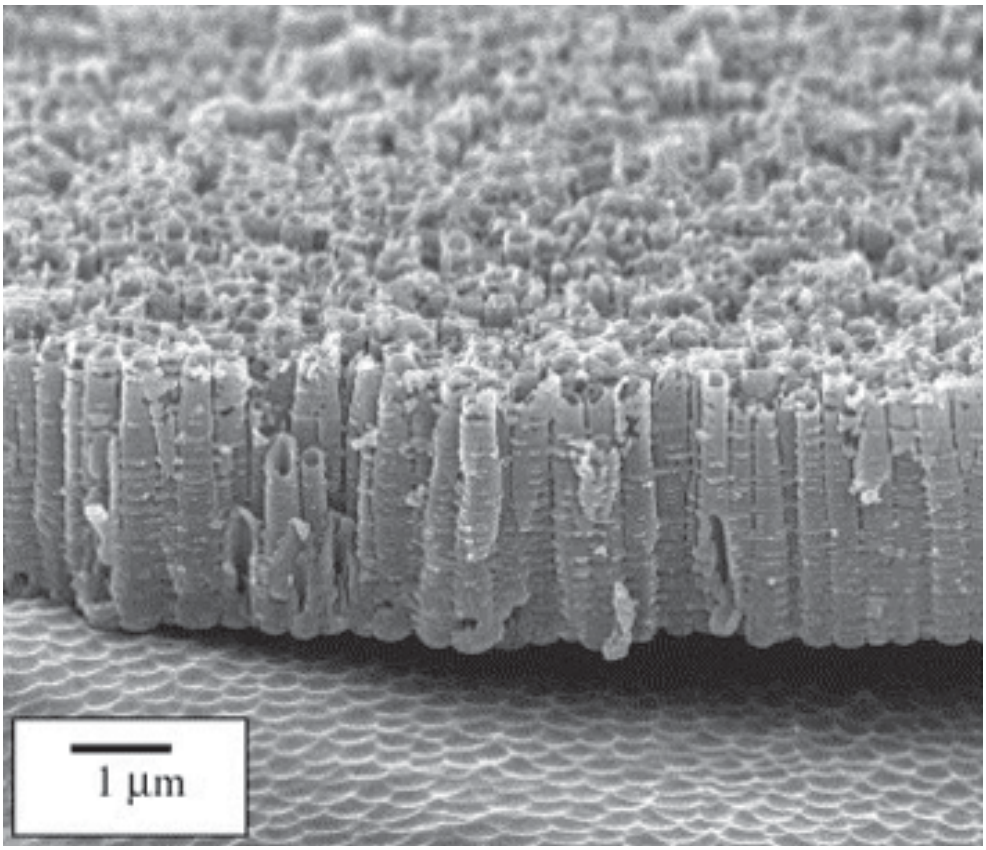

Fig. 2.24: FESEM cross-sectional image of 2.8 μm long TiO_2 nanotube array prepared by anodic oxidation of a titanium foil[71]. Reprinted with permission from Reference 71, M. Paulose, K. Shankar, S. Yoriya, H. E. Prakasam, O. K. Varghese, G. K. Mor, T. J. LaTempa, A. Fitzgerald, C. A. Grimes, Journal of Photochemistry and Photobiology A: Chemistry **178**, 8 (2006). © 2006, Elsevier.

their carbon-doped nanotube arrays with 3.3-μm tube lengths, claimed to be much higher than that of pure TiO_2 nanotube arrays at the same condition. And their total photocurrent was more than 20 times higher than that with a P-25 nanoparticulate film under white-light illumination. Their photoanode is prepared from titanium foil, firstly degreased by sonicating in 2-propanol and methanol and then rinsing with DI water and drying in a nitrogen flow.

2.4. References

[1] N. Auner and S. Holl, Energy **31**, 1395 (2006).

[2] O. V. Kravchenko, K. N. Semenenko, B. M. Bulychev and K. B. Kalmykov, J. Alloy Compd. **397**, 58 (2005).

[3] M.-q. Fan, L.-x. Sun and F. Xu, Energ. Convers. Manage. **51**, 594 (2010).

[4] A. V. Parmuzina and O. V. Kravchenko, Int. J. Hydrogen Energ. **33**, 3073 (2008).

[5] H. Z. Wang, D. Y. C. Leung, M. K. H. Leung and M. Ni, Renew. Sust. Energ. Rev. **13**, 845 (2009).

[6] H. Balat and E. Kirtay, Int. J. Hydrogen Energ. **35**, 7416 (2010).

[7] J. R. Rostrup-Nielsen, J. Sehested and J. K. Nørskov, Advances in Catalysis **65** (2002).

[8] K. Geissler, E. Newson, F. Vogel, T.-B. Truong, P. Hottinger and A. Wokaun, Physc. Chem. Chem. Phys. **3**, (2001)

[9] J. D. Holladay, J. Hu, D. L. King and Y. Wang, Catal. Today **139**, 244 (2009).

[10] A. Heinzel, B. Vogel and P. Hübner, J. Power Sources **105**, 202 (2002).

[11] C. Song, Catal. Today **77** 17 (2002).

[12] Mustafa Balat, Mehmet Balat, Elif Kirtay and Havva Balat, Energ. Convers. Manage. **50**, 3158 (2009).

[13] R. Farrauto, S. Hwang, L. Shore, W. Ruettinger, J. Lampert, T. Giroux, Y. Liu and O. Ilinich, Ann. Rev. Mater. Res. **33**, 1 (2003).

[14] Rostrup-Nielsen, J. In Encyclopedia of Catalysis; Horvath, I. T., Ed.; Wiley-Interscience, New York .Vol. **4** (2003).

[15] A. M. Adris, B. B. Pruden, C. J. Lim and J. R. Grace, Can. J. Chem. Eng. **74**, 177 (1996).

[16] M. Cargnello, N. L. Wieder, T. Montini, R. J. Gorte and P. Fornasiero, J. Am. Chem. Soc. **132**, 1402 (2009).

[17] F. P. Zamborini, S. M. Gross and R. W. Murray, Langmuir **17**, 481 (2000).

[18] P. S. Gradeff, F. G. Schreiber, K. C. Brooks and R. E. Sievers, Inorg. Chem. **24**, 1110 (1985).

[19] H. Chen, J. A. Cronin and R. D. Archer, Inorg. Chem. **34**, 2306 (1995).

[20] A. Machocki, A. Denis, W. Grzegorczyk and W. Gac, Appl. Surf. Sci. **256**, 5551 (2010).

[21] S. F. Wu and L. L. Wang, Int. J. Hydrogen Energ. **35**, 6518 (2010).

[22] F. Schüth, Angew. Chem. Int. Edit. **42**, 3604 (2003).

[23] T. Umegaki, K. Kuratani, Y. Yamada, A. Ueda, N. Kuriyama, T. Kobayashi and Q. Xu, J. Power Sources **179**, 566 (2008).

[24] A. C. Caputo, M. Palumbo, P. M. Pelagagge and F. Scacchia, Biomass Bioenerg. **28**, 35 (2005).

[25] K. S, L. K and C. ST, in *International conference for renewable energy* Bonn Germany, (2004).

[26] A. Demirbas, Energ. Source, Part A: Recovery, Utilization and Environmental Effects **30**, 475 (2008).

[27] T. A. Milne, C. C. Elam and R. J. Evans, *Hydrogen from biomass: state of the art and research challenges*, International Energy Agency Report IEA/H2/TR-02/001, 2002.

[28] A. Demirbas, Energ. Source, Part A: Recovery, Utilization and Environmental Effects **30**, 1120 (2008).

[29] B. Demirbas, ENERGY, EDUCATION, SCIENCE AND TECHNOLOGY Part A **26**, 10 (2010).

[30] M. Balat, Energ. Source, Part A: Recovery, Utilization and Environmental Effects **30**, 552 (2008).

[31] J. Li, BioResources **4**, 1520 (2009).

[32] J. Li, J. Liu, S. Liao and R. Yan, Int. J. Hydrogen Energ. **35**, 7399 (2010).

[33] J. Li, Y. Yin, X. Zhang, J. Liu and R. Yan, Int. J. Hydrogen Energ. **34**, 9108 (2009).

[34] J. R. Smith, T. H. Van Steenkiste and X.-G. Wang, Phys. Rev. B **79**, 041403 (2009).

[35] J. E. Funk, Int. J. Hydrogen Energ. **26**, 185 (2001).

[36] C. Perkins and A. W. Weimer, Int. J. Hydrogen Energ. **29**, 1587 (2004).

[37] A. Kogan, Int. J. Hydrogen Energ. **22**,481 (1997).

[38] A. Hammache and E. Bilgen, Int. J. Hydrogen Energ. **13**, 539 (1988).

[39] C. Perkins and A. W. Weimer, AIChE J. **55**, 286 (2009).

[40] A. Steinfeld, P. Kuhn, A. Reller, R. Palumbo, J. Murray and Y. Tamaura, Int. J. Hydrogen Energ. **23**, 767 (1998).

[41] A. Steinfeld, Int. J. Hydrogen Energ. **27**, 611 (2002).

[42] S. Yalçin, Int. J. Hydrogen Energ. **14**, 551 (1989).

[43] A. Kogan, Int. J. Hydrogen Energ. **25**, 1043 (2000).

[44] K. Wegner, H. C. Ly, R. J. Weiss, S. E. Pratsinis and A. Steinfeld, Int. J. Hydrogen Energ. **31**, 55 (2006).

[45] S. Abanades, P. Charvin, F. Lemont and G. Flamant, Int. J. Hydrogen Energ. **33**, 6021 (2008).

[46] W. Kreuter and H. Hofmann, Int. J. Hydrogen Energ. **23**, 661 (1998).

[47] R. de Levie, J. Electroanal. Chem. **476**, 92 (1999).

[48] O. V. Dorofeeva, Journal of physical and chemical reference data **32**, 879 (2003).

[49] C. A. Grimes, O. K. Varghese and S. Ranjan, *Light, water, hydrogen : the solar generation of hydrogen by water photoelectrolysis* (Springer, New York, 2008).

[50] P. Millet, M. Pineri and R. Durand, J. Appl. Electrochem. **19**, 162 (1989).

[51] L. L. Kazmerski, Renew. Sust. Energ. Rev. **1**, 71 (1998).

[52] L. L. Kazmerski, *Solar photovoltaic hydrogen [electronic resource] : the technologies and their place in our roadmaps and energy economics / L.L. Kazmerski, K. Broussard* (National Renewable Energy Laboratory, Golden, Colo. , 2004).

[53] Y. Yi, J. K. Lee, H. J. Lee, S. Uhm, S. C. Nam and J. Lee, Electrochem. Commun. **11**, 2121 (2009).

[54] A. Misra, J. Giri and C. Daraio, ACS Nano **3**, 3903 (2009).

[55] N. Osada, H. Uchida and M. Watanabe, J. Electrochem. Soc. **153**, A816 (2006).

[56] Anne Hauch, Sune Dalgaard Ebbesen, Soren Hojgaard Jensen and Mogens Mogensen, J. Mater. Chem. **18**, (20), 2331 (2008).

[57] A. Hagfeldt and M. Graetzel, Chem. Rev. **95**, 49 (1995).

[58] T. Bak, J. Nowotny, M. Rekas and C. C. Sorrell, Int. J. Hydrogen Energ. **27**, 991 (2002).

[59] N. Koriche, A. Bouguelia, A. Aider and M. Trari, Int. J. Hydrogen Energ. **30**, 693 (2005).

[60] H. Kato and A. Kudo, Catal. Today **78**, 561 (2003).

[61] Y. Li, G. Lu and S. Li, Appl. Catal. A: General **214**, 179 (2001).

[62] R. Brahimi *et al.*, J. Photoch. Photobio. A **186**, 242 (2007).

[63] A. A. Nada, M. H. Barakat, H. A. Hamed, N. R. Mohamed and T. N. Veziroglu, Int. J. Hydrogen Energ. **30**, 687 (2005).

[64] J. E. Moser and M. Grätzel, Chem. Phys. **176**, 493 (1993).

[65] G. Hodes, I. D. J. Howell and L. M. Peter, J. Electrochem. Soc. **139**, 3136 (1992).

[66] Chi CF, Liau SY and Lee YL, Nanotechnology **21**, 025202 (2010).

[67] Jing Tang, Yiying Wu, Eric W. McFarland and Galen D. Stucky, Chem. Commun. **14**, 1670 (2004).

[68] H. E. Prakasam, O. K. Varghese, M. Paulose, G. K. Mor, C. A. Grimes, Nanotechnology **17**, 4285 (2006).

[69] Ren-Jang Wu; Yo-De Ju, Chien-Chung Jeng, J. Nanosci. Nanotechnol.**10**, 4213, 2010.

[70] Y. Ling, J. Liao, X. Liu, X. Wu and X. Bai, J. Nanosci. Nanotechnol. **10**, 7020, 2010.

[71] M. Paulose, K. Shankar, S. Yoriya, H. E. Prakasam, O. K. Varghese, G. K. Mor, T. J. LaTempa, A. Fitzgerald, C. A. Grimes, J. Photoch. Photobio. A **178**, 8 (2006).

[72] A. Fujishima, K. Kohayakawa and K. Honda, J. Electrochem. Soc. **122**, 1487 (1975).

[73] J. H. Park, S. Kim and A. J. Bard, Nano Lett. **6**, 24 (2005).

3. CONCLUSION

Though very different from one another, all branches of hydrogen production pathways discussed in this review have reason for their existence. The methods of hydrogen production from fossil fuels, including the catalytic decomposition and steam reforming of natural gas, the partial oxidation of heavy oil and coal gasification, are very effective and will still dominate for a relatively long time before the real depletion of fossil fuels. The gasification of biomass would become an increasingly more important way of hydrogen production when it is technically sophisticated enough and nanotechnology is expected to play an important role in this process. In the long run, most hydrogen methods would be expected to give their places to the direct water-splitting methods. Direct water-splitting, especially with renewable energy, is supposed to be one of the most effective solutions to the problems of carbon emission and global warming. The advanced methods of water-splitting like photoelectrolysis and photocatalytic decomposition of water still have efficiencies lower-than-feasible and need to make substantial progress with the help of technological developments. It is evident that nanomaterials and nanotechnology have a great role to play not only in the application of hydrogen production but also in the hydrogen energy storage.

PART II

GALLIUM-BASED LIQUID ALLOYS FOR PRODUCING HYDROGEN FROM WATER

4. INTRODUCTION

The present global economy depends heavily on carbon-based fossil fuels and hence is termed a carbon economy. It is estimated that the worldwide demand for energy will double by 2050 due to the rapid growth in population and industrialization of developing countries[1]. Because of the continuous depletion of fossil fuel reserves, the sustainability of the traditional carbon economy is severely challenged. Among all the theoretically conceived alternatives, the hydrogen economy, a systematization based on hydrogen throughout the whole energy cycle including generation, storage, transportation and usage, is considered most promising[2]. Because of its potential environmental and industrial advantages over the current carbon economy, the hydrogen economy is gradually growing from a mere concept into an increasingly practical alternative. However, two major concerns which are impeding the rapid transition from carbon-economy to hydrogen economy are safety and energy density within the storage and transportation stages. Novel hydrogen storage methods like usage of carbon nanotubes are broadly studied worldwide. However, the potential negative effect of hydrogen over-pressure on the stability of adsorbed H_2 was found to be a severe problem[3]. In addition, none of the techniques available to date meet the goal of achieving the desired energy storage density (equal to 6.5wt% and 62kg m^{-3} of hydrogen) comparable to a typical petrol-driven vehicle.

A straightforward solution to overcome the current difficulties is the in-situ production of hydrogen at the same time of the usage, i.e., to combine the receiving stage

and consumption stage of hydrogen in one system, in one device. By this means, the generation and usage, the initial step and the final step, are coupled/integrated together without necessity to regard the unsolved issues on storage and transportation. Several different ways dependent on their corresponding chemical or electrochemical reactions can be employed in this process. Among these methods, utilization of metals, especially aluminum[4], as an energy material to reduce water into hydrogen is considered as an effective, user-friendly and safe approach. Aluminium metal, theoretically, can react with water directly and produce hydrogen: $Al+3H_2O=Al(OH)_3+3/2H_2\uparrow$.

The only reason we rarely see the above reaction happening in our daily life is the passivation of the aluminium surface caused by the dense film of aluminium oxide that prevents its further reaction with water. The process of passivation usually begins when an amorphous layer of oxide film, whose thickness is several nanometers[5], forms on the surface of aluminum metal. The amorphous layer gets crystallized, becomes dense and subsequently prevents further reaction of aluminium with water. If the passivation process can be avoided, aluminium can become an ideal candidate for generating hydrogen. The theoretical ability of one kilogram of aluminum to generate hydrogen is 1245 liter[6], much higher than its already-high counterpart, magnesium, one kilogram of which could theoretically generate 950 liter hydrogen. Secondly, the price of aluminium metal is low enough for either industrial or commercial use owing to both the abundance in the Earth's crust and, more importantly, the mature techniques in producing aluminium metal. It is also expectable to use the mature producing techniques to recycle the $Al(OH)_3$ generated in the process of hydrogen production.

One very simple way to avoid the passivation process is to use highly basic

solutions such as NaOH solution instead of pure water. However, this method is not viable for residential and vehicle usage because of the dangerously corrosive nature of strong basic solution. Meanwhile, it is also not economical for industrial usage because the manufacture of strong bases like NaOH and KOH consumes a very large amount of energies themselves. Another possible approach is to use aluminium nanoparticles instead of regular aluminum powder. In theory, if the particle size of aluminium is of the same scale of, or even smaller than, the thickness of the passivation layer, its reaction with water would also be complete enough to produce hydrogen. The major obstacles against the practical usage of the reaction between Al nanoparticles with water includes the relatively high cost of preparing nanoparticles, the difficulty in controlling the velocity of reaction due to the nature of nanoparticles and very importantly, the storage problem of the reactive nanoparticles which is ready to react with oxygen and humidity in the air. For example, a very commonly studied and used aluminum nanopowder produced by the plasma-explosion process, Alex powder, loses up to 70% of the original quantity of active aluminum in 8-12 days during some tests[7,8] where the temperature varied from room temperature to 60 ºC, with relative air humidity of 75%. Also, the generally lower density of nanoparticles resulting in a lower energy capacity per unit volume and the potential explosion and health hazard of nanoparticles are also concerns about the usage of aluminium nanopowders.

A recent and alternate approach is to have aluminium metal activated by liquid eutectics. When the surface of the aluminium is moistened by the amalgamation, the aluminium would readily react with water to produce hydrogen. The liquid eutectics themselves would not react with either aluminium or water in the process, thus behaving

like catalysts. Mercury was the amalgamation studied in early stages. While it successfully prevents the formation of the aluminium oxide film on its surface, its toxic properties prohibited its real-life application[6].

Recently it has been shown that Ga-In eutectic alloys can be useful to activate aluminum powders for generating hydrogen. Ga and In are both nontoxic and already widely used in various fields of science and technology. Their eutectic has a melting point lower than room temperature and the alloy is very easy to generate from Ga metal and In metal. Motivated by those reports we prepared alloys using five metals (Ga, In, Zn, Sn, Bi) and examined their performance as a catalyst in the reaction between water and Aluminum.

4.1. References

1 P. Kruger, Int. J. Hydrogen Energy **30** (15), 1515 (2005).

2 J. A. Turner, Science **305** (5686), 972 (2004).

3 A. C. Dillon, K. M. Jones, T. A. Bekkedahl, C. H. Kiang, D. S. Bethune and M. J. Heben, Nature **386** (6623), 377 (1997).

4 H. Z. Wang, D. Y. C. Leung, M. K. H. Leung and M. Ni, Renewable Sustainable Energy Rev. **13** (4), 845 (2009).

5 A. A. Gromov, U. Förter-Barth and U. Teipel, Powder Technol. **164** (2), 111 (2006).

6 A. V. Parmuzina and O. V. Kravchenko, Int. J. Hydrogen Energy **33** (12), 3073 (2008).

7 G. Sakovich, V. Arkhipov, A. Vorozhtsov, S. Bondarchuk and B. Pevchenko, Nanotechnol. Russ. **5** (1), 91 (2010)

8 M. M. Mench, K. K. Kuo, C. L. Yeh and Y. C. Lu, Combust. Sci. Technol. **135** (1-6), 269 (1998).

5. EXPERIMENTS

5.1. Preparation of Ga-In and Ga-In-Sn alloy

Ga-In-Sn liquid alloy was prepared using 65 wt% of gallium, 25 wt% of indium and 10wt% of tin. Firstly, physically mixed gallium and indium was heated to 150 °C until the phase charged to homogeneous liquid form (the alloy from these two metals of this ratio has a melting point of 15 °C according to the phase diagram). At this temperature, tin powder was added into the metallic liquid and stirred continuously for approximately 5 min. After cooling down to room temperature, the Ga-In-Sn eutectic maintained its liquid form.

Ga-In alloy was prepared with the same ratio between gallium and indium.

5.2. Preparation of Ga-In-Sn-Zn and Ga-In-Sn-Bi alloys

Ga-In-Sn-Zn liquid alloy was prepared using 65wt% gallium, 20wt% indium, 10wt% tin and 5wt% zinc. Gallium and indium were physically mixed and heated to 150 °C into liquid form. Tin powders were added into this metallic liquid and stirred continuously for approximately 5 min. Then zinc flakes were dispersed into the liquid alloy with stirring. Meanwhile, the temperature of the mixture was further increased to 180 °C to dissolve all the zinc flakes. Zn is added to the liquid alloy for its electrochemical properties in Al-based alloy. Also Zn may increase the defects and cracking of the protective alumina layer, which facilitated the diffusion of the deposited In (supposedly, Ga as well) into the surface layers and improved Al reactivity [1].

Ga-In-Sn-Bi liquid alloy was prepared using 65wt% gallium, 22wt% indium, 7wt% tin and 4wt% bismuth. Similar to the preparation of theGa-In-Sn-Zn alloy, the Ga-In-Sn alloy was firstly prepared and heated and bismuth is dispersed into it with increased temperature of 200 °C. Bi, is used as an alloying component to aluminum, it has been proven to lower the operating potential for more than 300 mV compared with that of pure aluminium[2]. Also, it is a nontoxic material stable in water and with its low melting point of 271.3 °C, it is often used together with Sn and In as an alloy for making low melting point alloy.

5.3 Activation

There are generally two ways of using Ga-based alloy as a catalyst on the reaction between aluminum and water:

The first method is to initially mix all the metals including Al and Ga and then co-heat them at high temperature in a vacuum or inert gas atmosphere, making a bulk alloy as a whole that contains Al. After that, the bulk of alloy could be directly put into water and generate hydrogen gas in the required situation. The advantage of this method is that the bulk alloy can be previously prepared and kept ready to use until the desired time. However, once synthesized, the alloy is quite reactive, even with normal moisture and oxygen levels in the air and this makes the alloy extremely difficult to store for any long period of time.

To solve the problem in this method, an efficient storage method is desired. A polymer layer that prevents the activated alloy from reacting with air would be a good solution if the polymer could also be removed immediately in the presence of water.

The second method for preparing Ga-based liquid alloy excludes the involvement of Al at the beginning. After the amalgamation-like alloy is formed, it could be mechanically mixed with fine Al powders. The mixture then could be used to produce hydrogen with the same effect as the alloy bulk in the first method. This method will cause relatively more complexity at the time of using, but by storing liquid alloy and Al powders separately, their shelf-lives are much longer. Although unstable and sensitive to changes in reacting conditions, both methods are separately reported to reach almost theoretical efficiencies[7,4]. This indicates that all the energy stored in the Al metal can be released locally into hydrogen energy through reaction with water with the help of Ga-based alloys.

The advantage of this method over the first method is that both Al before activation and Ga-based liquid alloys are easier and safer to store separately before activation, although currently, this method does not achieve the high efficiency of the first method.

For all four compositions of alloys, our hydrogen production rate data (which will be discussed later) were based on the aluminum activated with the second method, by directly mechanical mixing of aluminum powders and liquid alloy. Aluminum powders used here possessed an average diameter of 20 microns.

5.4. Apparatus for H_2 yield recording

A simple setup is used here for measuring the amount of hydrogen produced. As shown in Fig. 5.1, activated aluminum is reacting with water in the flask, generating hydrogen. The produced hydrogen will drive the same volume of water into the middle container into the graduated flask. Since the pressure in the space between the two water

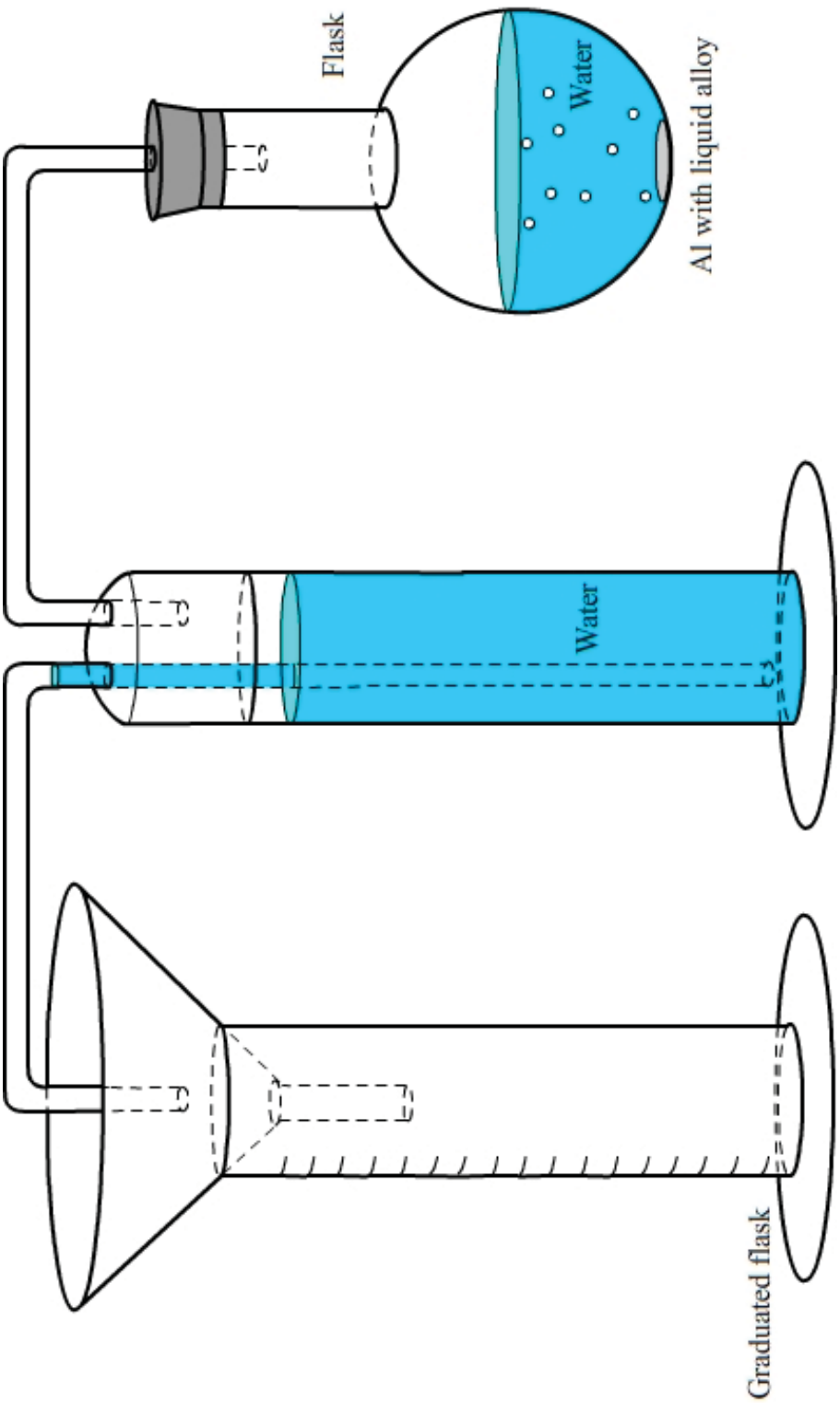

Fig. 5.1. Schematic diagram of apparatus used in H_2 production experiments

surfaces is almost the same as that of atmosphere, with merely a difference of a few centimeters of water column, the hydrogen produced can be treated as ideal gas with molar volume of approximately 22.4 L/mol. By measuring the volume of water transferred into the graduated flask, the amount of hydrogen produced through this process can be determined.

5.5. References

[1] H. A. El Shayeb, F. M. Abd El Wahab and S. Zein El Abedin, Corros. Sci. **43** (4), 655 (2001).

[2] S. B. Saidman and J. B. Bessone, Electrochim. Acta **42** (3), 413 (1997).

[3] A. V. Parmuzina and O. V. Kravchenko, Int. J. Hydrogen Energy **33** (12), 3073 (2008).

[4] O. V. Kravchenko, K. N. Semenenko, B. M. Bulychev and K. B. Kalmykov, J. Alloys Compd. **397** (1-2), 58 (2005).

6. RESULT AND DISCUSSION

6.1. SEM images on liquid alloy surface

SEM characterization of the surface of the Ga-In-Sn liquid alloy is done with a Hitachi S3000-N.

As seen in Fig. 6.1, the liquid phase of the alloy is not directly exposed to the atmosphere in the SEM chamber and is instead covered by a very thin layer of solid, which consists of oxides. This thin layer of solid results in both a solid-liquid interface and a solid-gas interface rather than a single liquid-gas interface. This may help to account for the reason the liquid alloy does not evaporate quickly like other liquid metallic materials (e.g., mercury), making it much safer for the health of users. Also, it

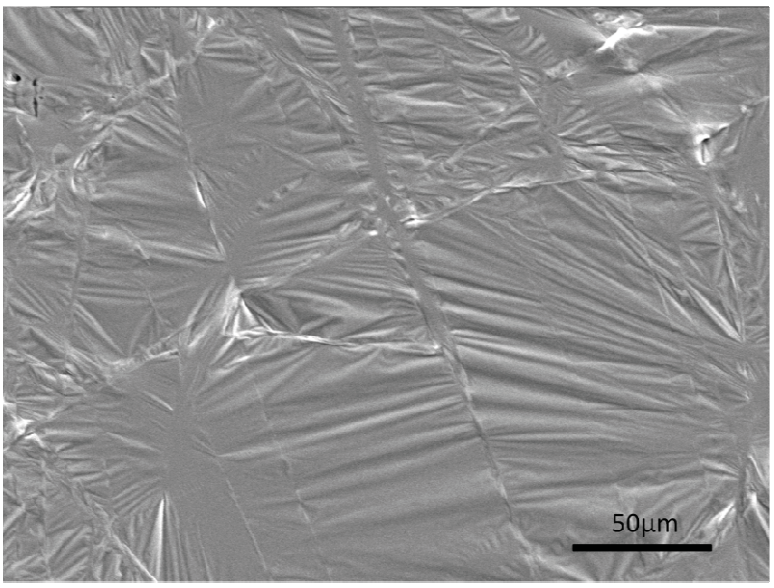

Fig. 6.1. SEM image of the surface of Ga-In-Sn liquid alloy recorded at room temperature.

may contribute in preventing the oxidization of the liquid alloy itself from ambient oxygen in air.

For those alloys which have already activated aluminum several times, the surface layers become more complicated. As can be seen in Fig. 6.2, instead of a very thin, smooth layer, the solid phase is thicker while more roughly and randomly distributed. It is mostly likely that, after each round of hydrogen production reaction, a small portion of Al_2O_3, or possibly unreacted Al, was left over on the surface of the liquid alloy, together with the already existing thin solid layer of alloy itself. Through the hole indicated on the left image of Fig. 6.2, we did EDX characterization of the inner material.

In Fig. 6.3, it can be seen that only Ga, In and Sn are found by EDX and no detectable amount of Al was examined inside. This supports the conclusion that the remaining Al_2O_3 (possibly partly of left over Al after the hydrogen production reaction) is inclined to attach to the outer surface of the alloy instead of dispersing into the liquid phase inside. Furthermore, this result suggests that, 1) a large volume of liquid alloy usage will not negatively influence the hydrogen production rate, because activated aluminum will always be released to the outer surface of the alloy to react with water, instead of staying inside; 2) removal of the Al_2O_3 is relatively easy since it is always on the surface; and 3) removal of the surface Al_2O_3 is important because this thick layer may hinder further hydrogen production reaction once the activated aluminum released from the alloy is covered by this outer layer of Al_2O_3.

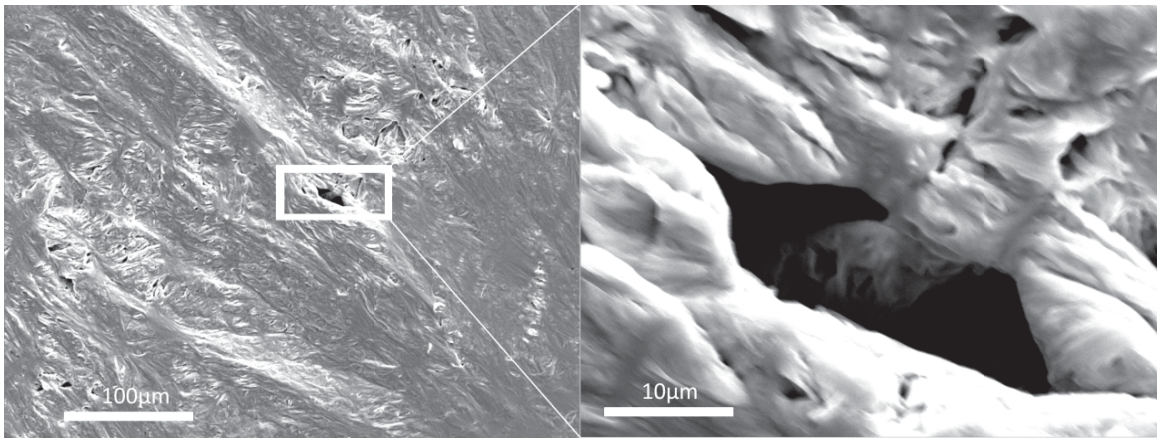

Fig. 6.2. The porous structure on the surface of alloy which was used for activation several times

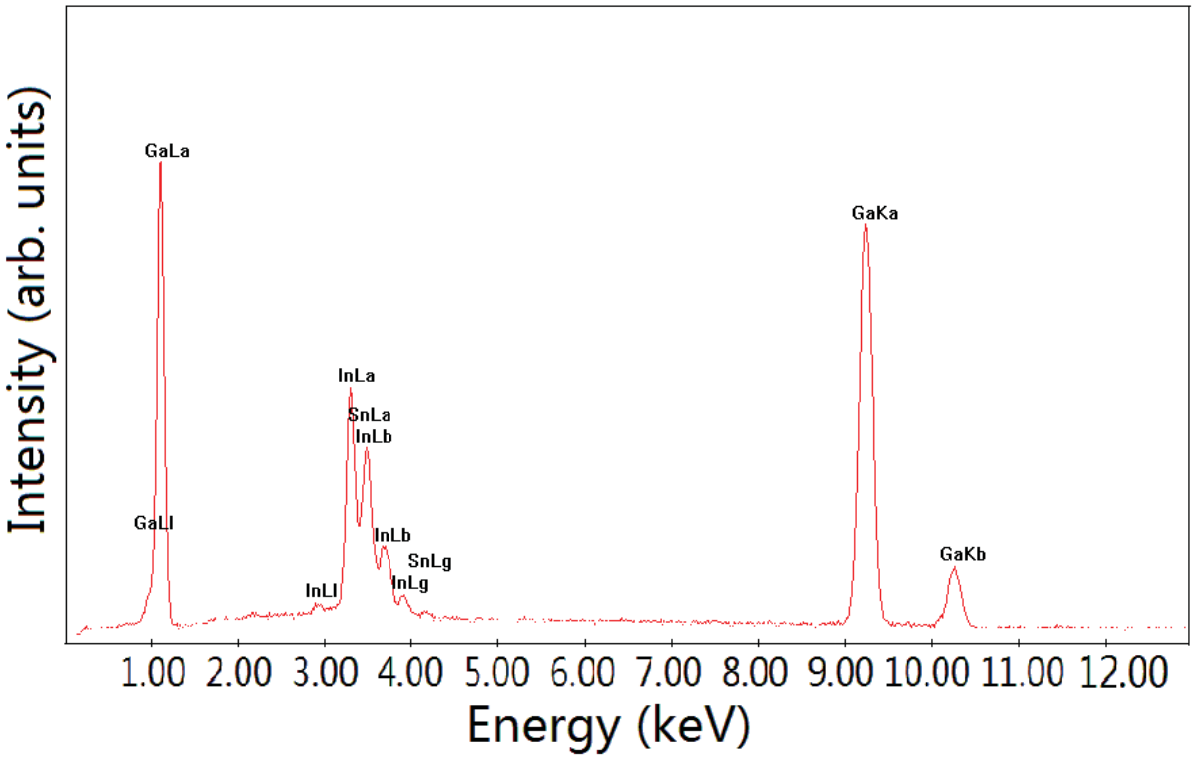

Fig. 6.3. EDX characterization of the inner part of the material

6.2. SEM images of Al before, during and after activated by liquid alloy

Fig. 6.4 is the SEM micrograph of the commercial Al powders. This image shows the size of aluminum at approximately 20 microns before activation with a fine and smooth spherical shape. Fig. 6.5 is taken after putting the freshly mixed Al and alloy into the SEM chamber.When Al powder is mixed with the liquid alloy, a homogeneous distribution of Al is expected throughout the whole material. It can be observed that the Al powders are either bound or absorbed into the randomly distributed liquid alloy. Fig. 6.6 is taken after 2 h of activation, when part of the liquid alloy became physically separatable from the Al powders. This image shows that part of the Al powders was reformed into a completely different structure, while other particles still retain their original spherical shape.

6.3. Activation time versus exposing time

The activation process of aluminum is affected by two competing factors of time: the longer the process is, the more complete the activation can be made; however, if the process is too long, the already activated aluminum will begin to oxidize from moisture and oxygen in the air. Therefore, an optimized time range to finish the activation process becomes a necessary reference for potential industrialized usage.

As shown in Table 6.1, in each group, 0.05g Al was mixed with approximately 1g of Ga-65 In-25 Sn-10 liquid alloy for 5 min and left alone for further activation in air during a certain amount of time. Water used in each group for hydrogen production reaction was 60 ml with a temperature of 70 degrees Celsius.

Observed from the trend, the total activation time between 1 h (60 min) and

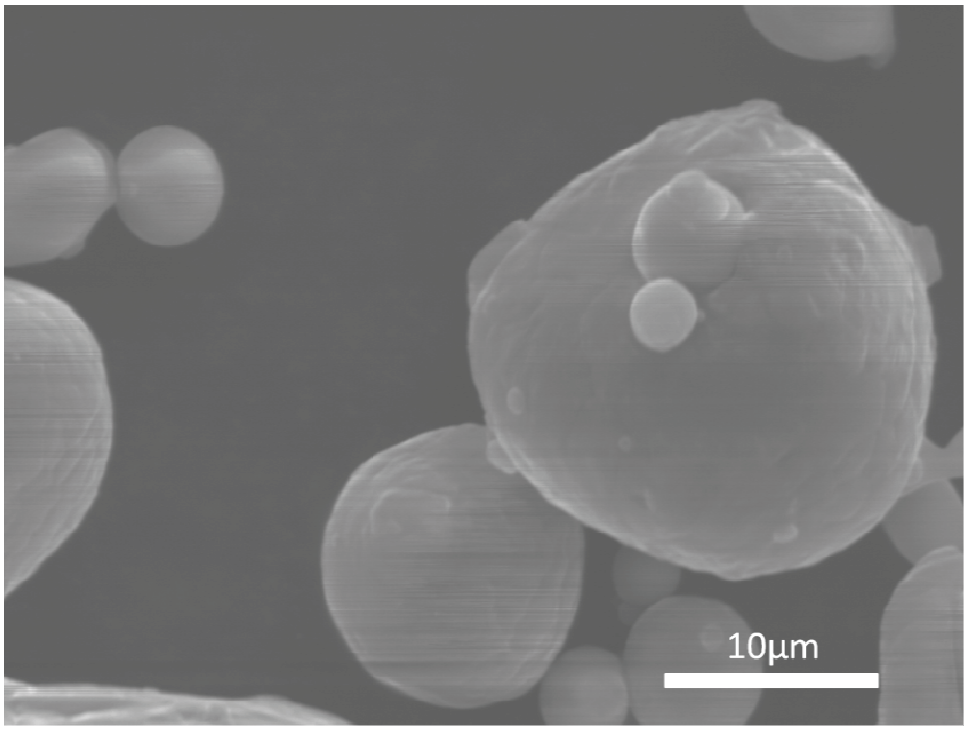

Fig. 6.4 SEM micrograph of aluminum sample before activation

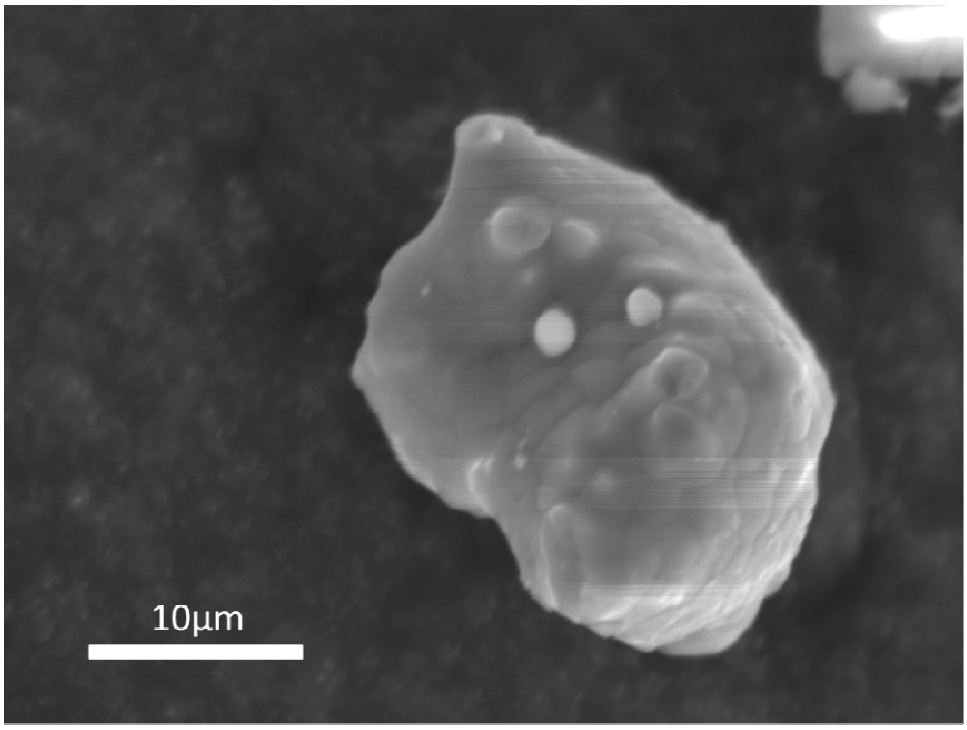

Fig. 6.5 SEM micrograph of aluminum sample during activation

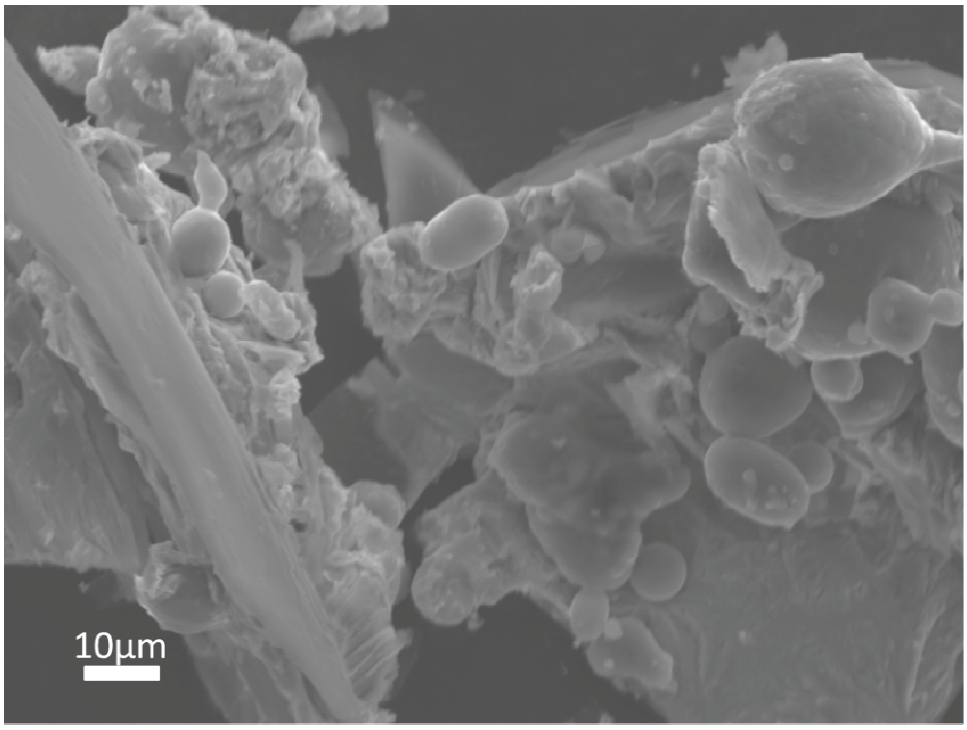

Fig. 6.6 SEM micrograph of aluminum sample after activation

Table 6.1. Total activation times and their influences on hydrogen production rates

Amount of Al (g)	Water temperature (degrees Celsius)	Total activation time (min)	Stirring time (min) (included in activation time)	Hydrogen produced in total (ml)	Reacted/Theoretical (%)
0.05	70	5	5	19	31
0.05	70	10	5	21	34
0.05	70	15	5	24	39
0.05	70	60	5	35	56
0.05	70	1440	5	36	58
0.05	70	4320	5	27	43
0.05	70	7200	5	19	31

1 day (1440 min) provides an optimized and relatively stable hydrogen production rate of approximately 56%-58% completeness. When less than 60 min, part of the aluminum would contact water too early to be fully activated and if more than 1440 min, oxidization of activated aluminum would cause gradual decrease in the production amount.

6.4. Influence of water temperature

Another very important factor on the production rate is the temperature of the Al-water where reaction is taking place. Critical temperature, below which hydrogen production reaction would be impeded, was reported to exist in Al-Ga binary alloy reacting with water at between 26 degrees Celsius and 27 degrees Celsius[1]. Although no such critical condition was observed in our experiments, temperature still plays an important role in the production rate of hydrogen in the reaction.

In our study, each group of 0.05g Al was activated by liquid alloy Ga-65 In-25 Sn-10 for 5 min and then immediately reacted with 60 ml water of different temperatures. As Fig. 6.7 indicates, the amount of hydrogen produced is positively correlated with an increase in water temperature and the difference between that of 70 °C is especially distinct as compared with 60 °C. The explanation can be either the high temperature provided by hot water boosted the activation process between alloy and Al before the Al is completely reacted or passivated by water, or Al with the same degree of activation tend to react more thoroughly with hotter water because of kinetic reasons, or both of them. The highest production rate achieved at 70 °C exhibits the theoretical yield, assuming pure H_2 is produced.

6.5. Viscosity and wetting of Ga-In-Sn alloy

Viscosity can be an important factor in the process of activation. A drop of Ga-In-Sn alloy was put into ice-water mixture. Instead of solidification, the drop remains liquid, but with very high viscosity. When picked up out of water and dried, the alloy at this status shows weak ability to wet and activate Al. This observation indicates that high viscosity is possibly among the reasons high hydrogen production rate was achieved with high water temperature.

The wetting of Ga-In-Sn alloy on Al is qualitatively observed to be determined by viscosity, thus by the temperature. Meanwhile, a more precise experiment of the wetting on Al at room temperature would be of reference value.

As shown on the images of Fig. 6.8, at room temperature, the contact angle of the Ga-In-Sn alloy on Al surface is smaller than on many other surfaces like glass surface, indicating a better wetting on Al. However, even though the contact angle of liquid alloy

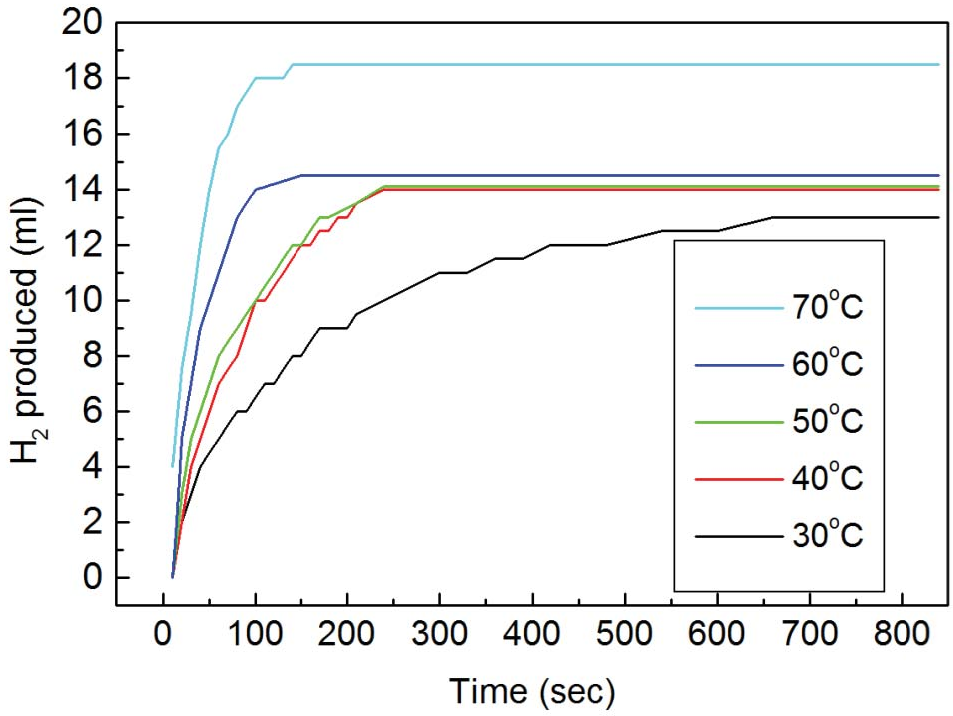

Fig. 6.7. Hydrogen production rates in different temperatures

on Al is larger, it is still smaller than 90°, which confirms that an increased temperature would still be helpful for optimized wetting conditions.

As shown in Fig. 6.9, it is also worth mentioning the effect of the alloy on the Al foil, which is used as the Al surface in Fig. 6.8, left image. Staying on the Al foil for 90 min, the alloy not only activated the area it directly contacts, but also affected the surrounding area of the foil, causing its reaction with air.

6.6. Alternative compositions

Gallium is the element that makes the reaction possible because many of its alloys could exist in liquid phase, which acts like amalgamation and moistening agents of the

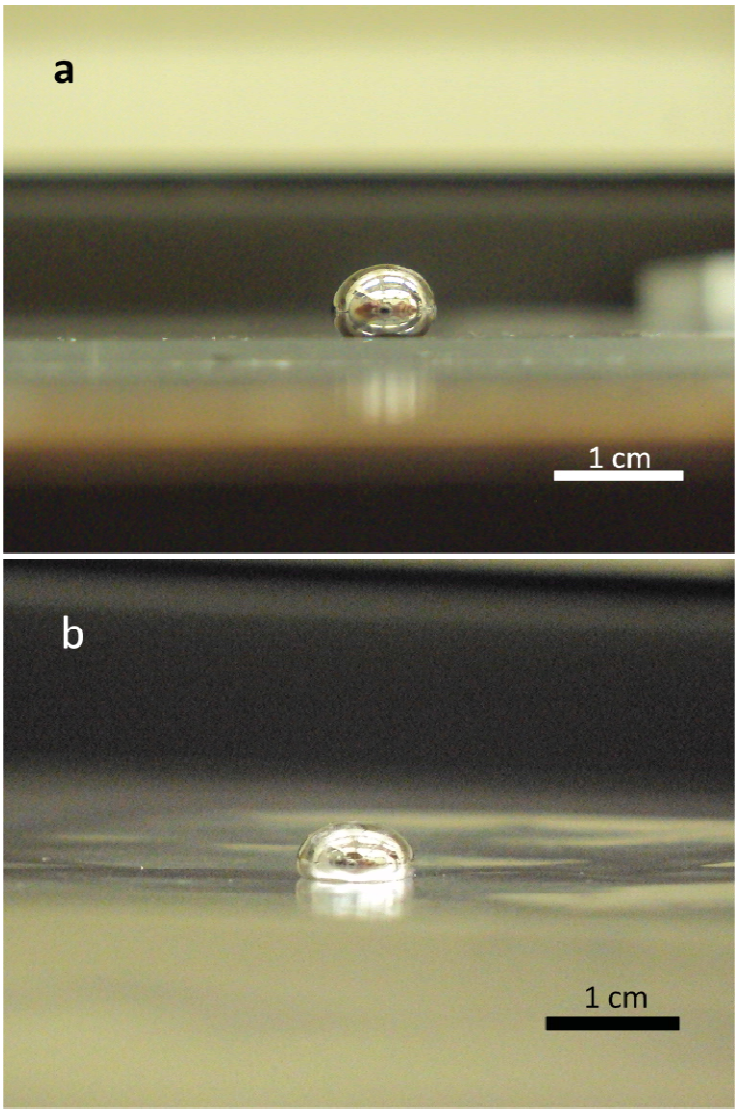

Fig. 6.8. Wetting of Ga-In-Sn alloy on Glass (a) and Al (b)

Fig. 6.9. Effect of Ga-In-Sn alloy on Al foil

aluminum surface to prevent the formation of the aluminum oxide film on its surface; Indium makes a liquid alloy with gallium when heated together with a ratio near the eutectic point. Tin further decreases the melting temperature of the alloy; and zinc could increase the defects and cracking of the protective alumina layer, which can facilitate the diffusion of the deposited In (supposedly, Ga as well) into the surface layers and improve Al reactivity. This is supposed to further decrease the melting temperature of the alloy, though so far Zn is proved extremely hard to mix into the existed alloy of Ga-In-Sn at relatively low temperature. Bi which was not commonly used for this kind of application was also tested in place of Zn because of its chemical and physical properties such as the ability to lower the melting point of alloys.

6.6.1. Ga-In alloy

Aluminum activated by Ga-In alloy produces less hydrogen than activated Ga-In-Sn alloy under the same conditions. After 5 min activation with minimum mechanical mixing, aluminum activated by Ga-In generated 8 ml hydrogen which is 13% of theoretical production, compared to 31% activated by Ga-In-Sn; after 60 min of total activation time including 5 min of mechanical mixing, aluminum activated by Ga-In generated 18 ml hydrogen which is 29% of theoretical production, compared to 56% activated by Ga-In-Sn.

It is also observed that, unlike Ga-In-Sn alloy which shows little change after ten to twenty activation cycles, part of the Ga-In alloy separated as fine droplets (size varying from less than 0.1 mm to slight more than 1 mm) from the main liquid alloy drop after each reaction cycle. These separated droplets show very weak capability to activate aluminum and there is no method for effectively merging them back into the main alloy drop. After approximately six reaction cycles, the entire alloy degraded into this status.

Subsequent SEM images as in Fig. 6.10 show that the degradation is mainly due to the alumina fractions attaching on these droplets, preventing them merging or having contact with Al. The EDX result proves that the fractions are alumina. The reason of alumina less likely attaching onto Ga-In-Sn alloy than onto G-In alloy is yet to be examined.

6.6.2. Ga-In-Sn-Zn alloy and Ga-In-Sn-Bi alloy

In the experiments, the introduction of Zn into the Ga-In-Sn alloy did not increase the hydrogen production rate as expected. After 5 min of activation with minimum mechanical mixing, aluminum activated by Ga-In-Sn-Zn generated 12 ml hydrogen

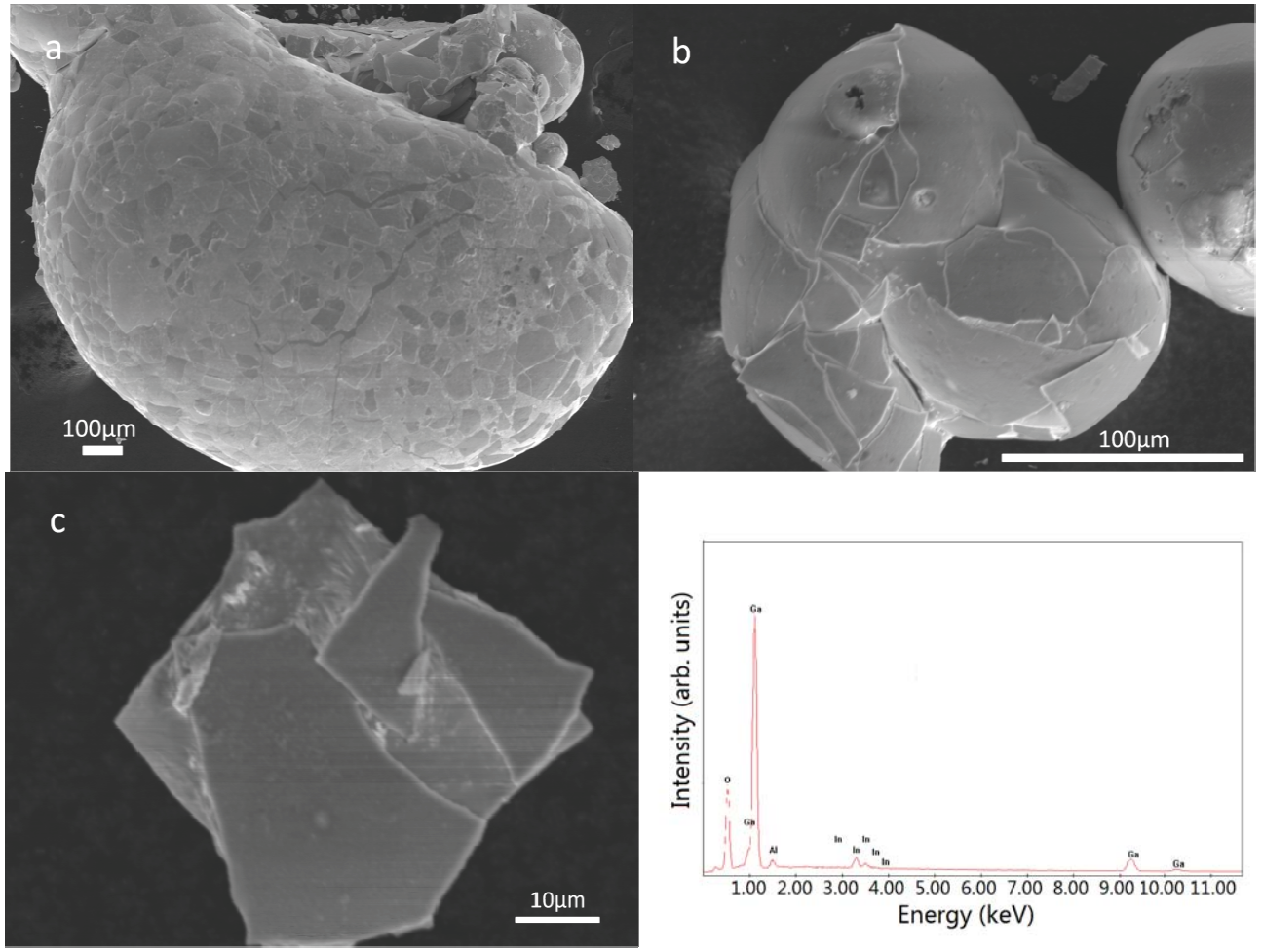

Fig. 6.10 Degraded Ga-In alloy which shows weaker capability to activate aluminum

which is 19% of theoretical production, compared to 31% activated by Ga-In-Sn-Zn. Also, after 60 min total activation time, including 5 min mechanical mixing, aluminum activated by Ga-In generated 16 ml hydrogen which is 26% of theoretical production, compared to 56% activated by Ga-In-Sn.

In the parallel experiment on Bi, it also failed to improve the Ga-In-Sn alloy. After adding Bi, the liquid alloy behaved in a manner consistent with a substance that possessed two or more separated phases, possibly due to the fact that the temperature used to merge Bi into Ga-In-Sn alloy was not high enough. Al activated by this alloy only produced trace amounts of hydrogen, regardless of the time of activating and the water temperature.

6.7. Mechanisms

Although there is not a uniform agreement on the mechanisms of activation, many researchers provided reasonable hypotheses to explain this phenomenon.

One theory is known as the metal dissolution-deposition[1], illustrating this phenomenon as an electrochemical plating process where alloying elements cathodic versus aluminum, such as In and Sn, plating back onto the aluminum surface and locally separate the covered oxide film[2]. This localized de-filming process is believed to be the result of the retention and agglomeration of high mobile metallic species upon the interface[3].

Another explanation is based on the study of Rebinder's effect of aluminum[4]. This illustration focuses on the eutectic penetration of the alloy into aluminum grain boundaries, destroying the intercrystal contacts and forming aluminum monocrystal powders covered by eutectic thin film[5].

Referring to these hypotheses and combining them with our observation, Fig. 2.9 is presented here to explain the mechanisms of reaction.

In Fig. 6.11 (a), Al particle is covered by the Ga-In-Sn liquid alloy with the aforementioned 65-25-10 composition and its surface will be physically broken apart by the alloy because of the Rebinder's effect. Then both alloy and Al are contacted with water as shown in Fig. 6.11 (b). Then we can see in Fig. 6.11 (c) these physically shattered tiny parts of Al tend to react with water nearby to generate hydrogen. These parts tend to move towards water because of the density and concentration difference and also the fact that the alloy layer covering each Al particle is very thin. The these parts of monocrystal Al react with water and generate hydrogen while due to the metal dissolution-deposition process, alloy elements keep preventing the formation of Al oxide films. Although as shown in Fig. 6.11 (d) that Al could be constantly shattered by the alloy, it is very difficult to make 100% Al reacted. This is because the main particle of Al would very likely react with water soon and form an oxide layer on its surface. When the passivation layer covering the particle is completely formed, the metal dissolution-deposition process no longer acts to activate the Al. To prove this, we did a minor experiment that if Al powders were immersed in water for 1 h before activation, it is unable to be activated it with any of the four types of liquid alloy anymore.

Although the analysis in the last paragraph could serve as an explanation of the activation mechanism, not enough evidence is readily available to confirm the effects in these reactions. A more straightforward way to consider the reactions is the dissolution of aluminum metal into the liquid alloy. Because according to the phase diagrams, the Ga-based liquid alloy could actually absorb a relatively large ratio of aluminum, it is valid

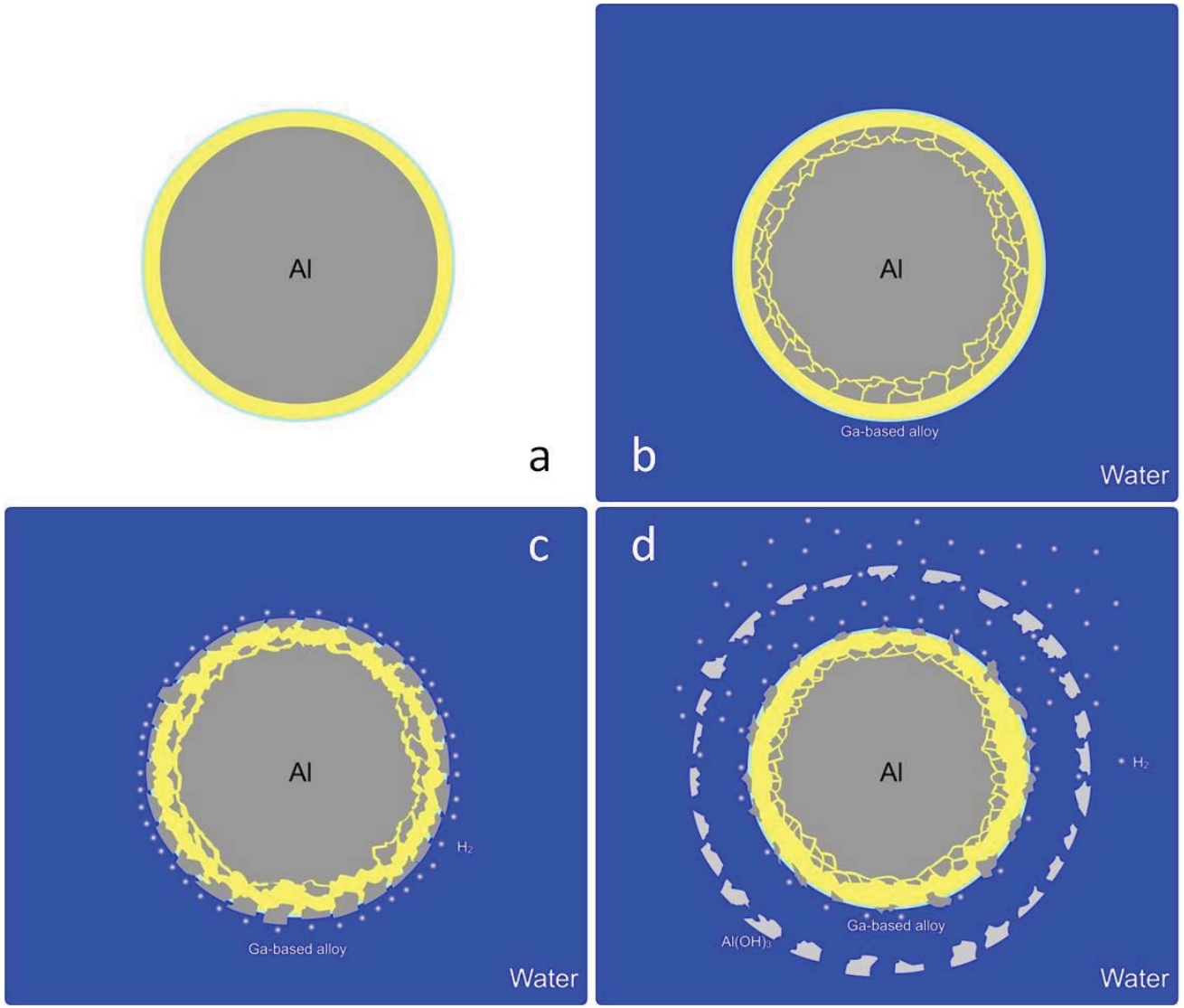

Fig. 6.11. Schematic diagram of activation and hydrogen production cycle

to consider that the liquid alloy absorbs aluminum and then the absorbed aluminum, as an element in the metal solution, reacts with water to produce hydrogen. This alternative mechanism provides another viewpoint on these hydrogen production reactions other than activation. It is also matches with the water temperature effect data for if the solubility of Al in Ga-based liquid alloy influences its reactivity, it is obvious that the solubility is dependent on temperature.

6.8. References

[1] Ziebarth, J.. "Use of the aluminum gallium indium tin system for energy storage and conversion". Ph.D. diss., Purdue University ,2010. In *Dissertations & Theses: Full Text* [database on-line]; available from http://www.proquest.com (publication number AAT 3417965; accessed May 8, 2011).

[2] H. Z. Wang, D. Y. C. Leung, M. K. H. Leung and M. Ni, Renewable Sustainable Energy Rev. **13** (4), 845 (2009).

[3] M. C. Reboul, Corrosion **40** (7), 366 (1984).

[4] M. Kliskic, J. Radosevic, S. Gudic and M. Smith, Electrochim. Acta **43** (21-22), 3241 (1998).

[5] A. V. Parmuzina and O. V. Kravchenko, Int. J. Hydrogen Energy **33** (12), 3073 (2008).

7. CONCLUSION

Both the hydrogen production reaction from Al-water reaction and the activation process between Al and Ga-based liquid alloy was studied in our research. The hydrogen production rate was observed to be affected by both activation time and reaction temperature. Higher temperature leads to faster reaction and more hydrogen produced while a optimized activation time was found between 60 min to 1440 min. The surface of liquid alloy was found to be covered by a thin layer of solid, which became thicker after reacting with Al, possibly because of the oxide of Al absorbed on the surface. The activation process of Al was also examined by SEM, showing the changes taken place during this process.

A commonly indicated drawback of hydrogen production through activated Al alloy is the fact that, when Al is part of the alloy composition, the chemical activity of the alloy would be too hard to retain at room temperature. With Ga-based alloy prepared beforehand and only activating Al 1 h to 1 day before usage, this storage problem can be circumvented.

PART III

COPPER BORON OXIDE / TITANIUM OXIDE HETEROJUNCTION AND COPPER ALUMINUM OXIDE / TITANIUM OXIDE HETEROJUNCTION FOR PHOTOCATALYTIC WATER SPLITTING

8. INTRODUCTION

Solar energy is always considered a renewable energy source for water splitting. To convert the energy of sunlight into the chemical energy of hydrogen, many methods are used, such as thermolysis[1,2] thermochemical decomposition[3,4,5] and the electrolysis of water using the electrical energy collected by solar cells[6]. Of all these routes, photoelectrolytic and photocatalytic processes are considered most promising[7]. The general operating principle of a photoelectrochemical cell (PEC) in the aphotoelectrolytic process is illustrated as the following.

The working electrode, also knownas the "semiconductor electrode", is usually an n-type semiconductor photoanode that functions as the working electrode, absorbing photons and evolving oxygen with the reaction between the photogenerated holes h^+ with water at the interface between the photoelectrode and electrolyte. The generated hydrogen ions H^+, travel through the aqueous electrolyte to the cathode. Meanwhile, the counter electrode, reducing H^+ ions into H_2, can either be a metal cathode like platinum or a p-type semiconductor cathode. However, if the counter electrode is chosen as a p-type semiconductor cathode, the working electrode can also be a metal anode. In general, at least one of two the electrodes should be a semiconductor, in which n-type is anode and p-type is cathode and the semiconductor electrode is photoactive.[8]

Within a photoelectrolytic process, the conversion of UV light and/or visible light into electrical current and the chemical transformation of H_2O into H_2 are integrated into a single step with a single electrode.

In a photocatalytic water decomposition, both of the following reactions:

$$2H^{+}+2e^{-}\rightarrow H_2\uparrow \quad (25)$$

$$2h^{+}+H_2O\rightarrow 1/2O_2\uparrow+2H^{+} \quad (26)$$

simultaneously take place at the same site, i.e., on the surface of the photocatalyst instead of separately occurring at the photoanode and the photocathode.[9]

A photocatalytic water-splitting device works with the semiconductor particles acting as photocatalysts. [8]The photocatalyst simultaneously functions as both the working electrode and the counter electrode of the photoelectrochemical cell. Hydrogen and oxygen mixture gas are generated from water splitting with light absorbed. Afterwards, the mixture of gases is usually separated with respective separation membranes. This separation process could be done easily at relatively low temperature.

Although both oxide and nonoxide semiconductors could potentially serve the function of photocatalysts in the photocatalytic process, oxide semiconductors attracted considerably more attention from researchers in the water-splitting field since 1977, when Scherauzer and Guth carried out the photocatalytic decomposition of water vapor under UV light, resulting in the simultaneous cogeneration of oxygen and hydrogen, with TiO_2-based photocatalysts[10].

Delafossite-type oxides, especially delafossite $CuAlO_2$, were discovered to be very promising candidates as oxide semiconductor photocatalysts. Delafossite $CuAlO_2$ is a p-type semiconductor with a small band gap depending on materials processing parameters[11]. The photocatalytic performances of $CuAlO_2$ were widely studied. $CuAlO_2$ nanoparticles can be used in thermal photocatalytic generation of H_2 in H_2O without

involvement of other chemicals while keeping a stable generation rate at temperature as high as 187–237 °C[12]. At lower temperature ranging from room temperature to 60 °C, hole scavengers like S^{2-} and $S_2O_3^{2-}$ are frequently used to make the hydrogen production reaction consistent[11]. And it is discovered that the heterosystem of $CuAlO_2$ and TiO_2 is the preferred way to improve the effiency of the photocatalytic process by means of permitting a physical separation of charge carriers with electrons injected from activated $CuAlO_2$ into activated TiO_2[13].

Copper boron oxide ($CuBO_2$), a relatively newer member of copper delafossite series, exhibits some similar physical and chemical properties as $CuAlO_2$. This material was discovered and synthesized by MichaelSnure and AshutoshTiwari in 2007[14]. Because the predicted band gap of $CuBO_2$, which is approximately 2.2 eV and slightly higher, matches well with the photon energy of 2.46 eVin Equation (3.3) derived from Equation (3.4) with the water splitting threshold energy of 1.23eV[7],it is highly expected that $CuBO_2$ can play a matching role as a photocatalyst in water splitting.[14]

$$\Delta G^0 = -nF \cdot \Delta E^0 \quad (27)$$

$$H_2O + h\nu \rightarrow H_2 + 1/2O_2 \quad (28)$$

In this work, $CuBO_2$ particles are synthesized with simplified methods and we studied its water splitting capability at 30 °C in basic environment with the present of S^{2-} as hole scavenger. The potential synergy of its heterosystem with TiO_2 was also investigated. For comparison, hydrogen production rates in groups of $CuAlO_2$ and $CuAlO_2/TiO_2$ were also recorded in the same experimental environment.

8.1. References

[1] J. E. Funk, Int. J. Hydrogen Energy **26**, 185 (2001).

[2] A. Kogan, Int. J. Hydrogen Energy **22**, 481 (1997).

[3] C. Perkins, A. W. Weimer, Int. J. Hydrogen Energy **29**, 1587 (2004).

[4] C. Perkins, A. W. Weimer, AIChE Journal **55**, 286 (2009).

[5] A. Steinfeld, P. Kuhn, A. Reller, R. Palumbo, J. Murray, Y. Tamaura, Int. J. Hydrogen Energy **23**, 767 (1998).

[6] L. L. Kazmerski, Renewable Sustainable Energy Rev. **1**, 71 (1997).

[7] C. A. Grimes, O. K. Varghese, S. Ranjan, *Light, water, hydrogen : the solar generation of hydrogen by water photoelectrolysis*, Springer, New York (2008).

[8] Journal of Nanoscience and Nanotechnology **11**, 3719 (2011).

[9] T. Bak, J. Nowotny, M. Rekas, C. C. Sorrell, Int. J. Hydrogen Energy **27**, 991 (2002).

[10] G. N. Schrauzer, T. D. Guth, Journal of the American Chemical Society **99**, 7189 (1977).

[11] N. Koriche, A. Bouguelia, A. Aider, M. Trari, Int. J. Hydrogen Energy **30**, 693 (2005).

[12] J. R. Smith, T. H. Van Steenkiste, X.-G. Wang, Physical Review B **79**, 041403 (2009).

[13] R. Brahimi, Y. Bessekhouad, A. Bouguelia, M. Trari, Journal of Photochemistry and Photobiology A: Chemistry **186**, 242 (2007).

[14] M. Snure, Applied physics letters **91**, 092123 (2007).

9. EXPERIMENTAL

9.1. Materials Preparations

9.1.1. Preparation of $CuBO_2$ and heterojunction$CuBO_2/TiO_2$

The $CuBO_2$ particles were prepared with a solution-based reaction. Firstly, B_2O_3 (Alpha Aesar99.98%) was dissolved in DI water with a stoichiometric amount of $Cu(NO_3)_2 \cdot 3H_2O$ (Fisher Science Education 98+%). The two solutions were mixed for 1 h with a magnetic stirrer and completely evaporated on a hot plate. Solids dehydrated from the mixed solution were collected and grounded for 40 min. Afterwards, the ground solids were transferred to an unglazed crucible. The solid was then calcinated at 750°C.

$CuBO_2/TiO_2$ heterojunctions were prepared by coheating of aforementioned $CuBO_2$ particles and commercial TiO_2-P25 (AEROXIDE®) nanopowders in a hydrothermal reactor. With a molar ratio of 1:1, both particles were mixed in 60 ml DI water and heated in the hydrothermal reactor at 200 °C for 20 h. The high pressure generated under this temperature in a hydrothermal reactor would result in a junction structure between these particles.

9.1.2. Preparation of $CuAlO_2$ and heterojunction$CuAlO_2/TiO_2$

The $CuAlO_2$ particles were prepared in a similar way as producing $CuBO_2$. Fine particle size was obtained by ball milling. Separately, a stoichiometric amount of $Al(NO_3)_3 \cdot 9H_2O$ (Alpha Aesar 97+%) was dissolved in DI water and CuO (Puratronic 99.995%) in concentrated nitric acid. The two solutions were then mixed for 1 h with a

magnetic stirrer and completely evaporated on a hot plate. Solid dehydrated from the mixed solution were collected and grounded for 40 min. Afterwards the ground solids were transferred to an unglazed crucible. The solid was then calcinated at 1150°C.

In order to get smaller sizes of $CuAlO_2$ particles, ball milling was applied on the obtained powders. The weight ratio between the zirconia milling balls and $CuAlO_2$ samples was taken as 10:1, with an operating time of 20 h.

$CuAlO_2/TiO_2$ heterojunction was prepared by coheating of the ball-milled $CuAlO_2$ particles and commercial TiO_2-P25 nanopowders in a hydrothermal reactor at 200 °C for 20 h with a molar ratio of 1:1.

9.2. Materials characterization

X-ray diffraction (XRD), Scanning electron microscope (SEM) and Energy-dispersive X-ray spectroscopy (EDX) characterizations were performed upon all solid samples. Powder XRD patterns of CuBO2, CuAlO2, $CuBO_2/TiO_2$ heterojunction and $CuAlO_2/TiO_2$ heterojunction were obtained with a Philips X'pert Diffractometer. Then those obtained patterns were analyzed with X'pert Highscore Plus software. SEM micrographs of $CuBO_2$, $CuAlO_2$, TiO_2, $CuBO_2/TiO_2$ heterojunction and $CuAlO_2/TiO_2$ heterojunction were also captured with a Hitachi S-3000N Scanning Electron Microscope, while some of these samples were examined with EDX.

9.3. Water splitting measurements

Quantified measurement of water splitting using various catalysts was operated by recording mass change of water. Five identical beakers (50ml) were filled with the same amount of DI water (30ml) and all of them were boiled to eliminate the oxygen from air

dissolved in the water. When the water reached room temperature, 0.05M $Na_2S \cdot 9H_2O$ as a hole scavenger and 0.1M NaOH as a pH modifier were added. The pH value of the solution was maintained at 12.8 at room temperature. Then 50 mg of each of the catalysts was dispersed into the four different beakers. The solution in the fifth beaker works as the control group because evaporation is the only form of water loss in this group. The initial mass of all three beakers was measured on a scale (Ohaus, Adventurer SL). All three beakers were then kept at 30°C and exposed to 1.5 AM solar radiation (Solar Light Model 16S). The remaining mass of each beaker was weighted after every 40 min. The mass of water loss because of evaporation in each group is estimated by measuring the mass change in the control group and the mass of split water in either experimental group was calculated by ruling out the mass of evaporated water from the mass of total water loss in that group.

10. RESULTS AND DISCUSSION

10.1. SEM and XRD characterization results

Micrographs of $CuBO_2$ and $CuBO_2/TiO_2$ heterojunction were taken, as well as those of $CuAlO_2$ particles after ball milling, and $CuAlO_2/TiO_2$heterojunction materials formed using the hydrothermal method. As shown in Fig. 10.1, after the hydrothermal process, both the $CuBO_2/TiO_2$ heterojunction and the $CuAlO_2/TiO_2$ heterojunction presents in the form of agglomeration of ultrafine particles of precursor materials and P-25 TiO_2 nanopowders. As shown in Fig. 10.2, a further proof from EDX characterization targeted on the particle in Fig. 10.1 (c), (d) shows no impurity peak existing in the agglomeration except for the carbon peaks, which are from the carbon paste substrates used for SEM sample preparation.

XRD results of $CuBO_2$ and $CuAlO_2$ are shown in Fig. 10.3. There is no obvious change of patterns of $CuAlO_2$ after it hydrothermally reacted with TiO_2, except for the presence of the corresponding TiO_2 peaks. However, in the case of $CuBO_2$, very severe change of patterns was observed after the hydrothermal reaction. This may be one of the reasons $CuBO_2$ showed no improved performance after forming a heterosystem with TiO_2.

10.2. ***Results of water splitting measurement*****s**

In all four experimental groups, i.e., $CuBO_2$ and $CuBO_2/TiO_2$, $CuAlO_2$, $CuAlO_2/TiO_2$, continuous water splitting data were observed, which indicates a positive yield of hydrogen.

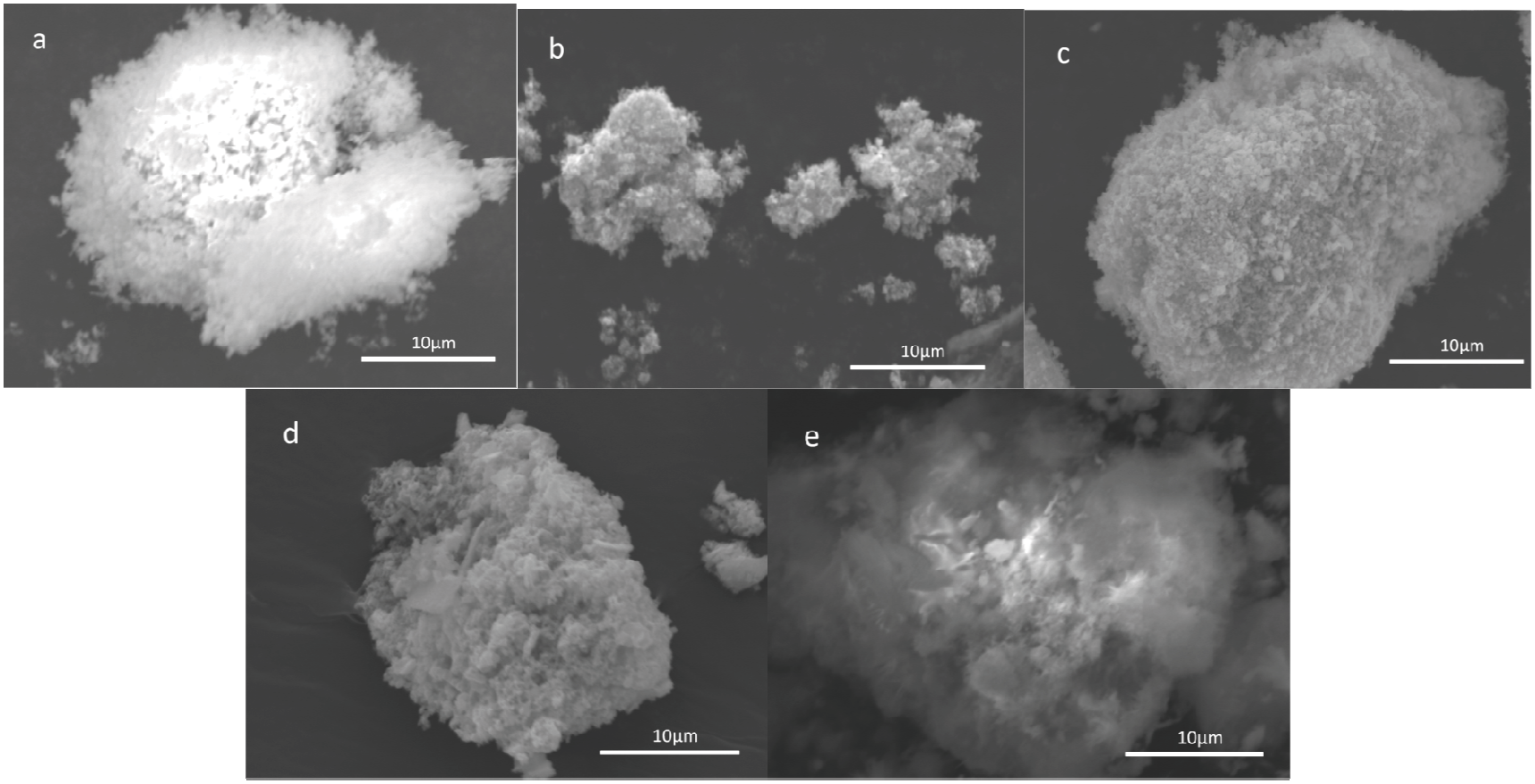

Fig. 10.1.SEM micrographs of $CuAlO_2$ after ball milling (a), commercial P-25 TiO_2 (b), $CuAlO_2/TiO_2$ heterojunction (c), $CuBO_2$ as prepared (d) and $CuBO_2/TiO_2$ heterojunction (e)

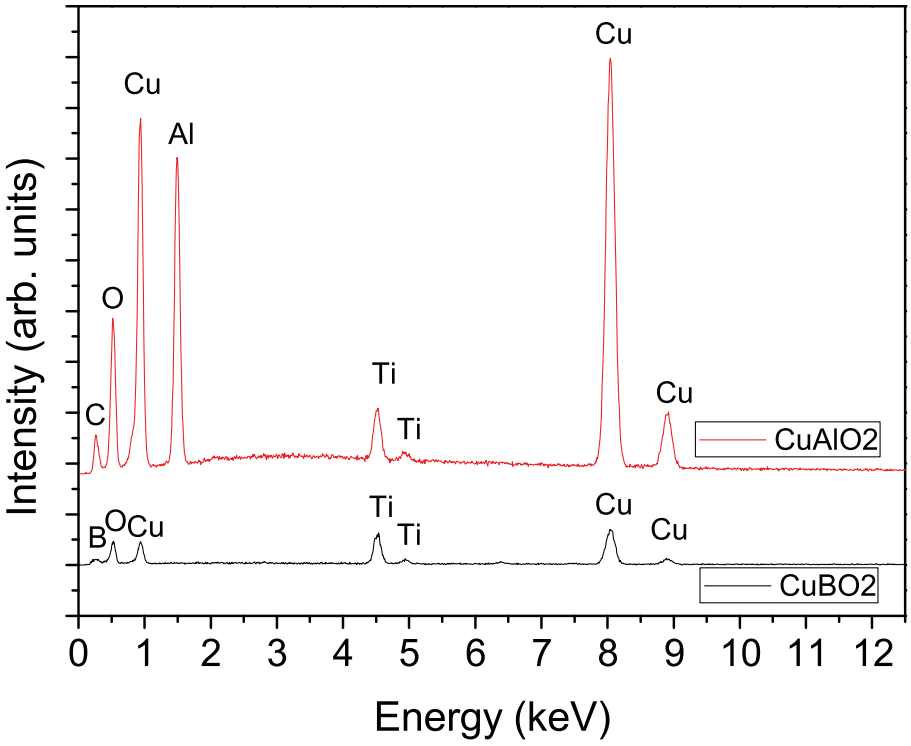

Fig. 10.2. EDX characterization of $CuBO_2/TiO_2$ heterojunctionand $CuAlO_2/TiO_2$ heterojunction

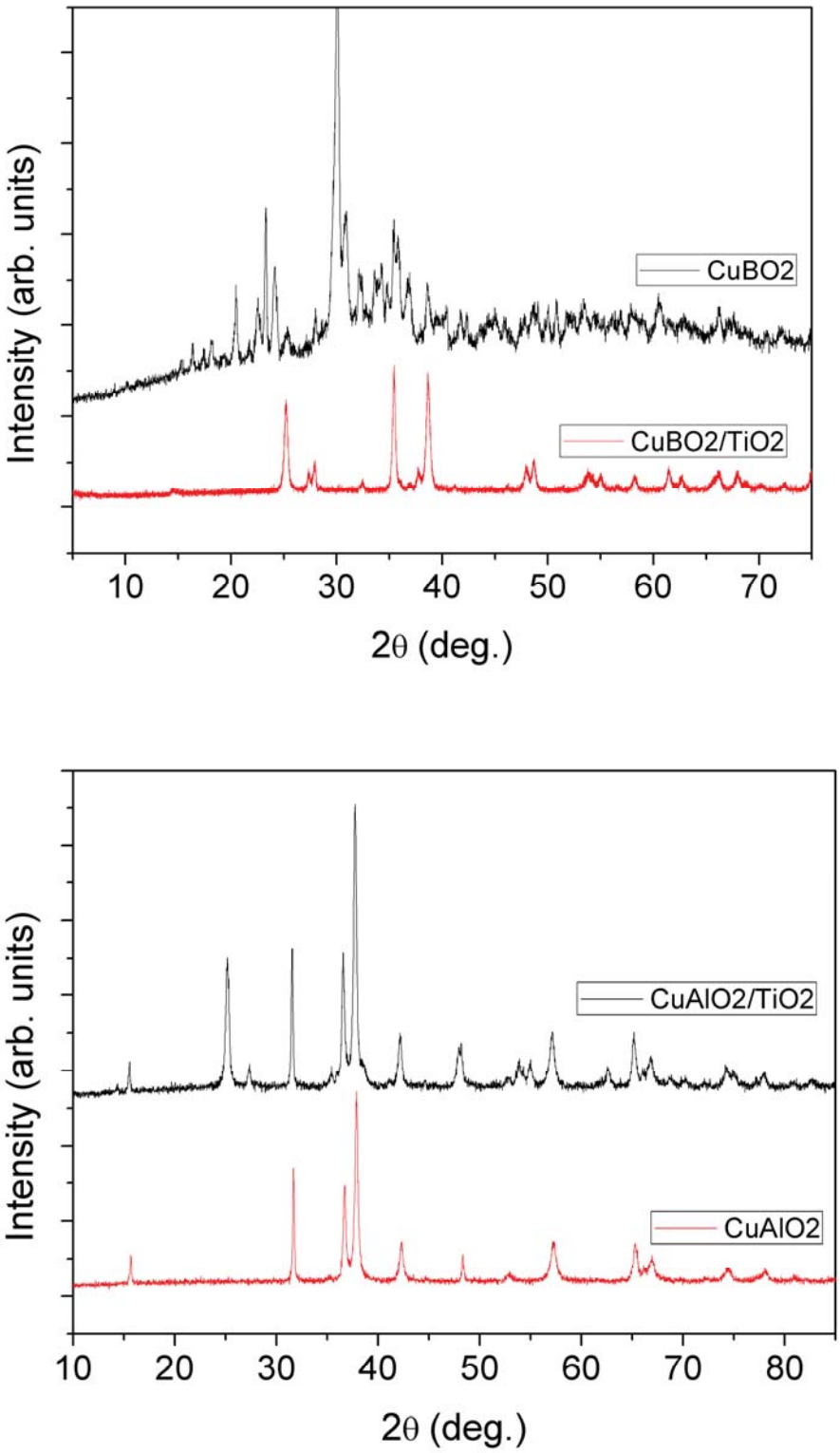

Fig. 10.3. XRD patterns of $CuBO_2$, $CuBO_2/TiO_2$ heterojunction,$CuAlO_2$ and $CuAO_2/TiO_2$ heterojunction

In the quantified measurement of water splitting using $CuAlO_2$ and $CuAlO_2/TiO_2$ heterojunction, as shown in Fig. 10.4, an average hydrogen production of 0.479mmol/min was achieved when only $CuAlO_2$ was used as the photocatalyst. Meanwhile, a higher average production rate of 0.509mmol/min was reached when using the synthesized $CuAlO_2/TiO_2$ heterojunction as the photocatalyst. These results indicate a boost of 6.33% in water-splitting rate, which can be explained by the earlier studies on $CuAlO_2/TiO_2$ heterojunction by R. Brahimi et al.[1]

As indicated in Fig. 10.4, when only $CuBO_2$ sample was used as the photocatalyst, an average 0.979 mmol/min production rate was obtained. It is apparent that a much larger amount of water was split when $CuBO_2$ was used than when using either $CuAlO_2$ or $CuAlO_2/TiO_2$ heterojunction. When $CuBO_2/TiO_2$ heterojunction was used, a much smaller production rate of 0.484 mmol/min was attained. This fact indicates that, with the 1:1 weight ratio, the synergy of $CuBO_2$ and TiO_2 was much lower than in the case of $CuAlO_2/TiO_2$ heterojunction. On the contrary, because only half the weight amount of $CuBO_2$ exists in the $CuBO_2/TiO_2$ group compared to the pure $CuBO_2$ group, without significant heterojunction effect, the production rate was also approximately a half as a result.

10.3. Discussion

Both $CuBO_2$and $CuAlO_2$ belong to delafossites[2]. Delafossite structured materials, along with scheelite (monoclinic) structured materials (e.g., $BiVO_4$) and perovskite structured materials (e.g., $AgNbO_3$), were found to show photocatalytic activities under certain conditions[3],[4] . Within these materials, Cu delafossites like $CuBO_2$ and $CuAlO_2$ are special due to various reasons. Some of these specialties are owing to the $3d_{10}$ related

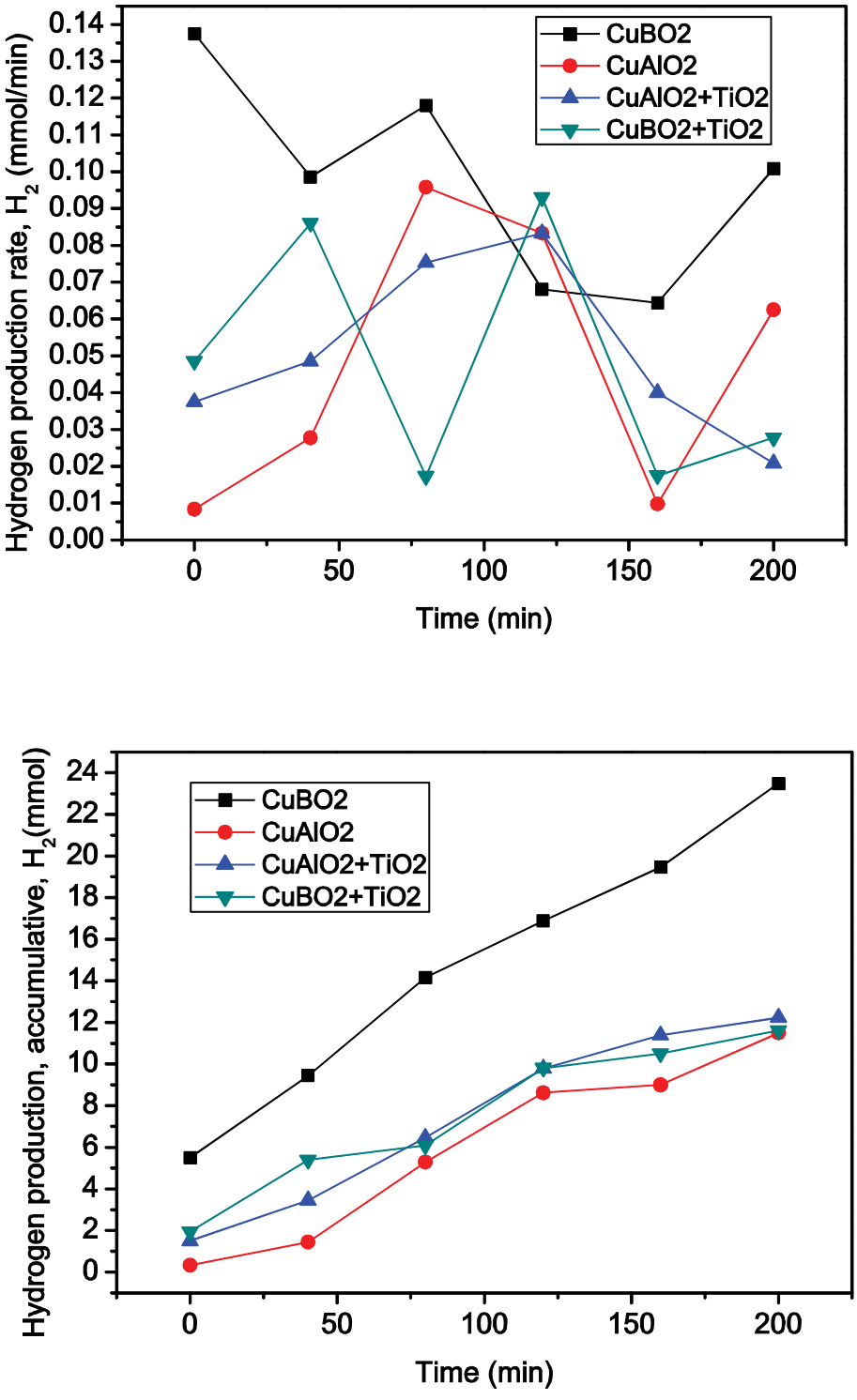

Fig. 10.4. Hydrogen evolution amount from water splitting as a function of illumination time, with $CuBO_2$, $CuAlO_2$, $CuBO_2/TiO_2$ heterojunction and $CuAlO_2/TiO_2$ heterojunction as photocatalysts, under AM1.5, 1000W/m^2, room temperature

electronic configurations in Cu. While forming a continuous valence band, the weak d_{10}-d_{10} interactions in Cu highly influence the features of band structure of $CuBO_2$ and $CuAlO_2$ because the Al orbitals have a negligible participation in the valence band of the material [5],[6]. This is also the possible reason for $CuBO_2$ achieving better results in water splitting, because with the delafossite structure and the same Cu-induced electronic configurations, B contributed more to the valence band than Al. However, because the chemical and physical properties of $CuBO_2$ are only preliminarily investigated, the detailed influence of B on band structure of $CuBO_2$ is yet to be extrapolated.

As indicated on Fig. 10.5, $CuBO_2$ is predicted to be positioned on the preferred energy level in the water solution of this pH level. The conduction band of $CuBO_2$ is well matched to $E_{H2O/H2}$ and its valence band lies just below $E_{H2O/H2}$. A possible explanation for $CuBO_2$ showing such a high hydrogen production rate even without TiO_2 or other materials to form a heterosystem is that the charge transfer between $CuBO_2$ and water is so fast that the charge recombination within the same particle is comparably extremely slow, thus exhibiting negligible effects. Another possibility besides the very fast charge transfer rate is that, during our synthesizing process, a small amount of oxides of either Cu or B were left over to play the role of charge transfer media and electron accumulator and this media matches $CuBO_2$ very well at this pH value.

It is also seen on Fig. 10.5 that, $CuAlO_2/TiO_2$ heterojunction works in favor of photocatalytic processes mainly because, when $CuAlO_2$ is simulated by photons, the generated electrons can be spontaneously injected into the conduction band of TiO_2. So compared to pure $CuAlO_2$, instead of Reaction (10.6), with the presence of $CuAlO_2/TiO_2$ heterojunction, Reaction (10.7) and Reaction (10.8) would take place. When the electrons

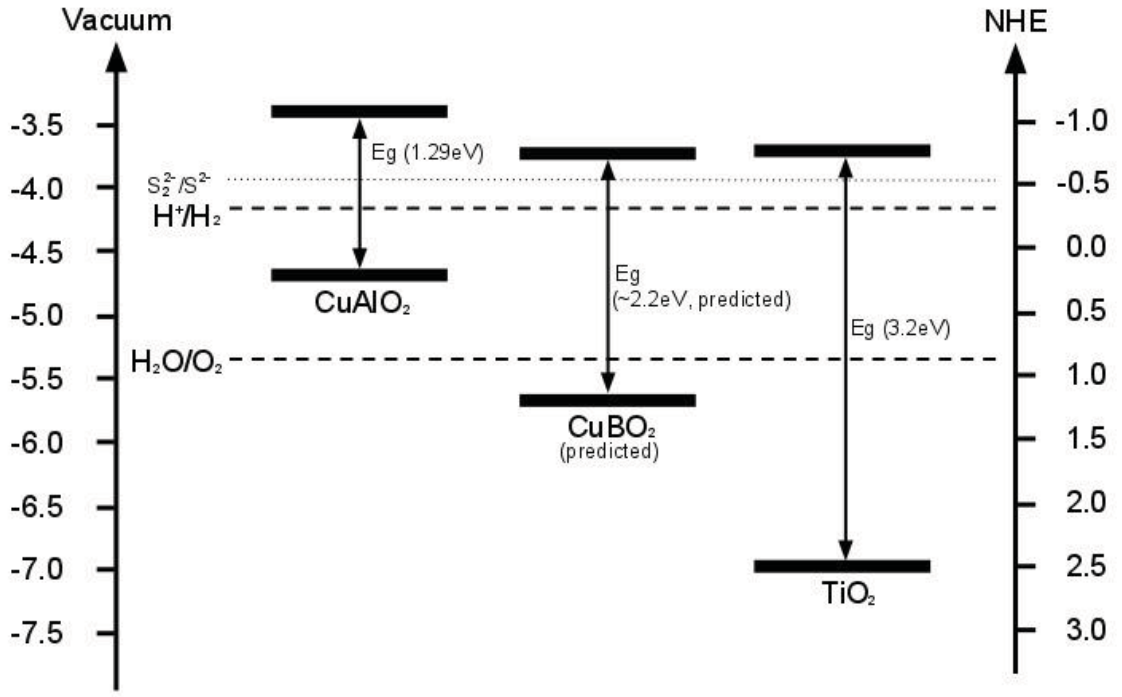

Fig. 10.5. Schematic energy diagram of $CuBO_2$, $CuAlO_2$ and TiO_2 at pH 12.8; the conduction and valence band of $CuBO_2$ was predicted according to the analysis of Michael Snure[2]

are injected into TiO_2, charge separation against recombination would be improved because of the stronger driving force resulting from the better matching of TiO_2 conduction band and $E_{H2O/H2}$.[1]

$$CuAlO2 + (h\nu) \rightarrow CuAlO2\ (e^-, h^+) \quad (29)$$

$$CuAlO2\ (e^-) + H2O \rightarrow CuAlO2 + (1/2)H2 + OH^- \quad (30)$$

$$CuAlO2\ (e^-) + TiO2 \rightarrow CuAlO2 + TiO2\ (e^-) \quad (31)$$

$$TiO2\ (e^-) + H_2O \rightarrow TiO_2 + (1/2)H_2 + OH^- \quad (32)$$

It is yet unknown about the interaction between $CuBO_2$ and TiO_2 when a heterojunction is formed. But since the involvement of TiO_2, in our case, hindered rather than boosted the photocatalytic capability of $CuBO_2$, it is reasonable to presume that, as drawn in Fig. 10.5, the conduction band edge of $CuBO_2$ is positioned slightly more positive than that of TiO_2 (NHE as reference). In this case, the electron injection from conduction band of $CuBO_2$ would not be spontaneous due to lack of driving force. Therefore, no similar electron flow as observed in the heterosystem of $CuAlO_2/TiO_2$ would happen in heterojunction $CuBO_2/TiO_2$.

10.4. References

[1] R. Brahimi, Y. Bessekhouad, A. Bouguelia, M. Trari, Journal of Photochemistry and Photobiology A: Chemistry **186**, 242 (2007).

[2] M. Snure, Applied physics letters **91**, 092123 (2007).

[3] H. Kato, H. Kobayashi, A. Kudo, The Journal of Physical Chemistry B **106**, 12441 (2002).

[4] A. Kudo, H. Kato, I. Tsuji, Chemistry Letters **33**, 1534 (2004).

[5] M. Gratzel, Nature **414**, 338 (2001).

[6] A. Kudo, Int. J. Hydrogen Energy **31**, 197 (2006).

11. CONCLUSION

In summary, the water-splitting performance of delafossite structured materials $CuBO_2$ and $CuAlO_2$ are studied in the present work with several improvements. A new route of forming heterosystem through hydrothermal method is used. $CuBO_2$ is synthesized and tested as a photocatalytic material for the first time and showed even better experimental photocatalytic properties than $CuAlO_2$ and heterojunction $CuAlO_2/TiO_2$ with the same standard light source and environmental conditions.